Development and application of computational tools for high content image analysis (HCA) of neural cells

Dissertation to obtain the degree
Doctor Rerum Naturalium (Dr. rer. nat.)
at the Heinrich-Heine-University Düsseldorf

submitted by

Martin Roland Schmuck

from Würzburg

Düsseldorf, November 2015

Entwicklung und Anwendung von informatischen Methoden für die "High Content" Bildanalyse (HCA) von neuralen Zellen

Inaugural-Dissertation

zur Erlangung des Doktorgrades
der Mathematisch-Naturwissenschaftlichen Fakultät
der Heinrich-Heine-Universität Düsseldorf

vorgelegt von

Martin Roland Schmuck

aus Würzburg

Düsseldorf, November 2015

Angefertigt am Leibniz Institut für umweltmedizinische Forschung (IUF) gGmbH
an der Heinrich-Heine Universität Düsseldorf.

Gedruckt mit der Genehmigung der
Mathematisch-Naturwissenschaftlichen Fakultät der
Heinrich-Heine-Universität Düsseldorf

Referentin: Prof. Dr. Ellen Fritsche

Korreferent: Prof. Dr. Lutz Schmitt

Tag der mündlichen Prüfung: 10.12.2015

Table of Contents

1. Introduction 1
   1.1. Developmental neurotoxicity (DNT) testing: 1
   1.2. Paradigm shift in toxicology 3
   1.3. Primary neural progenitor cells (NPCs) as an *in vitro* model for DNT testing 5
   1.4. High Content Image Analysis (HCA) 8
   1.5. *In silico* methods and fingerprint libraries 10
   1.6. Objectives of the thesis: 13
2. Manuscripts 14
   2.1. 'Omnisphero: A novel computational approach for high content image analyses (HCA) of organoid neurosphere cultures *in vitro* 15
   2.2. Automatic counting and positioning of 5-bromo-2-deoxyuridine (BrdU) positive cells in cortical layers of rat brain slices. 17
   2.3. Developmental Neurotoxicity of Epigallocatechin Gallate (EGCG) Is Triggered by Interference with β1-Integrin Function in Human Neural Progenitor Cells. 19
3. Discussion 22
   3.1. HCA for medium throughput DNT substance screening in the Neurosphere Assay 23
   3.2. Phenotypic screening of NPCs to classify modes of action (MOA) for developmental neurotoxicity (DNT) *in vitro* 33
   3.3. Integration of Omnisphero/BrdeLuxe into flexible software platforms for HCA image analysis of cell phenotypes 37
4. Abstract 42
5. Zusammenfassung 43

List of abbreviations 44

References 46

Acknowledgements 55

Eidesstattiche Erklärung/Declaration 56

1.Introduction

1.1. Developmental neurotoxicity (DNT) testing:

Developmental neurotoxicity (DNT) describes functional and morphological effects of exogenous noxae on the developing nervous system which, through pre- or postnatal exposure, result in pathological changes in the brain (Slikker 1994). Neurodevelopmental toxicants have shown to be a serious threat for the society, clearly demonstrating the need for DNT testing for any kind of registered chemical (Goldman and Koduru 2000). DNT effects become evident already during childhood by children having e.g. a lower intelligence quotient (IQ), learning disabilities or attention-deficit disorders. This results in immense costs for the society due to medication and individual support for those children. Epidemiological studies in the USA showed that about 17% of all children below 18 suffer from neurological deficits originating from genetic background and social environment but are also linked to exposure to DNT substances (Schettler 2001). The relevance of DNT for socioeconomic development of societies was demonstrated by a study of the Mt. Sinai Childeren's Environmental Health Centre which revealed that already a decrease of the average IQ of a population by five points leads to an increase of mentally retarded individuals by 57% resulting in a significant increase of costs (Bellanger et al. 2013; Landrigan et al. 2002). However, out of the chemical universe only 12 substances are known human DNT compounds (Grandjean and Landrigan 2014). This is attributed to sparse DNT testing: Regulatory agencies only demand DNT testing for substances that exert neurotoxic or endocrine disruption potential (EU, USA) or need registration as pesticides (USA). This is due to the fact that DNT studies following the OECD testing guideline 426 and the U.S. EPA guideline OPPTS 870.6300 (OECD 2007; USEPA 1998) are money and time demanding (Crofton et al. 2012) and require large animal numbers.

The developing nervous system is particularly vulnerable towards various chemicals (Rice and Barone 2000; Rodier 1995), since brain development is driven by complex and strongly regulated biological processes: Amongst them proliferation, migration, differentiation and apoptosis. Fig. 1 gives a brief overview over essential processes of brain development.

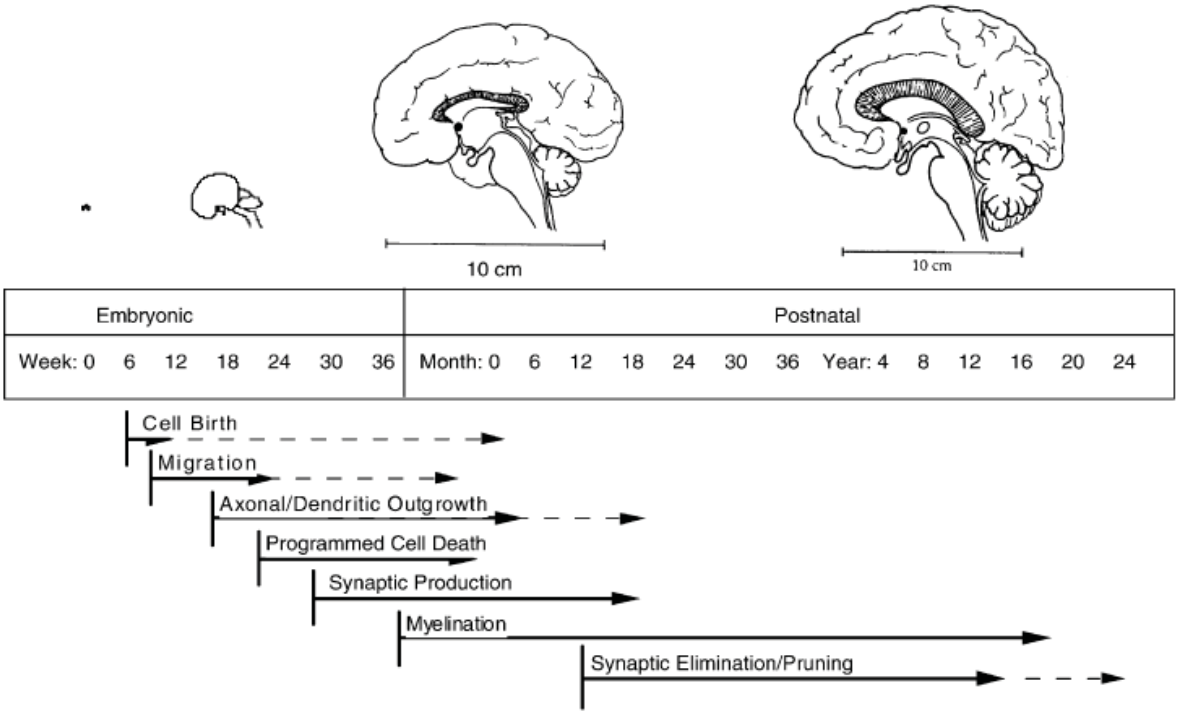

Fig. 1: Schematic representation of brain development: Essential processes of human pre- and postnatal brain development: Cell birth, migration, neurite outgrowth, apoptosis, synaptogenesis, myelination and synaptic elimination and pruning (Andersen 2003).

Single processes last from weeks over month to even years (e.g. myelination) spanning specific critical periods in which exogenous noxae can disturb brain development from the embryonic stage throughout childhood. However, due to the still devloping blood-brain-barrier (Liebner et al. 2011), prenatal exposure to chemicals is of highest concern, since not only lipophilic substances but also hydrophilic and ionic substances can enter the embryonic/fetal brain (Claudio et al. 2000; Pardridge 2006; Slikker 1994). Furthermore, xenobiotic metabolism for excretion of exogenous noxae is not fully developed during the prenatal stage (Bondy and Campbell 2005).

Serious human intoxications with DNT compounds in the past like e.g the contamination with methylmercury (Minamata Bay (Eto 1997)) or polychlorinated biphenyls (used in transformers and electronic isolation (UNEP 1999)) clearly demonstrated the potential of chemicals to disturb brain development (Grandjean and Landrigan 2006). Therefore, stakeholders all over the world agreed that evaluating the DNT potential of chemicals should be a crucial part for risk assessment (Bal-Price et al. 2015a; Crofton et al. 2011). In this context the ISTNET (International STakeholder NETwork) initiative was established to create a DNT testing road map for regulatory purposes.

1.2. Paradigm shift in toxicology

In 2007 the National Research Council (NRC) published the report 'Toxicity Testing in the 21st Century: A Vision and a Strategy' introducing a paradigm shift in toxicology to meet evolving regulatory needs (NRC 2007). The new testing paradigm proposes a shift away from the classical animal models towards alternative model organisms like *C.elegans* or *drosophila* and *in vitro* based methods (Collins et al. 2008; Krewski et al. 2010; NRC 2007) in combination with toxicogenomics, high content image analysis (HCA), systems biology and *in silico* methods (Fig. 2).

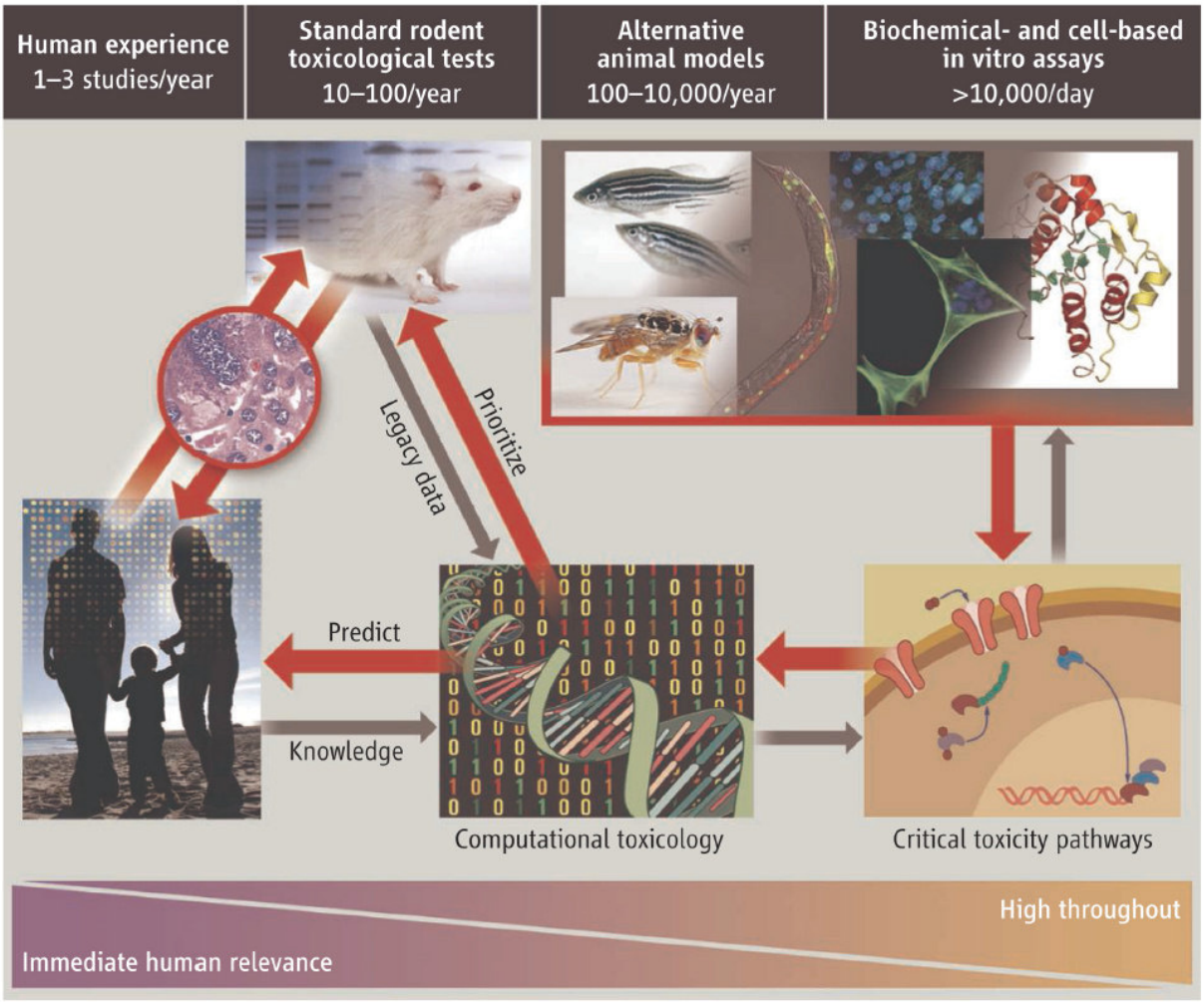

Fig. 2: Paradigm shift in toxicology: Within the new paradigm in toxicology described in Tox21 a shift away from the classical animal models for substance screenings towards human *in vitro* based systems is proposed. This will enhance the throughput, overcome species differences and help to reduce animal numbers in line with the 3R principle. This paradigm shift includes the use of novel technologies such as HCA to screen for critical toxicity pathways in combination with computational toxicology to link *in vitro* data with legacy data from animal studies for a better prediction for risk assessment in humans (Collins et al. 2008).

Within the new testing paradigm it is proposed to screen for critical toxicity pathways in *in vitro* assays (systems biology) and to use obtained data in computational toxicology to prioritize substances for further animal testing. This will reduce the number of animal experiments which is well in line with the 3R's principle (Reduce, Refine, Replace) introduced by Russell and Burch (Russell and Burch 1959). Furthermore, the comparability

between the human and animal situation will be elucidated by a comparison of human *in vitro* data with legacy animal *in vivo* data to allow better extrapolation towards the human *in vivo* situation. This paradigm is crucially dependent on three major factors: 1) The applied *in vitro* system has to mimic organ relevant endpoints and has to be physiologically relevant, 2) suitable techniques like HCA, metabolomics or genomics have to be available to screen for critical toxicity pathways in the given *in vitro* system and 3) *in silico* methods have to be developed to analyze data obtained from 2) to allow substance priorization and read-across approaches. The data obtained from this new testing paradigm will be integrated into 'Adverse Outcome Pathway' (AOP) frameworks and into the so called 'Integrated Approaches to Testing and Assessment' (IATA).

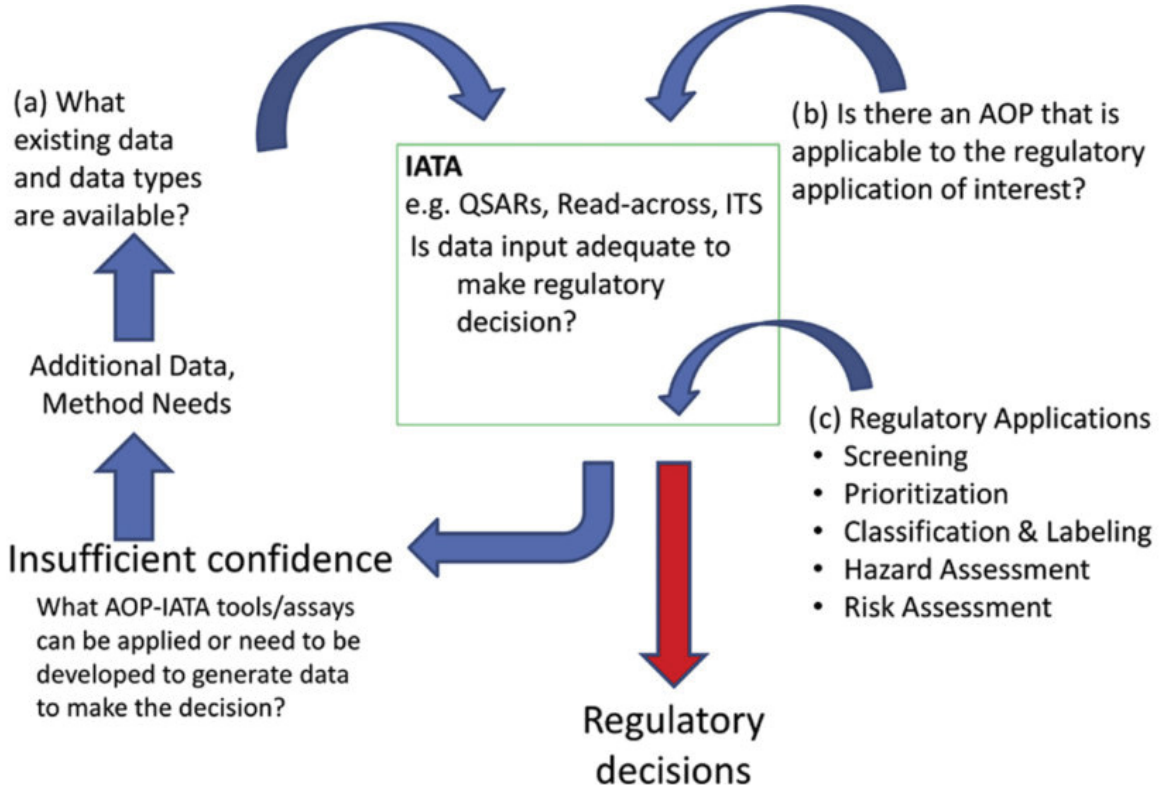

Fig. 3: AOP informed IATA concept: The concept starts with gathering available data sources (a), checks whether any AOP is available (b) and c) involves any regulatory applications. Data are evaluated by non-experimental approaches (e.g. QSAR and read-across) and experimental approaches (e.g. ITS) and data is weighted for reliability to make regulatory decisions. In case the data level is insufficient, proposals were given for the development of AOP-IATA tools/assays. New data is consequently added to the existing data and is revalidated, whether the new data set is sufficient to drive regulatory decisions (Tollefsen et al. 2014).

The AOP concept connects existing knowledge on molecular initializing events (MIE) and the cascade of intermediate or key events (KEs) at molecular, cellular, organ and tissue level that result in a specific adverse outcome (AO) at the individual or population level (Ankley et al. 2010; OECD 2013). In contrast to animal studies, which are based on apical endpoints, the AOP concept gives insight into the mechanistic mode of action (MOA) of compounds. IATA are structured approaches which gather available data from non

experimental data (*in silico*) and experimental data (*in chemico*, *in vitro* and *in vivo*) and weigh them to drive safety and regulatory decisions (Ankley et al. 2010; Bal-Price et al. 2015b). Since IATA are not necessarily build around mechanistic rationales, there is growing support to integrate the AOP concept into the IATA resulting in so called 'AOP-informed IATA' (OECD 2013; Tollefsen et al. 2014). The IATA should therefore ideally comprise as many MIEs and KEs as possible from the AOP. The basic principle of the IATA is given in Fig. 3.

In an initial step all data sources (literature, AOPs and regulatory applications) are gathered and weighted with the help of *in silico* methods like SAR, qualitative (Q)SAR and integrated testing strategies (ITS). Within an ITS different test batteries of mechanistic pathways are combined and organized in a hypothesis-driven decision scheme to ensure efficient analysis of available data and serve to assist for making hazard or risk assessments. Since AOPs should be included into the IATA it is important that ITS comprise as many MIEs and/or KEs as necessary from the AOP. In case of insufficient confidence of the analyzed data the IATA proposes AOP-IATA-tools or assays to fill the data gap. The newly generated data is added to the existing one and revalidated within the IATA.

1.3. Primary neural progenitor cells (NPCs) as an *in vitro* model for DNT testing

One essential requirement for the new toxicity testing paradigm described in Fig. 2 is the use of an *in vitro* system which is able to mimic organ-relevant endpoints and is physiologically relevant. The three-dimensional (3D) neurosphere system is such a promising candidate for DNT substance testing since it is able to mimic basic processes of brain development: proliferation, neuron and glia differentiation, migration and apoptosis (Baumann et al. 2014; Breier et al. 2010; Fritsche et al. 2005; Gassmann et al. 2010; Moors et al. 2009, 2010). Neurospheres spontaneously form by aggregation of primary neural progenitor cells (NPCs; Fig. 4) in the presence of epidermal growth factor (EGF) and fibroblast growth factor (FGF) in suspension culture (Buc-Caron 1995; Chalmers-Redman et al. 1997; Reynolds et al. 1992; Svendsen et al. 1995). They maintain their proliferative character in culture over several months allowing to passage them by mechanical dissociation (Svendsen et al. 1997). Upon withdrawal of growth factors neurospheres attach on poly-D-lysine (PDL) and laminin coated surfaces followed by radial cell migration. NPCs within the migration area differentiate to a heterogeneous cell population expressing markers of NPCs (Nestin) as well as characteristic proteins expressed in the three major cell types of the brain (Brannen and Sugaya 2000; Lobo et al. 2003; Piper et al. 2001; Reubinoff et al. 2001): neurons (βIII-tubulin), astrocytes (GFAP) and oligodendrocytes (O4).

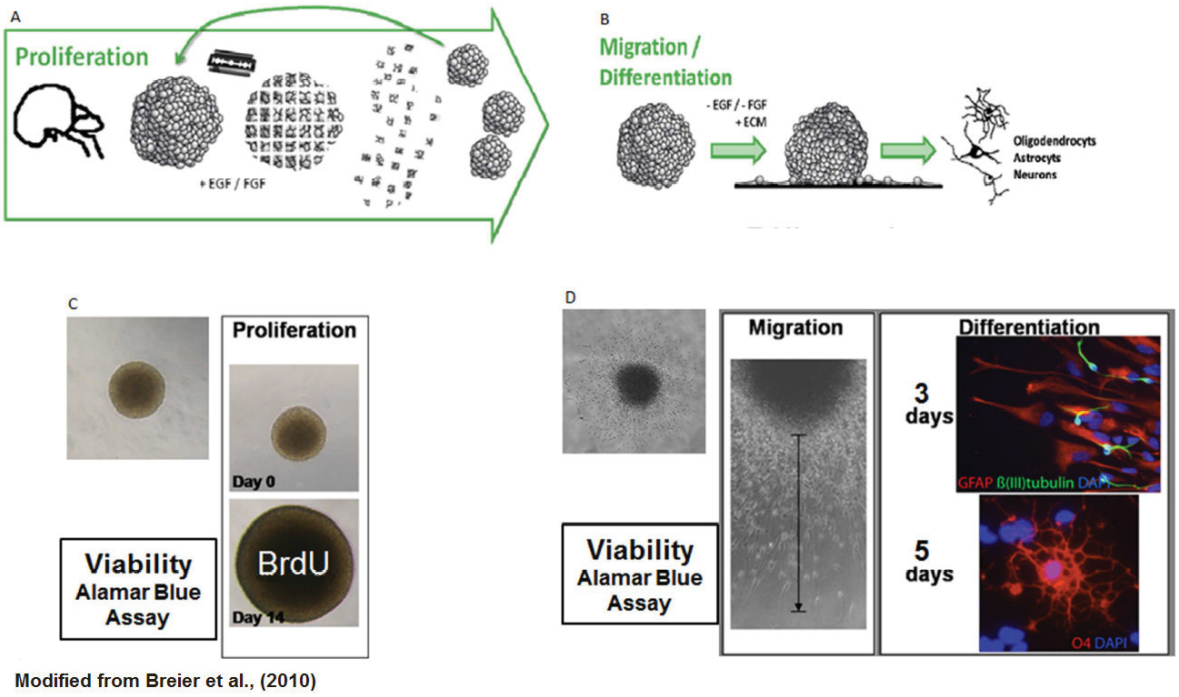

Modified from Breier et al., (2010)

Fig. 4: The 'Neurosphere Assay': Primary NPCs obtained from whole brain homogenates spontaneously aggregate in presence of mitogenic growths factors like EGF and FGF to cell clusters called neurosheres. Neurospheres can be passaged mechanically and can be kept in culture for several month maintaining their proliferative character. They are able to mimic the basic fetal processes of brain development: proliferation, migration, differentiation. Proliferation is assessed indirectly by measuring the diameter increase over time or directly by BrdU incorporation. Upon withdrawal of growth factors neurospheres are able to attach to ECM coated surfaces and cells start to radially migrate out. Thus, cell migration can be assessed by measuring the average distance from the neurosphere core to the furthest migrated cells. NPCs within the formed migration area differentiate into the three major cell types of the brain: neurons, oligodendrocytes and astrocytes. Individual cell types can be visualized with immunocytochemistry and can be quantified either manually or utilizing automated image analysis software.

The proportion of cell types present in the neurosphere migration area thereby seems to reflect the *in vivo* situation (Baumann et al. 2014) indicating their physiological relevance. Furthermore NPCs are able to undergo caspase-dependent and independent apoptosis (Moors et al. 2009) and are thus able to mimic cell-regulatory processes of brain development. Within the so called 'Neurosphere Assay' these endpoints are assessed after substance exposure (Baumann et al. 2014; Breier et al. 2010; Fritsche et al. 2005, 2011; Moors et al. 2009, 2010). Cell viability is assessed via the CellTiter-Blue® assay (CTB, Promega), which quantifies mitochondrial reductase activity. Proliferation is gauged in suspension culture either indirectly by measuring the diameter increase over time or directly by quantification of DNS synthesis via bromodeoxyuridine (BrdU) incorporation. For differentiation assays neurospheres are plated on ECM coated surfaces in multi-well-plates or on cover slides. Migration distance is measured as the average distance from the neurosphere core towards the furthest migrated cells and different cell types are visualized by immunocytochemical stainings. Automated image acquisition is performed using the ArrayScan VTI (Thermo Scientific) with a 20x objective. The ArrayScan VTI is a conventional inverted fluorescence microscope with an implemented micrometer stage allowing to scan complete wells of microtiter plates (196 image per well of a 96 well plate). Apoptosis is detected via immunocytochemical staining by co-staining with Hoechst33342 and PI (paragraph 1.4.).

So far, DNT testing is not implemented in the Tox21/ToxCast testing strategies. However, predictive assays for human DNT hazard and risk assessment are required that have the ability to feed DNT AOPs within a potential DNT IATA for regulatory decisions (Bal-Price et al. 2015b). Such assays will preferably be based on human cells as the prediction of animals for humans is in many cases insufficient (Leist and Hartung 2013). The Neurosphere Assay, covering neurodevelopmental processes during early fetal development, could be part of such a strategy. In addition, assays are needed including earlier developmental time-points as well as later neurodevelopmental processes (Fig. 5).

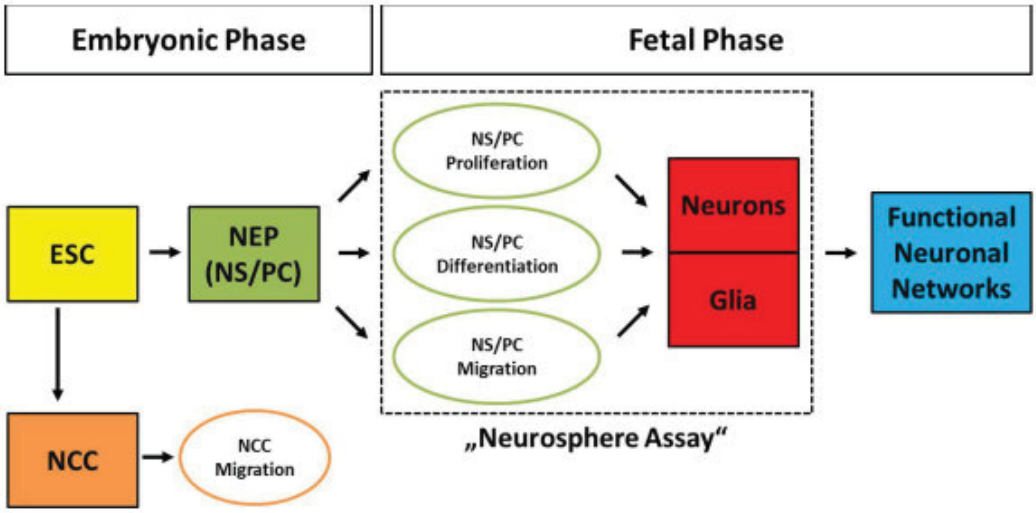

Fig. 5: DNT *in vitro* testing strategy: Endpoints obtained by the Neurosphere Assay covering the early fetal development are integrated into assays comprising endpoints of the embryonic phase like neural induction from e.g. human induced pluripotent stem cells (hiPSCs) to hiPSC-derived neuroepithelial precursors (NEP), neural crest cell (NCC) generation and migration. The addition of functional networks will further complete the neurodevelopmental key events (Baumann et al. 2015).

Such a modulatory testing strategy is necessary due to the spatiotemporal nature of developmental processes. Assays complementing the Neurosphere Assay could include human induced pluripotent stem cell (hiPSC)-based tests like neural induction from hiPSC to hiPSC-derived neuroepithelial precursors (NEP), neural crest cell (NCC) generation and migration, neuronal network and synapse formation as well as neuronal subtype specification (Fig. 5; Baumann et al. 2015). Since we demonstrated earlier that the Neurosphere Assay is capable of automated neurosphere sorting and plating (Gassmann et al. 2012), medium throughput screening of compounds for DNT seems feasible utilizing automated imaging techniques like HCA for evaluation of such *in vitro* assays. Such a testing strategy enables compound priorization or generates data, which serve for AOP-building (Ankley et al. 2010; Bal-Price et al. 2015b). The ultimate goal will be the integration into AOP-informed IATA (Tollefsen et al. 2014) for DNT.

1.4. High Content Image Analysis (HCA)

Besides a suitable *in vitro* system novel techniques like HCA are required within the new testing paradigm in toxicology to assess the relevant endpoints in a medium to high throughput manner. HCA describes the process of extracting high levels of information from images of *in vitro* or *in vivo* samples utilizing a combination of automated microscopy and automated image analysis. In recent years development of complex cellular imaging tools has driven the development of HCA applications. Within the field of DNT HCA applications have been established for a wide spectrum of endpoints, including NPC proliferation, neuronal differentiation, neuronal maturation and cell migration. Especially the group around William R. Mundy and Timothy Schafer from the US-Environmental Protection Agency (US-EPA) investigated this topic within the ToxCast program. One HCA application, developed by this group assesses proliferation and viability of the ReNcell CX neural progenitor cell line (Breier et al. 2008 ; see Fig. 6 1). This application is based on a dual staining for 4',6-diamidino-2-phenylindole (DAPI) for nucleus staining and either propidium iodide (PI) as a viability or bromodeoxyuridine (BrdU) as a proliferation marker. Within the DAPI channel (Fig. 6 1A) the assay detects nuclei as single particles fulfilling predefined shape and area constraints, utilizing a watershed algorithm (Thermo_Fisher_Scientific 2010b). Identified nuclei are marked with dark blue circles (Fig. 6 1B). The obtained nucleus mask is enlarged to account for the cell soma area, which is slightly larger than the identified nucleus and is applied on the second fluorescence channel (Fig. 6 1E). Within this mask the intensity values originating of the staining of either PI or BrdU is determined. When the value lies above a certain threshold the cell nuclei is defined as positive (Fig. 6 1E,F indicated by the white arrows) allowing to determine the ratio of viable/dead cells and proliferating cells.

Neuronal differentiation and neuronal maturation are analyzed utilizing the Neuronal Profiling bio-application developed by Thermo Fisher (Thermo_Fisher_Scientific 2010a) which proved its value in many studies covering a wide spectrum of *in vitro* systems (Harrill et al. 2010, 2011a; Radio and Mundy 2008; Radio et al. 2010). This application is used to quantify neurons and to assess their morphology (see Fig. 6 2). The application is based on a dual staining using DAPI/Hoechst33342 for the nucleus and e.g. βIII-tubulin to stain the cytoskeleton of neurons. In the Hoechst33342 channel cell nuclei are identified using a watershed algorithm executed on a fixed thresholded nucleus image (Fig. 6 2A,D; Thermo_Fisher_Scientific 2010a). In the βIII-tubulin channel a ring is placed at a certain distance around the nucleus and the intensity of the βIII-tubulin staining is quantified within this ring (Thermo_Fisher_Scientific 2010a; Fig. 6 2E). If the intensity values are above a certain threshold the nucleus is assigned to a neuron and starting from the identified soma of the neuron the neurite tracing is performed using a skeletonization algorithm (Fig. 6 2F; Thermo_Fisher_Scientific 2010a).

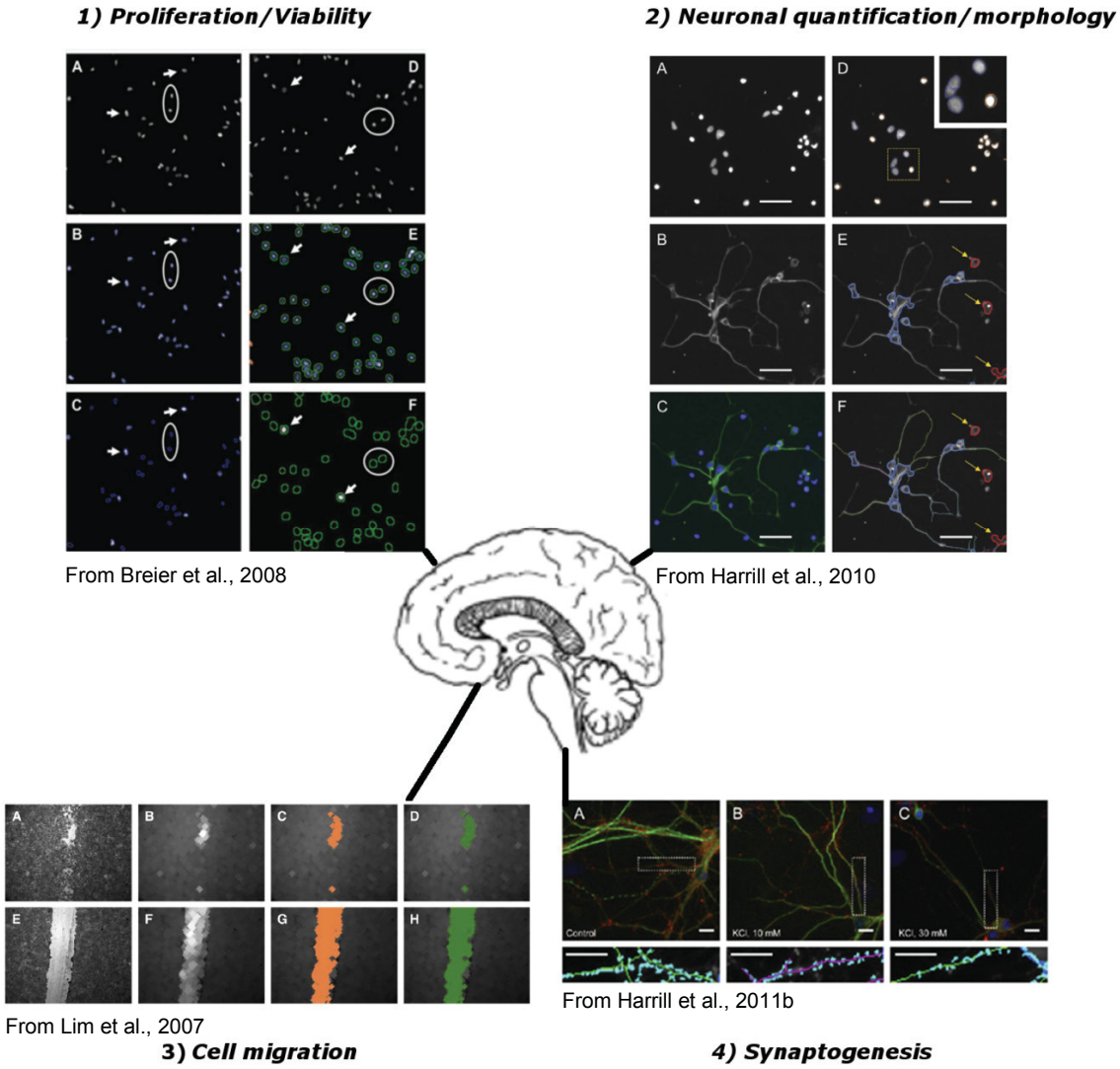

Fig. 6: HCA applications for relevant endpoints of brain development: 1) Proliferation and viability can be assessed via a dual staining of cell nuclei for Hoechst33342/DAPI and either PI for cell viability or BrdU for cell proliferation. A) The upper box shows a representative fluorescence image of cell nuclei and (B,C) the nuclei identification. Panel D shows the respective fluorescence image for BrdU staining and E-F the evaluation mask. White arrows indicate positive cells (Breier et al. 2008). 2) Panel A and B show representative images for Hoechst33342/DAPI and βIII-tubulin fluorescence images and C the overlay of both channels. The panels D-F display the evaluation mask. Identified cell nuclei are indicated by dark blue circles, neuron cell bodies by light blue circles and neurites as colored lines (Harrill et al. 2010). 3) Panel E shows the transmission image of day 0 after introduction of the scratch and panel E the respective image at day 5. Transmission images were preprocessed (Panel B,F) using a morphology filter and thresholded (Panel C,G). The thresholded images were further processed by image morphometry analysis (Panel D,H) to extract the area information (Lim et al. 2007). 4) The upper panel shows fluorescence images of MAP2 and synapsin stained untreated (A) and KCl treated (B,C) cortical neurons. The lower panel shows representative magnifications and the evaluation mask of identified neurites (lines) and identified synapses (blue dots; Harrill et al. 2011b).

The Neuronal Profiling bio-application can be expanded to also quantify the number of synapses (Fig. 6 4) on neurites allowing to study the influence of substances on synaptogenesis (Harrill et al. 2011b). This work nicely demonstrates the advantage of assessing multiple endpoints at the same time without increasing the sample size. The assessment of synapse formation adds an indirect endpoint for assessment of neuronal network function to the endpoints neuronal quantification and neuronal morphology.

Astrocyte migration is currently studied in so-called scratch assays (Fig. 6 3), in which an artificial scratch is introduced into a cell layer and the time is measured which is required to

close the resulting gap (Lim et al. 2007). While this is an adequate assay to describe the process of wound healing it fails to mimic the process of guided cell migration important for brain development. In contrast, neurospheres display radial migration out of the neurosphere, which can be easily quantified by measuring migration distances of the cells out of the neurosphere core (Moors et al. 2007).

Although relevant DNT endpoints can be studied using HCA algorithms many studies lack analyses of a multiple set of endpoints at the same time. This is due to the fact, that none of the above-described *in vitro* cell culture models is able to mimic a larger variety of DNT-relevant endpoints. However, analyzing multiple *in vitro* systems enlarges the set of required samples and therefore will lower the throughput and increase the costs. Furthermore, both, the species (Culbreth et al. 2012; Harrill et al. 2011a; Mundy et al. 2010) and the type of cell (normal versus tumor cell; Wilson et al. 2014) can significantly alter the outcome of substance screenings. Because identification of the most sensitive endpoint across time and neurodevelopmental processes is necessary to determine Lowest Observable Adverse Effect Concentrations (LOAECs) for DNT, it is desirable to study as many endpoints as possible in one *in vitro* system. In this regard NPCs grown as neurospheres are a promising 3D *in vitro* system, because they are able to mimic multiple DNT endpoints *in vitro* (see Fig. 4). However, safety and efficacy testing of chemicals with 3D neurospheres by employing HCA requires advanced scanning and evaluation processes which is due to characteristic features of the culture: 1) a 3D sphere core, which leads to unfocused images, 2) a variable cell density within the migration area, 3) a heterogonous cell population of neurons and glia cells and 4) neurosphere-specific endpoints. Available applications were so far exclusively developed for conventional two-dimensional (2D) cell cultures with adjusted cell densities which allow appropriate object discrimination (Dragunow 2008; Harrill et al. 2010). Therefore, existing algorithms have to be re-validated for their capability to quantify neurons and to assess their morphology in high-density, heterogeneous *in vitro* systems or novel algorithms have to be developed to deal with this challenge. In order to assess endpoints involving the spatial distribution of cells within the entire well like cell migration and cell type distributions, novel algorithms have to be designed which operate on image montages covering complete wells.

1.5. *In silico* methods and fingerprint libraries

An essential part of the Integrated Approaches to Testing and Assessment (IATA) are the integration of *in silico* methods, which on the one hand gather existing information for SAR (structure–activity relationship)-based read-across approaches and on the other hand serve as models to predict MIEs or KEs (Tollefsen et al. 2014). However, although SAR-based

read across approaches are already widely used, a framework is required to transparently reveal the degree of uncertainty of this models (OECD 2014; Patlewicz et al. 2013). To tackle this challenge the European Chemicals Agency (ECHA) is currently establishing the read across assessment framework (RAAF), which characterizes the uncertainty of SAR-based read-across approaches (ECHA 2012). The SAR-based read-across is also referred to as the so-called tiered surrogate approach, which was published by the US-EPA to serve for priorization of substances for further testing and to disclose the MOAs. Substance priorization is achieved with the SAR approach, which links the effect of a substance on animal, human or environment to its molecular structure (Wang et al. 2012). This is mostly done by using either structurally identical molecules with altered functional groups in order to investigate altered toxicological effects within this group (Tong et al. 2003) or by using legacy data in combination with software algorithms providing quantitative assessment (similarity scores) for identifying and ranking potential structural analogs (Wu et al. 2010). This second approach is called the tiered surrogate approach, which is highly dependent on the available data set. Fig. 7 shows a general scheme of the tiered surrogate approach, which can be used as a decision tree. In case toxicity data from animal studies or epidemiological data for the chemical itself or for one of its moieties are known, a direct concentration-response assessment is performed assessing e.g. the no/lowest observed adverse effect level (NOAEL/LOAEL). If such data doesn't exist, a literature review is conducted to identify breakdown compounds or metabolites of the parent compound originated from biological or chemical transformation, which have known toxic properties. In case toxicity data are available for these breakdown compounds or metabolites, these data are used for the parent compound. If there is no data available either, the surrogate approach starts by searching for three categories of surrogates considering similar structure, metabolism and toxicity-like. While structure-related surrogates can be extracted from databases, the identification of metabolic surrogates requires knowledge on metabolites and kinetic precursors of the chemical of concern. The third type of surrogate, toxicity-like, is mostly found for chemical mixtures with known toxicity equivalent factor (TEF) or relative potency factor (RPF) for one index chemical and the rest of the mixture. These chemicals are mostly structurally similar and present comparable concentration-response curves (examples are dioxins, furans and PCBs (US-EPA 2000)). From the identified surrogates, only those with repeated dose toxicity values are considered and their physiochemical properties are gathered. In the next step all potential surrogates are pooled and it is checked for similarities among those like structure, toxic effect, endpoint specificity, biodegradation products, environmental fate and transport. Consequently, the unknown chemical is classified by computational models for potential organ endpoints, MOA and toxic effects and is compared with the data from the identified surrogates.

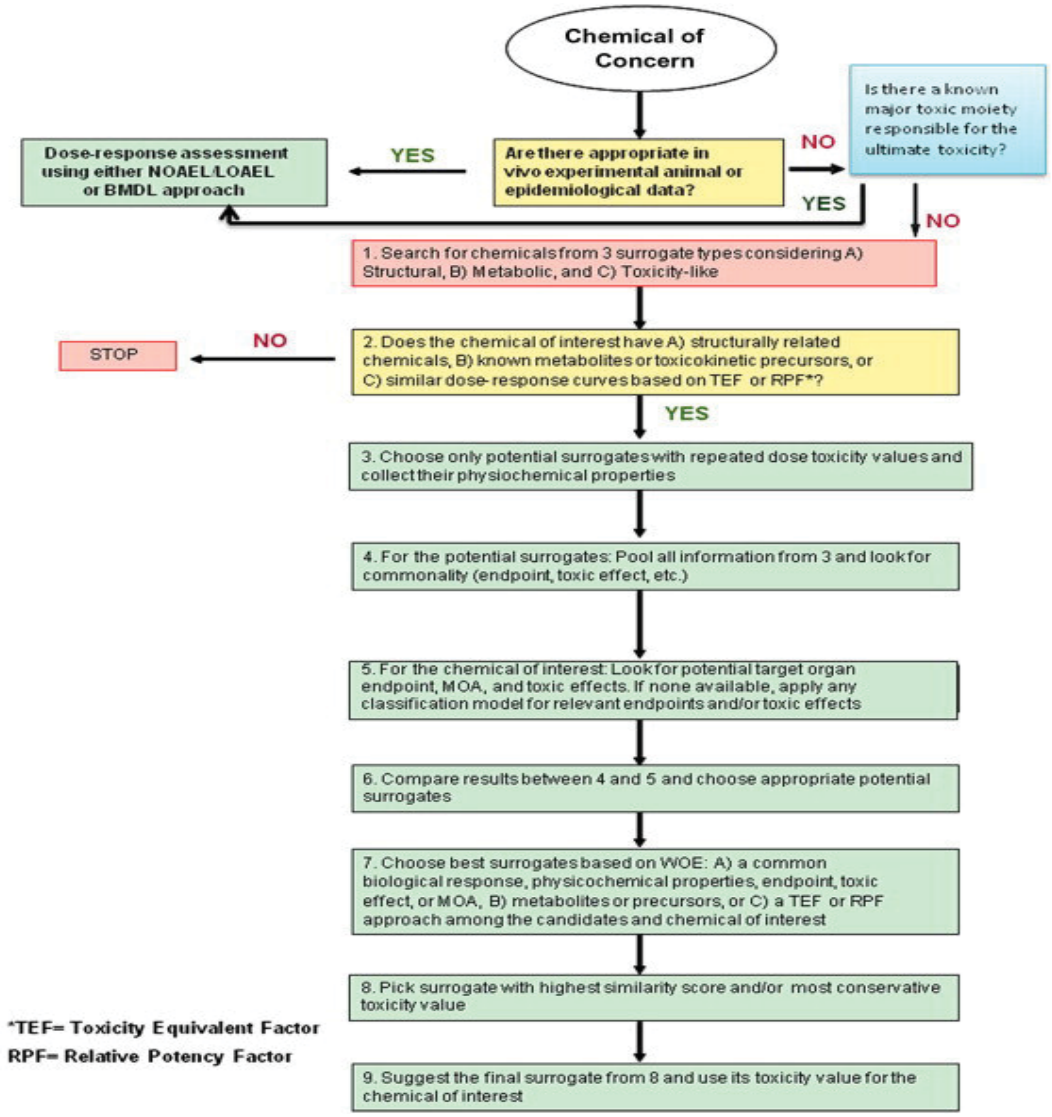

Fig. 7: Tiered surrogate approach. This SAR-based read across approach published by the EPA serves to identify toxicity surrogates for human health risk assessment. Within the tiered surrogate approach, toxicity data for unknown chemicals are assessed by using the data of the most similar available surrogate. This approach is based on similarity scores between the chemical of concern and potential surrogates. This similarities comprise structure, metabolism and toxicity-like (Wang et al. 2012).

In a further step a weight-of-evidence approach (WOA) is applied to filter potential surrogates. Potential surrogates are again compared with the chemical of concern but this time pointing the focus to toxicological similarity over structural similarity. From the remaining surrogates, the one with the highest similarity score is taken and toxicity data are used to classify the chemical of concern. Since this approach crucially relies on a sufficient number of potential surrogates (Wang et al. 2012), another approach is the phenotypic screening approach, in which a set of test chemicals with known MOA is used to create a fingerprint library by assessing as many relevant endpoints as possible from different *in vitro* systems.

Therefore a specific fingerprint can be attributed to one or more MOAs and allows to disclose the MOA of untested chemicals (Kleinstreuer et al. 2014). This, in line with the proposed paradigm shift in toxicology to priorize chemicals for further substance testing and

to cluster chemicals with comparable patterns to facilitate the surrogate approach in terms of available toxicity data (Collins et al. 2008).

1.6. Objectives of the thesis:

Chemical testing according to the current guidelines facilitating animal experiments is extremely time- and cost-intensive. Therefore in Tox21 a paradigm shift was proposed towards more *in vitro* based chemical testing in combination with novel technologies such as HCA. Regulatory agencies only demand DNT testing for substances that exert neurotoxic or endocrine disruption potential (EU, USA) or are registered as pesticides (USA) resulting in an immense data gap in the field of DNT with only 12 known DNT substances. Therefore HCA DNT screening utilizing *in vitro* systems is highly desirable. In order to reflect the *in vivo* situation as precisely as possible the use of complex 3D cell cultures was proposed by many studies which makes the neurosphere system a promising candidate for DNT testing. The overall aim of the thesis was to implement automated HCA workflows allowing a medium throughput safety and efficacy screening of substances in the Neurosphere Assay.

Therefore the objectives of this thesis were:

1) Establishment of protocols for sample preparation and image acquisition: Suitable single and multi cell-type staining protocols in 96 well plates have to be developed for all cell types present within the migration area of the neurosphere (neurons, oligodendrocytes and astrocytes). Furthermore image acquistion protocols utilizing the ArrayScan VTI have to be established.

2) Development of a novel software approach for a medium throughput HCA safety and efficacy screening: The software has to be able to identify neurons even in high density heterogeneous cell populations and to assess their morphology with high accuracy and precision. Additionally novel algorithms should be developed to assess neurosphere-specific endpoints like radial migration and neuronal density distributions.

3) Development of software to assess NPC distribution *in vivo*: Correct neuronal distribution within cortical layers is an essential process during brain development and therefore a direct comparison between *in vitro* and *in vivo* is highly desirable. Therefore the task was to develop a software which semi-automatically assesses NPC distributions, NPC numbers and cortical layer morphology in rat brain cortical tissue sections.

2. Manuscripts

The manuscripts emerged from this thesis are included below. The first manuscript (2.1) 'Omnisphero: A novel computational approach for high content image analyses (HCA) of organoid neurosphere cultures *in vitro* describes our self-developed software 'Omnisphero', which enables an automatic assessment of relevant endpoints of the Neurosphere Assay. Those comprise classical endpoints assessible also in 2D cell cultures like neuronal quantification and morphological analyses as well as neurosphere-specific endpoints involving the spatial distribution of cells within the entire well like radial migration and neuronal density distributions. The manuscript contains a detailed description of the software as well as a validation of the algorithms using three model substances with known effects on NPCs: EGF, methylmercury-chloride (MeHgCl) and acrylamide. Omnisphero's algorithms perform with comparable precision than manual evaluations for neuronal quantification as well as for neurosphere-specific endpoints like radial cell migration. Furthermore, Omnisphero added a so for not accessible endpoint, the neuronal density distribution, to the portfolio of endpoints within the Neurosphere Assay. The neuronal density distribution describes the spatial distribution of neurons within the migration area. Since endpoints like cell migration and cell distributions are crucial mechanisms for correct cortex layer development, our second publication (2.2: Automatic counting and positioning of 5-bromo-2-deoxyuridine (BrdU) positive cells in cortical layers of rat brain slices) describes the software BrdeLuxe, which assesses $BrdU^+$ cell distribution *in vivo*. BrdeLuxe is designed to quantify the total number of $BrdU^+$ cells, their density and their distribution among cortical layers as well as to describe cortical layer morphology by measuring layer area and thickness. This article describes the software and its advantages in terms of accuracy and evaluation time versus existing methods by comparison with a manual ground truth evaluation. Both software approaches were used for our third manuscript (2.3: Developmental Neurotoxicity of Epigallocatechin Gallate (EGCG) Is Triggered by Interference with β1-Integrin Function in Human Neural Progenitor Cells). In this article Omnisphero, described in manuscript 2.1, was used to quantify neurons and oligodendrocytes after different NPC differentiation times (1-5 days) in Epigallocatechin Gallate (EGCG)-exposed neurospheres. In addition, Omnisphero's algorithms assessed the EGCG-induced characteristic arborized migration phenotype by evaluating the homogeneity of the migration area as well as the average nucleus density. This altered NPC migration *in vitro* was compared to the *in vivo* situation utilizing BrdeLuxe to assess $BrdU^+$ cell distribution in EGCG treated rat brain slices.

2.1. 'Omnisphero: A novel computational approach for high content image analyses (HCA) of organoid neurosphere cultures *in vitro*

M. Schmuck*, T. Temme*, D. de Boer, A. Mosig, E. Fritsche

* Shared first authors

BIOINFORMATICS (submitted 10.11.2015)

Motivation: Ein kürzlicher Paradigmenwechsel in der Toxikologie empfiehlt die Nutzung von *in vitro* Systemen in Kombination mit "High Content" Bildanalyse (HCA)-techniken, um die Kosten zu senken, den Durchsatz zu erhöhen und die Prädiktivität für die humane Gefahrenabschätzung zu verbessern. Im Bereich der Entwicklungsneurotoxizität (ENT) stellen neurale Progenitorzellen (NPCs), die zu Neurosphären aggregieren ein geeignetes *in vitro* System dar, da sie einige wichtige Prozesse der fetalen Gehirnentwicklung, wie Migration und Differenzierung von NPCs, nachahmen. HCA von solchen 3D *in vitro* Systemen schafft neue Herausforderungen für automatische Auswertungen, da diese über ein variable Zelldichte, inkonsistente z-Ebenen und eine heterogene Zellpopulation verfügen.

Ergebnisse: In unserer Software Omnisphero setzen wir computergestützte Methoden ein, welche multiple Endpunkte des "Neurosphären Assays" mit einer vergleichbaren Präzision wie die manuelle Auswertung erfassen. Für die neuronale Quantifizierung erreicht Omnisphero eine Detektionsfähigkeit von 83,8% (DP) und eine Falscherkennungsrate (FPR) von 11% und übertrifft damit existente Ansätze, deren DP bei einer FPR über 50%, die 50%, nicht übersteigt. Die hohe FPR der existenten Ansätze führt zu inkorrekten Messungen der neuronalen Morphologie, die mit einer Überinterpretation von Chemikalieneffekten einhergehen. Omnisphero beinhaltet neue Algorithmen, um "Neurosphären-spezifische" Endpunkte wie radiale Migration und neuronale Dichteverteilungen innerhalb der Migrationsfläche zu analysieren. Weiterhin ermöglicht eine den Anwender unterstützende Parameteroptimierung, dass Omnisphero auch von nicht erfahren Endnutzern verwendet werden kann.

Verfügbarkeit: Die Open Source Software (unter der GPLv3 Lizenz) ist unter folgende Adresse zusammen mit Beispieldaten erhältlich: https://www.omnisphero.com.

10-Nov-2015

Dear Mr. Schmuck:

A manuscript titled Omnisphero: A novel computational approach for high content image analyses (HCA) of organoid neurosphere cultures in vitro (BIOINF-2015-1868) has been submitted by Mr. Martin Schmuck to the Bioinformatics.

You are listed as a co-author for this manuscript. The online peer-review system, ScholarOne Manuscripts, automatically creates a user account for you. Your USER ID and PASSWORD for your account is as follows:

Site URL: https://mc.manuscriptcentral.com/bioinformatics
USER ID: Martin.Schmuck@IUF-Duesseldorf.de
PASSWORD:
To enter your account, please do the following:

1. Go to: https://mc.manuscriptcentral.com/bioinformatics
2. Log in using this information:

Your USER ID is Martin.Schmuck@IUF-Duesseldorf.de Your case-sensitive PASSWORD is x2mk9cff

You can use the above USER ID and PASSWORD to log in to the site and check the status of papers you have authored/co-authored. This password is case-sensitive and temporary. Please log in to https://mc.manuscriptcentral.com/bioinformatics to update your account information and change your password.

Thank you for your participation.

Sincerely,
Bioinformatics

BIOINFORMATICS

Vol. 00 no. 00 2015
Pages 1–8

Omnisphero: A novel computational approach for high content image analyses (HCA) of organoid neurosphere cultures *in vitro*

Martin R. Schmuck [a,†], Thomas Temme [b,†], Denise de Boer [a], Axel Mosig [b,*], Ellen Fritsche [a,*]

[a] IUF - Leibniz Research Institute for Environmental Medicine, Auf'm Hennekamp 50, 40225 Düsseldorf, Germany
[b] Ruhr-University Bochum, Department of Biophysics, ND04/596, Universitätsstr. 150, 44780 Bochum, Germany
* to whom correspondence should be addressed
† The authors wish it to be known that, in their opinion, the first two authors should be regarded as Joint First Authors.

Received on XXXXX; revised on XXXXX; accepted on XXXXX

Associate Editor: XXXXXXX

ABSTRACT

Motivation: A recent paradigm shift in toxicology proposes the use of 3D *in vitro* systems in combination with high content image analysis (HCA) techniques to lower the cost, increase the throughput and enhance the predictivity for human hazard identification. In the field of developmental neurotoxicity (DNT), neural progenitor cells (NPCs) grown as neurospheres are such an *in vitro* system since they mimic several basic processes of brain development including neural progenitor cell migration and differentiation. HCA of such 3D *in vitro* systems creates new challenges for automated evaluations because they encompass variable cell densities, inconsistent z-layers and heterogeneous cell populations.

Results: We propose computational methods implemented in our *Omnisphero* software which assesses multiple endpoints of the 'Neurosphere Assay' and achieve precision comparable to manual evaluation. For neuronal identification *Omnisphero* reaches a detection power (DP) of 83.8% and a false positive rate (FPR) of 11%, thus largely improving the results obtained by an existing approach whose DP does not exceed 50% at an FPR above 50%. The high FPR of existing approaches results in incorrect measurements of neuronal morphological features accompanied by an overestimation of compound effects. *Omnisphero* additionally includes novel algorithms to assess 'neurosphere-specific' endpoints like radial migration and neuronal density distribution across the migration area. Furthermore, a user-assisted parameter optimization procedure makes *Omnisphero* accessible to non-expert end users.

Availability: Open source software (under the GPLv3 license) is available at https://www.omnisphero.com along with sample data.[1]

Contact: Ellen.Fritsche@IUF-Duesseldorf.de, Axel.Mosig@bph.rub.de

Supplementary information: Supplementary data are available at Bioinformatics online.

[1] For review purposes the software and the sourcecode can be downloaded from www.omnisphero.com/download/Omnisphero.zip

1 INTRODUCTION

In recent years, computational approaches for high content image analysis (HCA) have substantially supported and driven the development of high-throughput microscopy assays (Giuliano *et al.*, 2003; Starkuviene and Pepperkok, 2007). Such HCA methods entered the field of developmental neurotoxicity (DNT) testing to implement complex two-dimensional (2D) and three-dimensional (3D) cellular models for compound screening (Breier *et al.*, 2010; Dragunow, 2008) since testing for DNT according to the current guidelines is highly time- and cost-intensive (Bal-Price *et al.*, 2012). While most DNT approaches for HCA are designed for conventional (2D) mono-cell type cultures (Radio and Mundy, 2008; Breier *et al.*, 2008; Harrill *et al.*, 2010, 2011a,b, 2013; Wilson *et al.*, 2014), only few image analysis approaches exist for more complex heterogeneous 2D (Anderl *et al.*, 2009) and none for 3D cultures. However, HCA of 3D cell cultures have the potential to become fundamental tools for risk assessment since they reflect the *in vivo* tissue architecture more precisely than 2D cultures (Pampaloni *et al.*, 2007; Alépée *et al.*, 2014). The complex spatial organization of 3D cell culture assays and the presence of different cell types creates new challenges for computational image analysis.

The 'Neurosphere Assay'. For DNT testing *in vitro*, the 'Neurosphere Assay' is a promising module of an envisioned testing strategy (Baumann *et al.*, 2015) (Fig. 1*a,e*). It is based on 3D primary human neural progenitor cell (hNPC) clusters, which mimic several neurodevelopmental endpoints including migration as well as differentiation into neurons, astrocytes and oligodendrocytes *in vitro* (Moors *et al.*, 2009; Baumann *et al.*, 2014). Exposure of neurosphere cultures towards test compounds allows to assess disturbances of these processes (Moors *et al.*, 2007, 2009; Gassmann *et al.*, 2010; Schreiber *et al.*, 2010; Baumann *et al.*, 2015). When HCA is used to measure such neurosphere endpoints, advanced scanning and data analysis procedures are required because the neurospheres' 3D structure results in assay-specific challenges. First, neurospheres contain a 3D neurosphere-core, which, if not corrected for, leads

to unfocused images. Second, the density of cells within the migration area of a neurosphere is highly variable. Third, neurospheres consist of a heterogonous cell population of neurons and glia cells, and finally, they involve sphere-specific endpoints like radial glia migration and neuronal migration. For higher throughput of chemical testing, HCA algorithms are needed to tackle these challenges and evaluate those endpoints with a high accuracy and precision.

Neuronal morphology and motility in DNT assays. Automated quantification of neuronal counts and neuronal morphology in conventional 2D neuronal cultures are well-established and were shown to achieve a precision comparable to manual quantification by human experts (Ramm *et al.*, 2003). However, most studies rely on adjusting cell densities in the samples to facilitate object discrimination (Harrill *et al.*, 2010; Dragunow, 2008). In the neurosphere model, cell density cannot be adjusted. Thus, new and existing algorithms require re-evaluation for their applicability to quantify relevant cellular parameters of such complex, mixed cultures. In addition, new algorithms are needed to cover endpoints originating from the spatial distribution of cells within the entire well.

Overview of Contributions. We propose a novel computational approach for quantifying features of neurospheres that are relevant for DNT testing. Our approach relies on novel methods for the identification of the classical endpoints like neuron counting and characterization of their morphology as well as novel algorithms to assess endpoints like radial migration and neuronal density distributions, which originate from the morphology of the 'Neurosphere Assay'. Compared to existing approaches for neuron identification, our approach is based on analyzing morphology by explicitly identifying the major morphological constituents, in particular the length and number of neurites as well as potential branching points of neurites. To validate our method, we assessed its accuracy and sensitivity with respect to an extensive manual ground truth annotation, and compared results to the *Neuronal Profiling bioapplication V4.1 (NPBA)* module of the *vHCS-Scan (build 6585)* software. Our approach is implemented and made available in the *Omnisphero* software, which facilitates analysis of the full spectrum of endpoints of the complex organoid neurosphere system. *Omnisphero* is accessible to non-expert end users through a graphical user interface (GUI) and an automated parameter optimization. While our main target is to facilitate automated high-throughput DNT assays, our image analysis approaches may also be applied in other 3D *in vitro* systems such as in the migration assay of tumor spheroids (Vinci *et al.*, 2013).

2 METHODS

2.1 Sample preparation

Neurospheres were incubated with either epidermal growth factor (EGF), acrylamide or methylmercurychloride (MeHgCl) for 5 days under differentiating conditions with subsequent cell viability monitoring, immunostainging, and image acquisition (see Supplement 1). For each compound four individual experiments with three technical replicates were conducted.

2.2 Image preprocessing

Preprocessing. 16-bit microscopic images of complete microtiter well plates were generated for the nuclei channel (Hoechst 33258) and the neuron channel (βIII-tubulin) utilizing the ArrayScan VTI (Thermo Fisher Scientific) and the *vHCS Scan software (build 6585)*. Images were recorded in tiles, which were subsequently stitched to obtain a *whole-neurosphere image* which displays a complete well of a 96-well plate (Fig. 1*e*).

Identification of nuclei and neuronal cell bodies. Coordinates of nuclei were identified as centroid coordinates in the whole-neurosphere images using two different approaches. In the first approach, the nuclei channel was binarized using the isodata approach (Ball and Hall, 1965). These binarized images were watershed transformed, and nuclei coordinates identified as the centroids of all segments satisfying suitable size constraints (Fig. 1*f*). A second approach for nuclei identification was introduced for the sake of comparability with existing approaches. Here, nuclei centroids were identified using the *Spot Detector bioapplication*. Obtained nuclei coordinates from the *Spot Detector bioapplication* were used for further identification of neuron cell bodies by both *Omnisphero* (see Section 2.3) and the *NPBA* to compare obtained neuron coordinates of the two automated methods. Obtained coordinates are transferred to the whole-neurosphere images.

Neurosphere-core removal. The neurosphere-core is defined as the area with the highest intensity and cell density in the image. As detailed in Supplement 2.1, this area is determined by converting the image into a thresholded intensity matrix in which the neurosphere-core is identified as the largest connected component. The identified area is masked out from the image for further evaluations.

Skeletonization. For the neuron channel, the morphological skeleton S_N of every connected component N in the neuron binary channel is computed using a refined version of the approach from Wang *et al.* (2013) based on the method proposed by Bai *et al.* (2007) (see Fig. 1*h* and Supplement 2.2).

2.3 Determining standard analysis endpoints.

Automated quantification of neurons. We consider a nucleus as a candidate for a neuronal nucleus if there is a closed connected component in the overlay of the binarized neuron image and the binarized nucleus image, and if the nucleus is uniquely assigned to one skeleton S_N. A corresponding component in the nucleus channel is considered further as a neuron nucleus candidate if the size of the overlap component exceeds a predefined threshold (Fig. 1*g*). Those candidates are investigated further by the *Neuron Tracer* algorithm which utilizes the skeletonization results (Fig. 1*i*). A neuron nucleus candidate associated with a skeleton S_N is rejected if length or roundness of the skeleton falls below a user defined threshold. Furthermore, areas with low signal-to-noise ratio in the neuron channel are disregarded. Neuron nuclei candidates located on the remaining skeletons S_N are counted as neuron nuclei. Whenever no neuron nucleus candidate is associated to a skeleton, the nearest neighbor nucleus at the endpoints can be assigned if it is located within a certain distance and angle to an endpoint. The parameters involved in these steps are determined using an automated parameter optimization (Section 2.5).

Validation. As validation measures, we determined the numbers of true positives (TPs) and false positives (FPs) as identified by an automated algorithm compared to a manual ground truth annotation. Furthermore, we determined the detection power (DP) and false-positve rate (FPR), i.e., the ratio between TPs or FPs and the total number of cells annotated in the ground truth annotation. All validation measurements were derived from four independent experiments with three technical replicates per experiment. In order to obtain ground truth for validating the automated quantification, *Omnisphero* provides the user with a manual counting tool to quantify neurons. User-defined coordinates are saved in a separate matrix and serve for a one by one comparison of neuronal coordinates with an automated evaluation.

Neuronal morphology. Neuronal morphology is characterized on the single cell level through four features normalized per neuron, namely the total length of neurites, the average length of neurites, the number of branching

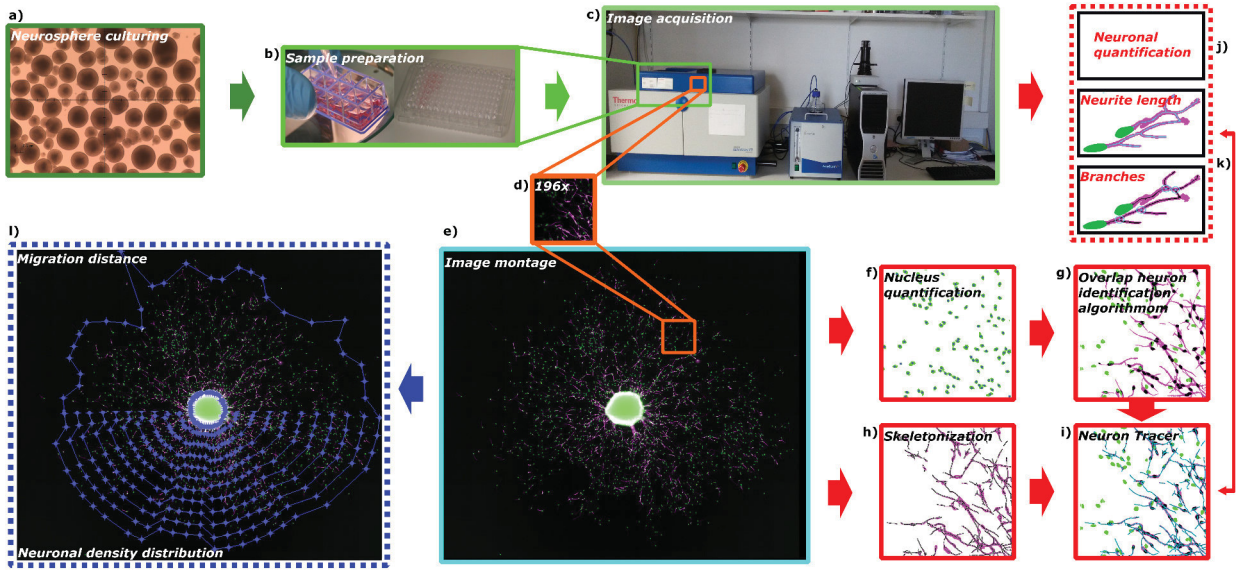

Fig. 1. ***Omnisphero*** **workflow.** Neurospheres *(a)* were plated on PDL/laminin coated multiwell- plates *(b)* and incubated with either acrylamide, MeHgCl or EGF over 5 days. *c)* Afterwards cells were fixed, stained and whole wells (196 images per well of a 96 well plate) were imaged (nuclei channel (green), neuron channel (magenta)) using the ArrayScan VTI (Thermo Fischer). The in build *NPBA* analyzes images for neuronal quantification *(j)* and neuronal morphology *(k)*. *e) Omnisphero* combines all 196 image tiles *(d)* to one large image montage. The complete image montage is binarized and binary nucleus images are used for nucleus quantification using a watershed algorithm *(f)*. Connected components in the overlap of the binarized nucleus channel and the binarized neuron channel are used for identifying neuron candidates *(g)*. The binary neuron image is further processed with a skeletonization algorithm *(h)*. *i)* Shows the final *Neuron Tracer* algorithm which uses the skeletons from *(h)* to verify the neuronal positions determined by the overlap neuron identification algorithm *(g)* and to assess neuronal morphology *(k)*. *l)* Beside these classical endpoints it is also possible to assess radial migration distance and neuronal density distributions utilizing spatial information of image montage.

points, and the number of neurites. In order to measure only morphological properties of the neurites, the cell soma has to be excluded. The soma of hNPCs can be considered equivalent to the area of the neuron nuclei. Therefore, all vertices covered by a nucleus N are not considered part of the respective skeleton S_N, resulting in a new set of subskeletons representing the neurites. Corresponding neurites whose lengths did not exceed 12 pixels were discarded. Whenever no nucleus would overlap a skeleton S_N, the nucleus with the shortest euclidean distance was connected to the skeleton as long as the distance did not exceed 20 pixels. Data are stored in a relational database (Supplement 3).

2.4 Determining extended analysis endpoints.

Migration area and migration distance. The average migration distance is defined as the distance between the boundary of the neurosphere core (Section 2.2) and the furthest migrated cells. It is computed by subdividing the image into 64 wedges centered at the centroid coordinate of the neurosphere-core C (Section 2.2). The migration area is then obtained by measuring the distance between the boundary of the neurosphere-core and the outmost cells for all wedges (see Supplement 4.1 and Fig. 1*l*).

Neuronal density distribution. The neuronal density distribution is assessed by subdividing the migration area into ten rings with equal width. Within each ring, the ratio of neurons to cell nuclei is calculated and normalized to the average ratio within the entire migration area, resulting in a distance dependent density function (Supplement 4.2).

2.5 Automated Parameter Optimization

The different analysis steps of our approach involve five major parameters: *(i)* the threshold for binarizing the neuron image; *(ii)* the threshold for binarizing the nucleus image; *(iii)* the minimum overlap between connected components in the two binary images for treating one nucleus as neuron; *(iv)* the minimum distance for connected components between the binarized neuron and nucleus channel for identifying neurons; and *(v)* the threshold for identifying and eliminating low signal-to-noise areas in the neuron channel. To avoid the obvious difficulty to adjust five parameters manually, we followed the idea pioneered by Held *et al.* (2011) and implemented an approach that uses a small annotated reference data set to optimize these parameters. For details, we refer to Supplement 5.

2.6 Statistical Analysis

Statistics were performed using Graphpad Prism v6 (La Jolla, California). Dose response curves for viability, neuronal quantification, neuronal morphology, migration distance and neuronal density distributions were obtained from four independent experiments with three technical replicates per condition. The raw values for viability (CTB: fluorescence signal) of each technical replicate within one plate were corrected by subtraction of a background control (containing only media and CTB reagent), averaged and normalized to the mean of the untreated controls (differentiation medium for acrylamide and EGF and 0.015% DMSO in differentiation medium for MeHgCl). Data were further analyzed as % of control and are presented as percent of control±SEM (standard error of the mean). Neuronal quantification, morphology and migration distance raw values (% of neurons as number neurons/number of nuclei, neurite length in μm, number of branching points and migration distance in μm) were averaged for all technical replicates within one plate. The resulting mean values were averaged among the four individual experiments. Data are presented as mean±SEM. For dose response curves EC_{50}-values (Neubig *et al.*, 2003) were determined by using a sigmoidal dose-response (variable slope) fit with values of untreated neurospheres as upper constraint and zero as lower constraint. For the neuronal density distributions the average slopes of the four independent experiments

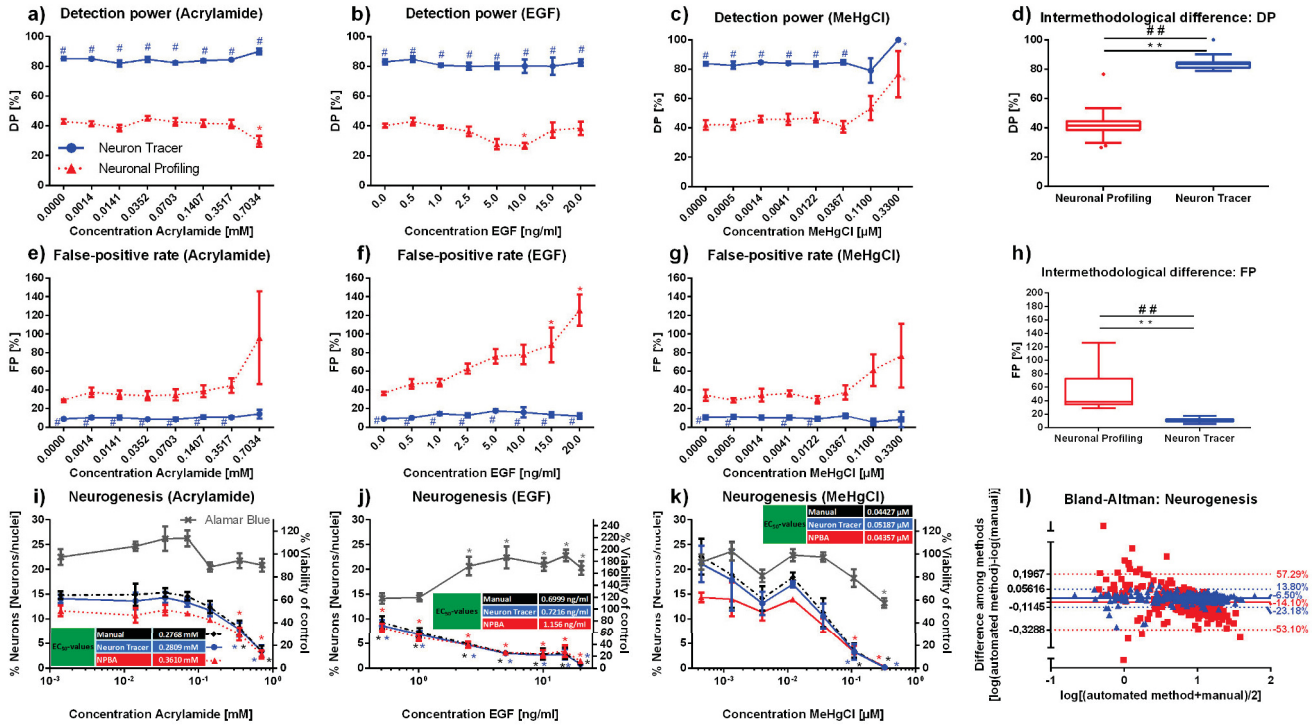

Fig. 2. Methodological comparison of neuronal quantification. *a-c)* DP of the *NPBA*, the *Neuron Tracer* algorithm and manual evaluation for acrylamide, EGF and MeHgCl. *e-g)* Corresponding FPR for all methods. *d)* Box blot representation of combined DP data of *a-c)* and *h)* respective box blot representation of FPR of *e-g)*. *i-k)* Dose response curves for neurogenesis and viability and respective EC_50-values. *l)* Bland-Altman diagram for comparison of manual evaluation versus automated evaluation. Data is plotted as average against differences of log transformed raw values. Bias are shown as continuous line and confidence intervals as dotted lines and are given as % values. Results are obtained from four independent experiments with three technical replicates per concentration and are presented as mean±SEM. Significant differences among one method are indicated as * and intermethodological significant differences as #. Significant differences of the mean in the box blot representation are indicated as ** and difference in the variance as ##.

were determined using a nonlinear fit (straight line). Results are shown as mean±SEM. Significant differences within one method were analyzed using the analysis of variance (ANOVA) with a *post hoc* Sidak test ($p<0.05$). Inter-methodological differences were analyzed using a multiple t-test assuming non consistent standard deviations and the Holm-Sidak-method for determining the statistical significance ($\alpha<0.05$). For Box-Plot diagrams the Tukey representation was chosen. Differences between two groups were calculated using unpaired t-test and F-test for comparison of variances. Bland-Altman diagrams were plotted as average against differences of automated methods and manual evaluation using raw values of each single well of all experiments. Raw values were transformed to logarithmic scale. Bias and 95% confidence intervals were retransformed to normal scale resulting in % values.

3 RESULTS

3.1 Methodological comparison: Neurogenesis.

The *Omnisphero Neuron Tracer* algorithm exhibits a significantly higher DP, lower FPR and a lower variance for those values among the full concentration range of the three model-substances compared to the *NPBA* (Fig. 2*a-h*). The quality of automated methods was evaluated by comparing automatically obtained neuron coordinates with manually annotated ground truth neuron coordinates. Comparison between automated and manual evaluation of neuron cell body coordinates revealed an average DP of 83.8% for our *Omnisphero Neuron Tracer* algorithm compared to 41.9% for the existing approach implemented in *NPBA*. The average FPR of our *Neuron Tracer* algorithm is 11.0%, and thus much lower than the 52.1% FPR of *NPBA*. Average DP and variation of both automated methods are represented as box-plot diagrams in Fig. 2*d*, and corresponding data for FPR in Fig. 2*h* respectively. Statistical analyses revealed a significant difference between the mean values of the automated methods for both DP and FPR (Fig. 2*d,h*). Variances between methods were compared using the F-test. The *Neuron Tracer* algorithm shows a significantly lower variance compared to the *NPBA*, revealing a much higher robustness of this method. The highest variance is found for the FPR of the *NPBA* especially for high concentrations indicated by the non symetric box plot in Fig. 2*h*. Comparison of concentration-response curves for % of neurons and calculated EC_{50} values obtained by automated methods and manual evaluation revealed no statistically significant inter-methodological differences (Fig. 2*i-k*). EC_{50} values are consistently higher for *NPBA* compared to manual and *Neuron Tracer* evaluation. Significant effects of tested substances on neurogenesis observed by automated and manual evaluations correspond to each other (acrylamide: 0.35 mM for all methods; EGF: 0.5 ng/ml for all methods; MeHgCl: 0.11 μM for all methods). Bland-Altman diagrams revealed a high accordance between manual and *Neuron Tracer* evaluation (Fig. 2*l*). The *NPBA* shows a proportional error overestimating values for high and

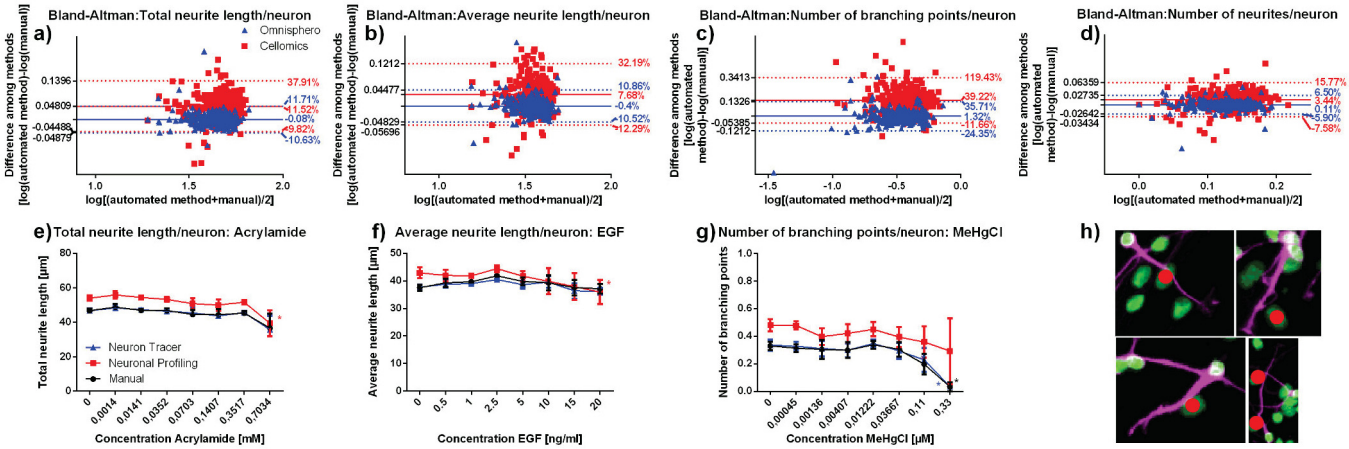

Fig. 3. Neuronal morphology. Bland-Altman-diagrams of combined data of all three model substances for total neurite length *a)*, average neurite length *b)*, number of branching points *c)* and number of neurites *d)* for comparison of the two automated evaluations versus manual evaluation. Examples of dose response curves for total neurite length *e)*, average neurite length *f)* and number of branching points *g)*. *h)* Representative images of FPs identified by *NPBA* visualized with the GUI of *Omnisphero* are indicated as red dots. Results are obtained from four independent experiments with three technical replicates per concentration and are presented as mean±SEM. Significant differences among one method are indicated as *. Bland-Altman-diagrams are plotted as average against differences of log transformed raw values. Bias are shown as continuous lines and confidence intervals as dotted lines and are given as % values.

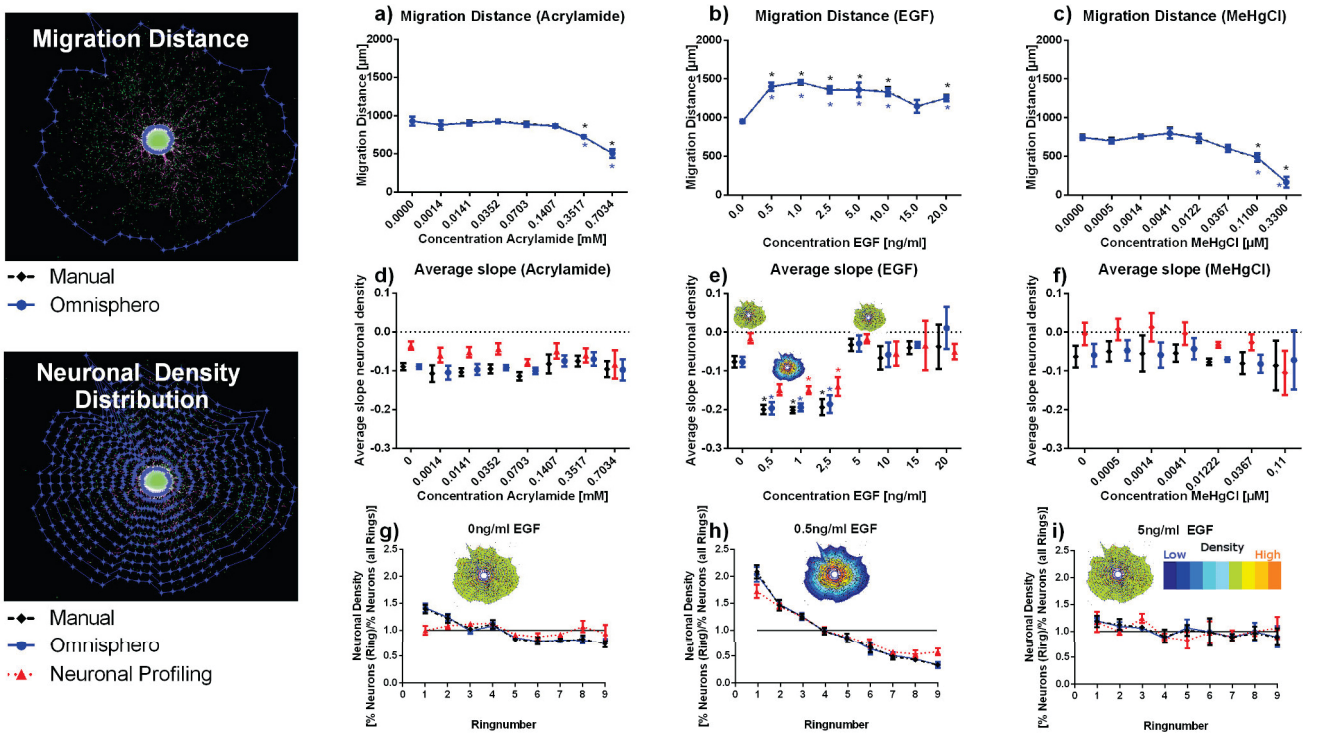

Fig. 4. Migration distance and neuronal density distributions. *a-c)* Migration distance obtained by manual and automated measurements of *Omnisphero* for the three model substances. *d-f)* Average slope of each neuronal density function obtained by manual evaluation, *Omnisphero* and *NPBA* for all three model substances and all concentrations. *g)* Neuronal density graphs of untreated samples and *h,i)* EGF treated samples (0.5 ng/ml and 5 ng/ml EGF). *g,i)* Equal distributions are indicated as homogeneous green colored migration areas and *h)* altered density distributions as color coded migration areas. Results are obtained from four independent experiments with three technical replicates per condition and are shown as mean±SEM. Significant differences among one method are indicated as *.

underestimating values for low concentrations resulting in a wide 95% confidence interval (from 57.3 to -53.1%).

3.2 Methodological comparison: Neurite outgrowth

In order to compare different methods, total neurite length, average neurite length, number of branching points and number of neurites were determined using the same skeletonization-based approach (see Section 2.2) for coordinates obtained by automated methods and by manual evaluation. Differences within the results can therefore be attributed to differences in identified neuron coordinates of the different methods. The manual evaluation was taken as the gold standard to study inter-methodological comparisons using the Bland-Altman representation. The *Omnisphero Neuron Tracer* showed the lowest bias and the lowest range of the 95% confidence interval among automated methods indicating the highest accordance towards manual evaluation (Fig. 3*a-d*). The *NPBA* tends to overestimate the morphological features which becomes most obvious for the number of branching points. This can be seen in Fig. 3*c* as well as in Fig. 3*g* where values determined using the coordinates identified by *NPBA* are between 25-30% higher compared to the manual evaluation. Calculation of the bias which is always positive for *NPBA* reveals a systematic error of the method. This systematic error leading to the overestimation of effects persists for average neurite length and total neurite length Fig. 3*a,b,e,f*, but not for the number of neurites Fig. 3*d*. Concentration-response curves for all endpoints and substances are shown in Supplementary Fig. S.6.

3.3 Novel endpoints: Migration distance and neuronal density distribution

Both manual evaluation and *Omnisphero* reveal an increase of migration distance upon EGF treatment, and a concentration-dependent decrease in migration distance induced by acrylamide and MeHgCl with no significant difference between methods (Fig. 4*a-c*). Average slope neuronal density distribution graphs showed no significant difference between manual evaluation, *Omnisphero* and *NPBA* (Fig. 4*d-f*). Untreated neurospheres showed a close to ideal equal distribution of neurons for all distances (Fig. 4*g*). Treatment with acrylamide and MeHgCl did not influence this neuronal density distribution at any concentrations indicated by a stable slope (Fig. 4*d,f*). Low concentrations of EGF (0.5 -2.5 ng/ml, Fig. 4*h*), however, significantly alter the neuronal density distribution. Under these concentrations the density of neurons was higher in the vicinity of the neurosphere-core and decreased with increasing distance. This effect disappears at higher concentrations (Fig. 4*i*).

4 DISCUSSION

In order to assess the relevance of the results obtained by our newly introduced approach for HCA-based DNT assays, two questions are of major concern: (i) how robust the new approach is to deliver reliable assessments of DNT screenings involving a large number of substances, and (ii) how the results acquired with the novel methods compare to existing approaches. This will finally allow to assess the suitability of a fully-automated HCA of neurosphere cultures as an assay for DNT testing.

Robustness of neuronal quantification. The recognition of neurons by *Omnisphero* clearly exceeds *NPBA* with a DP of 83.8% (compared to 41.9% by *NPBA*) and a FPR of 11% (compared to 52.1%). Remarkably, the performance of *Omnisphero* remains constant or improves compared to *NPBA* over the full range of concentrations for all substances. The FPR of *NPBA* increases significantly with increasing concentrations (Fig. 2*e-g*). The overall higher variability of *NPBA* shown in the Box-Plot diagram in Fig. 2*d,h* will narrow down the size of effects detectable with this approach. Besides this quantitative analysis of DP and FPR, the GUI of *Omnisphero* also facilitates to qualitatively assess the reliability of an automated method by displaying the neuron coordinates. In particular, it is possible to specifically display the coordinates of all unidentified or falsely identified neurons. We utilized this feature to identify potential subpopulations of cells not detectable or falsely detected by a specific algorithm in order to spot systematic errors of this algorithm. In fact, we identified a systematic error for *NPBA* which tends to assign glial nuclei as neuronal when passed by a neurite (see Fig. 3*h*). This can be explained by the algorithm used by *NPBA*, which identifies neurons by measuring relative overlap between the neuron fluorescence channel and a ring placed around the identified nucleus. Neurites crossing a non-neuronal nucleus will produce a corresponding overlap, so that areas with a high neuron density are particularly prone to produce false positive neurons. In contrast, the approach in *Omnisphero* is based on a combination of overlap criteria and a skeletonization, which prevents this particularly frequent source of false positive neurons as identified by the *NPBA*. Overall, our results strongly indicate that the quantification of neuronal features by *Omnisphero* is highly robust, and far exceeds the robustness of existing approaches, which can be explained by using morphological skeletonizations in addition to overlap criteria as a basis for quantification.

Assessment of classical endpoints and extended analysis endpoints. To validate the algorithms of *Omnisphero* for substance screening we treated neurospheres over 5 days with three model substances with described effects on endpoints of the 'Neurosphere Assay': Acrylamide (Park *et al.*, 2010), EGF (Ayuso-Sacido *et al.*, 2010) and MeHgCl (Moors *et al.*, 2009; Baumann *et al.*, 2015; Lewandowski *et al.*, 2003). All substances are expected to decrease neurogenesis in a concentration-dependent manner, yet by different mechanisms: inducing NPC apoptosis as well as general neurotoxicity (Erkekoglu and Baydar, 2014) in the case of acrylamide (Park *et al.*, 2010) and inhibiting neuronal differentiation by EGF (Ayuso-Sacido *et al.*, 2010) and MeHgCl (Baumann *et al.*, 2015). Concentration-response curves for all three substances were compared between manual evaluation and automated methods. All methods delivered comparable curve shapes with significant effects starting at 0.35 mM for Acrylamide, 0.5 ng/ml for EGF and 0.11 μM for MeHgCl (Fig. 2*i-k*). Calculated EC_{50}-values revealed no statistically significant difference between methods, but were always higher for *NPBA* (Fig. 2*i-k*). In order to figure out the reason for this overestimation we created Bland-Altman diagrams (Fig. 2*l*), demonstrating a proportional error of *NPBA*, leading to an overestimation of high concentrations and an underestimation for low concentrations. The overestimation of the percentages of neurons for high concentrations in the concentration-response curves is attributed to the high FPR of the *NPBA* (Fig. 2*h*). The underestimation for low concentrations is more likely attributed to the low DP of the *NPBA*. Since

high concentrations decrease the number of neurons to below 1% of the control value, even high FPR alterations will not significantly alter the curve fitting for determining the EC_{50} value. In contrast, the underestimation for low concentrations can play a more crucial role, especially when concentration-response curves display a slight slope. In such a case, the underestimation for low concentrations could result in missing of low concentration effects resulting in significantly higher EC_{50} values. Besides neuronal quantification we evaluated neuronal morphology on the single cell level after 5 days of differentiation in the same samples: total neurite length, average neurite length, number of branching points and number of neurites (Fig. 3*a-g*). MeHgCl reduced neurite outgrowth in rat, but not in human embryonic stem cell-derived neuronal cultures at non-cytotoxic concentrations (Harrill *et al.*, 2011a; Radio and Mundy, 2008). In line with these results, we observed that MeHgCl effected neuronal morphology of human NPC-derived neurons only for the highest concentration of MeHgCl tested (0.33 μM, Fig. 3*g*), which exceeds the concentration reducing neurogenesis (0.11 μM) and decreased cell viability (Fig. 2*k*). So far nothing is known for EGFs ability to interfere with neuronal morphology. Since EGF inhibits neuronal differentiation (Ayuso-Sacido *et al.*, 2010), we expected an EGF-induced delayed neuronal maturation possibly resulting in reduction of neurite outgrowth and branching. Indeed, we observed a reduction of total and average neurite length, number of branching points and a significant decrease of neurite number upon EGF exposure (Supplementary Fig. S.6) at concentrations not reducing viability (Fig. 2*j*). The effects of acrylamide on neuron morphology of developing neurons are, to the best of our knowledge, not known. Acrylamide's mode of actions are associated with three mechanisms suspected to induce neurite degeneration in fully differentiated neurons: inhibition of kinesin-based fast axonal transport, alteration of neurotransmitter levels, and direct inhibition of neurotransmission (Erkekoglu and Baydar, 2014). Since 5 days differentiated neurons from hNPC are relatively immature, acrylamide effects on neurite outgrowth are expected to be limited. This is in line with the automated and manual results: only the *NPBA* detects effects in total neurite length (Fig. 3*e*) for the highest acrylamide concentration applied, while the number of neurons was significantly reduced at a subcytotoxic concentration of 0.354 mM (Fig. 2*i*). However, one limitation of assessing neurite outgrowth is the dynamic range of values (Harrill *et al.*, 2011a), which for developing neurons in the neurosphere system (50-60 μm) is much lower compared to e.g. primary cortical cultures (129.8$\pm$12.6 μm). Therefore, small compound effects on this endpoint cannot be distinguished from *in vitro* model variability. Comparison of the evaluation performances for endpoints concerning neuronal morphology revealed similar curve shapes for manual and automated methods (Supplementary Fig. S.6). While curves of manual evaluation and of the *Omnisphero* algorithm correspond very precisely, the curve of *NPBA* indicates an overestimation of total neurite length (Fig. 3*a,e*), average neurite length (Fig. 3*b,f*) and, most notably, for the number of branching points (Fig. 3*c,g*). In order to identify a potential systematic error, we again generated Bland-Altman-diagrams (Fig. 3*a-d*), revealing a systematic error for *NPBA* as well as a higher variability compared to the *Neuron Tracer*. The *NPBA* algorithm overestimates the number of branching points by up to 39.2% (Fig. 3*c*). This overestimation effect tends to result in an artificially high sensitivity of *NPBA* for adverse outcomes. This is demonstrated by *NPBA* detecting significant effects of EGF on average neurite (Fig. 3*f*) and of acrylamide on total neurite length (Fig. 3*e*), which are not confirmed by either manual evaluation or the other algorithms. These significant effects on neuronal morphology originate from the higher measures of the control values (Fig. 3*e,f*). Additionally, the higher overall variability of *NPBA* leads to the loss of significant results for the total number of branching points in the case of MeHgCl (Fig. 3*g*). All model substances interfere with cell migration *in vitro* and/or *in vivo*. MeHgCl decreases migration *in vitro* and *in vivo*, acrylamide disturbs migration *in vivo* (Ogawa *et al.*, 2011; Kakita *et al.*, 2002) and EGF induces cellular migration *in vitro* and *in vivo* (Ayuso-Sacido *et al.*, 2010; Puehringer *et al.*, 2013). Both, manual and automatic evaluations of radial migration detected either concentration-dependent increases (EGF) or decreases (acrylamide, MeHgCl) for radial migration with no detectable inter-methodological differences (Fig. 4*a-c*). The last endpoint evaluated was the neuronal density distribution, which provides the unique opportunity of measuring specific neuronal migration *in vitro* and is, to the best of our knowledge, the first time assessed in a 3D *in vitro* system. Untreated neurospheres display a close to ideal equal distribution of neurons migrating on the glia scaffold (Baumann *et al.*, 2014) (Fig. 4*g*). MeHgCl did not alter neuronal migration by any applied concentration (Fig. 4*f*). Because MeHgCl interferes with SH-groups of proteins (Bernhoft, 2012) our data indicates that glial cell migration might be more sensitive to MeHgCl exposure (Fig. 4*c*) than neuronal migration itself. However, so far the precise molecular mechanisms behind neuronal migration disturbances in MeHgCl-exposed humans are not clarified (Kakita *et al.*, 2002), but based on our data there is room to speculate that disturbances of neuronal migration due to migrational defects of the glial scaffold might be involved. Acrylamide is also suspected to alter migration resulting in a distorted distribution of neurons (Ogawa *et al.*, 2011). Comparable to MeHgCl, acrylamide decreased the overall migration distance without specific effects on neuron positioning (Fig. 4*a,d*) pointing towards a non-neuron-specific effect on migration. In contrast to the other substances, EGF is reported to induce neuronal migration *in vivo* and *in vitro* [(Ayuso-Sacido *et al.*, 2010; Puehringer *et al.*, 2013); 20 ng/ml]. In the 'Neurosphere Assay', increased neuronal migration will manifest in a higher neuronal density towards the periphery of the migration area than close to the neurosphere-core, while inhibition of neuronal migration will accumulate neurons in areas close to the neurosphere-core. Very low concentrations of EGF (0.5-2.5 ng/ml) caused the latter with gathering in the central migration areas (Fig. 4*h*). Increasing EGF concentrations up to 20 ng/ml restored equal distribution of neurons across the migration area (Fig. 4*i*). Because all EGF concentrations enhanced the total radial migration distance (Fig. 4*b*), the restoration of equal neuronal distribution at higher EGF concentrations is actually only possible by increased neuronal migration. Thus, our HCA allows evaluation of migration of specific cell types in this mixed culture 3D system.

Automated parameter optimization. Investigation of different training set sizes in the automated parameter optimization of *Omnisphero* revealed that a manual evaluation time of roughly one hour delivers comparable precise results for parameter settings than those obtained by experts (manual: DP=82.4%; FP=11.8%; Quality Index (QI, defined in Supplement 5)=70.6% and reduced optimized: DP=81.0%; FP=13.8%; QI=67.2%). Manual validation times of few hours are reasonable if one considers that parameters among experiments remain comparable with the exception of the threshold

values which are related to different staining qualities. Therefore, parameters for a given time point, in our case 5 days of differentiation, within a given *in vitro* system, in our case hNPCs, can be assessed with a manual time expense of roughly 1 hour. This procedure, however, has to be readjusted when altering experimental setups or changing the *in vitro* system. A further reduction in manual annotation time can be accomplished by only using control or low-concentration spots for annotation, which, however, comes at the cost of slightly less accurate quantifications (see Supplement 5).

5 CONCLUSION

Our novel approach implemented in the *Omnisphero* software facilitates a highly robust HCA-based assay contributing to DNT *in vitro* testing. *Omnisphero* assesses effects of three model substances in the 'Neurosphere Assay', and achieves an accuracy and precision that is comparable to manual evaluation. In contrast to existing software, *Omnisphero* is also capable of analyzing spatial distribution of cells within the entire well including endpoints like radial migration and neuronal density distributions, which is of high relevance especially for 3D *in vitro* systems. Migration endpoints can be transferred to other 3D cell systems such as tumor spheroids, where radial migration is a measure for invasiveness (Vinci *et al.*, 2013). Furthermore, through automated parameter optimization, *Omnisphero* is highly automated and thus suitable for users without data analysis or programming experience in studies involving large numbers of experiments.

ACKNOWLEDGEMENT

Funding: This project was funded by the DFG through the research training group 1033 and by the German Ministry for Education and Research (16V0899).

REFERENCES

Alépée, N., *et al.* (2014). State-of-the-Art of 3D Cultures (Organs-on-a-Chip) in Safety Testing and Pathophysiology. *Altex*, **31**(4), 441–477.

Anderl, J. L., *et al.* (2009). A neuronal and astrocyte co-culture assay for high content analysis of neurotoxicity. *Journal of visualized experiments : JoVE*, (27), 1–6.

Ayuso-Sacido, A., *et al.* (2010). Activated EGFR signaling increases proliferation, survival,and migration and blocks neuronal differentiation in post-natal neural stem cells. *Journal of Neuro-Oncology*, **97**(3), 323–337.

Bai, X., *et al.* (2007). Skeleton pruning by contour partitioning with discrete curve evolution. *IEEE Transactions on Pattern Analysis and Machine Intelligence*, **29**(3), 449–462.

Bal-Price, A. K., *et al.* (2012). Advancing the Science of Developmental Neurotoxicity (DNT): Testing for Better Safety Evaluation. *ALTEX*, **29**(2), 202–15.

Ball, G. H. and Hall, D. J. (1965). ISODATA, A novel method of data analysis and pattern classification. *Stanford Research Institute, Menlo Park,United States. Office of Naval Research. Information Sciences Branch*.

Baumann, J., *et al.* (2014). Comparative human and rat "neurosphere assay" for developmental neurotoxicity testing. *Current protocols in toxicology*, **59**, 12.21.1–12.21.24.

Baumann, J., *et al.* (2015). Comparative human and rat neurospheres reveal species differences in chemical effects on neurodevelopmental key events. *Archives of Toxicology*.

Bernhoft, R. A. (2012). Mercury toxicity and treatment: a review of the literature. *Journal of environmental and public health*, **2012**, 460508.

Breier, J. M., *et al.* (2008). Development of a high-throughput screening assay for chemical effects on proliferation and viability of immortalized human neural progenitor cells. *Toxicological sciences*, **105**(1), 119–33.

Breier, J. M., *et al.* (2010). Neural progenitor cells as models for high-throughput screens of developmental neurotoxicity: state of the science. *Neurotoxicology and teratology*, **32**(1), 4–15.

Dragunow, M. (2008). High-content analysis in neuroscience. *Nature reviews. Neuroscience*, **9**(10), 779–88.

Erkekoglu, P. and Baydar, T. (2014). Acrylamide neurotoxicity. *Nutritional neuroscience*, **17**(2), 49–57.

Gassmann, K., *et al.* (2010). Species-specific differential AhR expression protects human neural progenitor cells against developmental neurotoxicity of PAHs. *Environmental health perspectives*, **118**(11), 1571–7.

Giuliano, K. a., *et al.* (2003). Advances in high content screening for drug discovery. *Assay and drug development technologies*, **1**(4), 565–577.

Harrill, J. a., *et al.* (2010). Quantitative assessment of neurite outgrowth in human embryonic stem cell-derived hN2 cells using automated high-content image analysis. *Neurotoxicology*, **31**(3), 277–90.

Harrill, J. a., *et al.* (2011a). Comparative sensitivity of human and rat neural cultures to chemical-induced inhibition of neurite outgrowth. *Toxicology and applied pharmacology*, **256**(3), 268–80.

Harrill, J. A., *et al.* (2011b). Use of high content image analysis to detect chemical-induced changes in synaptogenesis in vitro. *Toxicology in vitro*, **25**(1), 368–87.

Harrill, J. A., *et al.* (2013). Use of high content image analyses to detect chemical-mediated effects on neurite sub-populations in primary rat cortical neurons. *Neurotoxicology*, **34**, 61–73.

Held, C., *et al.* (2011). Comparison of parameter-adapted segmentation methods for fluorescence micrographs. *Cytometry Part A*, **79**(11), 933–945.

Kakita, A., *et al.* (2002). Neuronal migration disturbance and consequent cytoarchitecture in the cerebral cortex following transplacental administration of methylmercury. *Acta neuropathologica*, **104**(4), 409–417.

Lewandowski, T. a., *et al.* (2003). Effect of methylmercury on midbrain cell proliferation during organogenesis: Potential cross-species differences and implications for risk assessment. *Toxicological Sciences*, **75**(1), 124–133.

Moors, M., *et al.* (2007). ERK-dependent and -independent pathways trigger human neural progenitor cell migration. *Toxicology and applied pharmacology*, **221**(1), 57–67.

Moors, M., *et al.* (2009). Human neurospheres as three-dimensional cellular systems for developmental neurotoxicity testing. *Environmental health perspectives*, **117**(7), 1131–8.

Neubig, R. R., *et al.* (2003). International union of pharmacology committee on receptor nomenclature and drug classification. xxxviii. update on terms and symbols in quantitative pharmacology. *Pharmacological Reviews*, **55**(4), 597–606.

Ogawa, B., *et al.* (2011). Disruptive neuronal development by acrylamide in the hippocampal dentate hilus after developmental exposure in rats. *Archives of Toxicology*, **85**(8), 987–994.

Pampaloni, F., *et al.* (2007). The third dimension bridges the gap between cell culture and live tissue. *Nature reviews. Molecular cell biology*, **8**(10), 839–845.

Park, H. R., *et al.* (2010). Acrylamide induces cell death in neural progenitor cells and impairs hippocampal neurogenesis. *Toxicology letters*, **193**(1), 86–93.

Puehringer, D., *et al.* (2013). EGF transactivation of Trk receptors regulates the migration of newborn cortical neurons. *Nature neuroscience*, **16**(4), 407–15.

Radio, N. M. and Mundy, W. R. (2008). Developmental neurotoxicity testing in vitro: models for assessing chemical effects on neurite outgrowth. *Neurotoxicology*, **29**(3), 361–76.

Ramm, P., *et al.* (2003). Automated screening of neurite outgrowth. *Journal of biomolecular screening*, **8**(1), 7–18.

Schreiber, T., *et al.* (2010). Polybrominated diphenyl ethers induce developmental neurotoxicity in a human in vitro model: evidence for endocrine disruption. *Environmental health perspectives*, **118**(4), 572–8.

Starkuviene, V. and Pepperkok, R. (2007). The potential of high-content high-throughput microscopy in drug discovery. *British journal of pharmacology*, **152**(1), 62–71.

Vinci, M., *et al.* (2013). Tumor Spheroid-Based Migration Assays for Evaluation of Therapeutic Agents. *Target Identification and Validation in Drug Discovery*, **986**, 253–266.

Wang, C., *et al.* (2013). An image skeletonization-based tool for pollen tube morphology analysis and phenotyping. *Journal of integrative plant biology*, **55**(2), 131–41.

Wilson, M. S., *et al.* (2014). Multiparametric High Content Analysis for assessment of neurotoxicity in differentiated neuronal cell lines and human embryonic stem cell-derived neurons. *Neurotoxicology*, **42**, 33–48.

Omnisphero: A novel computational approach for high content image analyses (HCA) of organoid neurosphere cultures *in vitro*.

Supplementary Material

Martin Schmuck, Thomas Temme, Denise de Boer, Axel Mosig, Ellen Fritsche

Supplement S.1 Sample preparation

Human neural progenitor cells (hNPC, Lonza, Verviers, Belgium) from gestational week 16-20 were grown as neurospheres (Baumann *et al.*, 2014) in proliferation medium consisting of Dulbeccos modified Eagle medium (Life Technologies GmbH, Darmstadt, Germany) and Hams F12 (3:1) (Life Technologies GmbH, Darmstadt, Germany) supplemented with 2% B27 (Life Technologies GmbH, Darmstadt, Germany), 20 ng/ml epidermal growth factor (EGF, Life Technologies GmbH, Darmstadt, Germany), 20 ng/ml recombinant human fibroblast growth factor (FGF, R&D Systems, Wiesbaden, Germany) and 1% penicillin and streptomycin (Pan-Biotech, Aidenbach, Germany). For differentiation one neurosphere with a diameter of 0.3 mm is centered to the middle of the well of a PDL/laminin (Sigma Aldrich, Munich, Germany) coated 96-well plate containing 100 μl of differentiation medium [DMEM (Life Technologies GmbH, Darmstadt, Germany), Hams F12 (Life Technologies GmbH, Darmstadt, Germany) 3:1 supplemented with 1% of N2 (Life Technologies GmbH, Darmstadt, Germany) and 1% penicillin and streptomycin (Pan-Biotech, Aidenbach, Germany)] containing the respective treatment. One experiment contains neurospheres treated with seven different concentrations of acrylamide (Sigma Aldrich, Munich, Germany), EGF (Life Technologies GmbH, Darmstadt, Germany) or MeHgCl (in 0.015% DMSO, Sigma Aldrich, Munich, Germany) and the respective solvent in triplicates. For each substance four independent experiments were conducted. Neurospheres were differentiated over 5 days with half media exchange after 3 days. For staining, neurospheres were fixed by adding 50 μl 12% w/v paraformaldehyde (PFA, Merck, Darmstadt, Germany) to the media in each well resulting in a total volume of 150 μl and a final PFA concentration of 4% w/v. Plates were incubated for 45 min at 37°C. The supernatant was removed and 100 μl of phosphate-buffered saline (PBS, Biochrom, Berlin, Germany) were added to each well. The supernatant was removed and 50 μl of primary antibody solution were added to each well, containing βIII-tubuline antibody (1:200, anti-β-tubulin III rabbit, # T2200-200UL, Sigma Aldrich, Munich, Germany), goat serum (10% Sigma Aldrich, Munich, Germany) and phosphate-buffered saline Triton X (PBS-T) (0.1%, Roth, Karlsruhe, Germany). Plates were incubated 1 hour at 37°C and the wells were washed thrice with 100 μl of PBS. The supernatant was removed and 50 μl of secondary antibody solution was added to each well, containing Hoechst (0.2 mg/ml; 1:50, Sigma Aldrich, Munich, Germany), Alexa 546 anti rabbit (1:200; Alexa Fluor 546 goat anti- rabbit IgG #A11010, Life Technologies GmbH, Darmstadt, Germany) in PBS. Plates were incubated 30 min at 37°C and wells were washed thrice with PBS. Each well was covered with 200 μl PBS and stored at 4°C in the dark.

Supplement S.2 Image Preprocessing

S.2.1 Neurosphere-core removal.

The boundary of the neurosphere-core is determined by subdividing the nucleus channel image into a grid of 89×89 squared subregions, each subregion containing 80×80 pixels. In each subregion, the intensity values I_i of all pixels are integrated, resulting

in the 89×89 density matrix D_I of the nucleus image. This matrix is binarized using a user-defined threshold. In this binarized matrix, the connected component γ involving the largest entry in D_I (i.e., the highest density area) is identified as the neurosphere-core. The resulting area associated with γ is masked out from the image, and the centroid of the this area is calculated as the center of the neurosphere-core $C = (x_C, y_C)$. In order to account for error sources originating from bright objects not corresponding to the neurosphere such as bright edges of the well boundary, only areas exceeding a certain distance from the boundary of the image are considered as neurosphere cores.

S.2.2 Skeletonization

In order to extract morphological features of the neurite outgrowth a *morphological skeleton* of the binarized neuron fluorescence channel was computed using the method of Bai *et al.* (2007). More precisely, for each connected component N of the thresholded neuron channel, one skeleton S_N is represented as a graph as follows. A vertex $w \in W$ is introduced for each branching point, i.e., a point belonging to S_N with three ore more neighbours in its 8-neighbourhood. Edges are identified by sequences of points, i.e., points with exactly two neighbours. Finally, endpoints are represented by vertices in S_N as points which have precisely one neighbour in the skeleton. The resulting skeletons are postprocessed as described earlier by Wang *et al.* (2013). By eliminating the branching points, we split each S_N into a set of subskeletons. All subskeletons shorter than 12 pixels are eliminated, and branching points seperated by less than 30 pixels are summarized to a single branching point located at the corresponding weight point of the two summarized branching points. Remaining subskeletons are reconnected on their endpoints ensuring that each new connection point has only two neighbours and no other skeleton lines are touched. This ensures that no artifical branching points are created. Whenever this was not possible without touching another skeleton line, the shortest euclidean distance is selected.

Supplement S.3 Neuronal Morphology

Neuronal morphology is assessed at the level of individual neuronal cells (Supplementary Fig. S.1). Each neuron is described by the number of neurites, the total length of neurites and the average length of neurites adjacent to one neuron nucleus as well as the number of branching points present in the adjacent neurites. The single cell features are averaged in one well for all identified neurons and are further averaged as the mean of triplicates containing the same treatment. In order to only extract morphological features of neurites the cell soma has to be excluded. The size of the soma of neurons derived from neural progenitor cells roughly equals the area of the cell nucleus of the neuron. Therefore, all positions covered by a neuron nucleus, represented by a vertex $v \in V$, are not considered part of the skeleton S_N, resulting in a new set of subskeletons Y representing the neurites. In some cases, a nucleus identified as a neuronal nucleus may not exhibit any overlap with the skeleton S_N. In such cases, the nucleus is connected to the skeleton with the shortest euclidean distance whenever this distance does not exceed 20 pixels. Before extracting the morphological characteristics, again

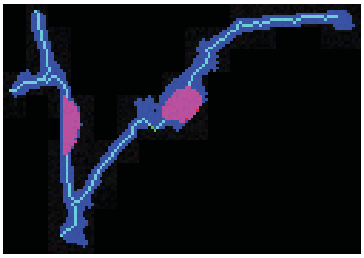

Supplementary Figure S.1. *Morphology of two individual neurons.* The post-processed neuronal morphology shows the two identified neuron nuclei (magenta areas) with three adjacent neurites (bright blue skeletons) and two branching points.

the method of Wang *et al.* (2013) is applied, to ensure that no new artifical branching points are created. The resulting morphological data describing the identified neurons and their neurite structure are exported to a relational Postgre SQL database. For an entity-relationship diagram, refer to Supplementary Fig. S.2, SQL statements for extracting neurite length, average neurite length, and numbers of neurites and branching points are provided in Supplementary Fig. S.3, S.4 and S.5, respectively. The resulting morphological features for total neurite length, average neurite length, number of branching points, and number of neurites for all methods and all model substances are exemplified in Supplementary Fig. S.6. The following morphological features are extracted:

- *Total neurite length/neuron.* The sum of the length of all subskeletons Y adjacent to one vertex v is averaged for all vertices in V resulting in the average total neurite length per neuron of one well.
- *Average neurite length/neuron.* The average length of all subskeletons Y adjacent to one vertex v is averaged for all vertices in V resulting in the average length of neurites per neuron of one well.
- *Neurite count/neuron.* The sum of the number of subskeletons Y connected to a vertex v is averaged for all vertices in V resulting in the average number of neurites per neuron of one well.
- *Total number of branching points/neuron.* The sum of elements w within all subskeletons Y connected to a vertex v is averaged for all vertices in V resulting in the average total number of branching points per neuron of one well.

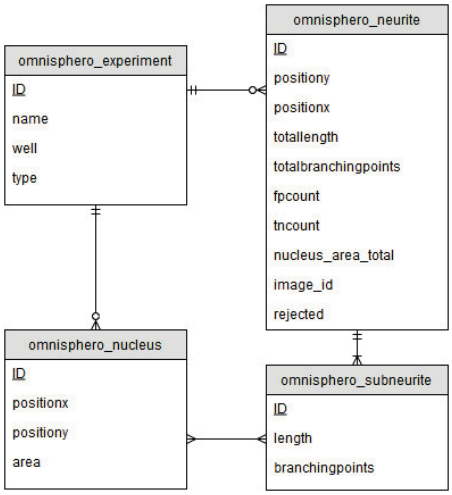

Supplementary Figure S.2. *Entity-relationship diagram of the database structure for representing neuronal morphology.* The database consists of four tables and a mapping table connecting neurites and nuclei. All identified neuron nuclei and morphological skeletons of one experiment are saved in the database. *Omnsiphero_neurite* comprises the morphological skeleton S_N and *omnisphero_subneurite* all neurites obtained by eliminating all vertices covered by a nucleus N from S_N. Neuron nuclei can be assigned to multiple neurites.

```
SELECT expname,typeid,wellname, avg(sublengthtotal) as
Total_Subneuritelength_PerNucleus FROM
(
  SELECT nuc.id,ex.name as expname,ex.well as wellname,ex.type as typeid,
  sum(sub.length) as sublengthtotal FROM OMNISPHERO_NUCLEUS nuc
  INNER JOIN OMNISPHERO_SUBNEURITE_NUCLEUS_MAPPING map ON
  map.nucleusid=nuc.id
  INNER JOIN OMNISPHERO_SUBNEURITE sub on sub.id = map.subneuriteid
  INNER JOIN OMNISPHERO_NEURITE neu on neu.id = sub.neuriteid
  INNER JOIN OMNISPHERO_EXPERIMENT ex ON neu.experiment_id = ex.id
  WHERE ((neu.totallength > 10 AND neu.totallength <= 100
  AND neu.totalbranchingpoints <3 )
  OR (neu.totallength > 100 AND neu.totallength <= 200
  AND neu.totalbranchingpoints <4 )
  OR (neu.totallength > 200 AND neu.totallength <= 300
  AND neu.totalbranchingpoints <4) OR (neu.totallength > 300
  AND neu.totallength <= 360 AND neu.totalbranchingpoints <5))
  AND sub.id not in(
    SELECT subid FROM
    (
       SELECT sub.id as subid, ex.name,ex.type,ex.well,
       count(distinct nuc.id) as distinctNuclei
       FROM OMNISPHERO_NUCLEUS nuc
       INNER JOIN OMNISPHERO_SUBNEURITE_NUCLEUS_MAPPING map
       ON map.nucleusid=nuc.id
       INNER JOIN OMNISPHERO_SUBNEURITE sub on sub.id = map.subneuriteid
       INNER JOIN OMNISPHERO_NEURITE neu ON sub.neuriteid=neu.id
       INNER JOIN OMNISPHERO_EXPERIMENT ex on neu.experiment_id = ex.id
       GROUP BY ex.name,ex.type, ex.well, sub.id order by sub.id asc
  ) as innerResult WHERE innerResult.distinctNuclei >= 3)
  GROUP BY nuc.id, ex.name, ex.well,ex.type
)
as mainneurite group by expname, wellname, typeid order by expname,
typeid, wellname
```

Supplementary Figure S.3. *SQL statement for extracting total neurite length per neuron.*

```
SELECT expname,typeid,wellname, avg(sublength) as
Average_Subneuritelength_PerNucleus FROM
  (SELECT nuc.id,ex.name as expname,ex.well as wellname,ex.type as typeid,
  avg(sub.length) as sublength FROM OMNISPHERO_NUCLEUS nuc
  INNER JOIN OMNISPHERO_SUBNEURITE_NUCLEUS_MAPPING map ON
  map.nucleusid=nuc.id
  INNER JOIN OMNISPHERO_SUBNEURITE sub on sub.id = map.subneuriteid
  INNER JOIN OMNISPHERO_NEURITE neu on neu.id = sub.neuriteid
  INNER JOIN OMNISPHERO_EXPERIMENT ex ON neu.experiment_id = ex.id
  WHERE ((neu.totallength > 10 AND neu.totallength <= 100
  AND neu.totalbranchingpoints <3 )
  OR (neu.totallength > 100 AND neu.totallength <= 200
  AND neu.totalbranchingpoints <4 )
  OR (neu.totallength > 200 AND neu.totallength <= 300
  AND neu.totalbranchingpoints <4)
  OR (neu.totallength > 300 AND neu.totallength <= 360
  AND neu.totalbranchingpoints <5))
  AND sub.id not in
    (SELECT subid FROM
      (SELECT sub.id as subid, ex.name,ex.type,ex.well,
      count(distinct nuc.id) as distinctNuclei FROM OMNISPHERO_NUCLEUS nuc
      INNER JOIN OMNISPHERO_SUBNEURITE_NUCLEUS_MAPPING map
      ON map.nucleusid=nuc.id
      INNER JOIN OMNISPHERO_SUBNEURITE sub on sub.id = map.subneuriteid
      INNER JOIN OMNISPHERO_NEURITE neu ON sub.neuriteid=neu.id
      INNER JOIN OMNISPHERO_EXPERIMENT ex on neu.experiment_id = ex.id
      GROUP BY ex.name,ex.type, ex.well, sub.id order by sub.id asc) as
      innerResult WHERE innerResult.distinctNuclei >= 3)
      GROUP BY nuc.id, ex.name, ex.well,ex.type
) as mainneurite group by expname, wellname, typeid
order by expname,typeid, wellname
```

Supplementary Figure S.4. *SQL statement for extracting average neurite length per neuron.*

```
SELECT expname,typeid,wellname,
avg(sublengthtotal) as Total_Subneuritelength_PerNucleus,
avg(numberbranchingpoints) as numberbranchingpoints,
avg(distinctsubneurites) as distinctsubneurites FROM
  (SELECT nuc.id,ex.name as expname,ex.well as wellname,ex.type as typeid,
  sum(sub.length) as sublengthtotal,
  sum(sub.branchingpoints) as numberbranchingpoints,
  count(distinct map.subneuriteid) as distinctsubneurites
  FROM OMNISPHERO_NUCLEUS nuc
  INNER JOIN OMNISPHERO_SUBNEURITE_NUCLEUS_MAPPING map
  ON map.nucleusid=nuc.id
  INNER JOIN OMNISPHERO_SUBNEURITE sub on sub.id = map.subneuriteid
  INNER JOIN OMNISPHERO_NEURITE neu on neu.id = sub.neuriteid
  INNER JOIN OMNISPHERO_EXPERIMENT ex ON neu.experiment_id = ex.id
  WHERE ((neu.totallength > 10 AND neu.totallength <= 100
  AND neu.totalbranchingpoints <3)
  OR (neu.totallength > 100 AND neu.totallength <= 200
  AND neu.totalbranchingpoints <4)
  OR (neu.totallength > 200 AND neu.totallength <= 300
  AND neu.totalbranchingpoints <4)
  OR (neu.totallength > 300 AND neu.totallength <= 360
  AND neu.totalbranchingpoints <5))
  AND sub.id not in
    (SELECT subid FROM
      (SELECT sub.id as subid, ex.name,ex.type,ex.well,
      count(distinct nuc.id) as distinctNuclei FROM OMNISPHERO_NUCLEUS nuc
      INNER JOIN OMNISPHERO_SUBNEURITE_NUCLEUS_MAPPING map
      ON map.nucleusid=nuc.id
      INNER JOIN OMNISPHERO_SUBNEURITE sub on sub.id = map.subneuriteid
      INNER JOIN OMNISPHERO_NEURITE neu ON sub.neuriteid=neu.id
      INNER JOIN OMNISPHERO_EXPERIMENT ex on neu.experiment_id = ex.id
      GROUP BY ex.name,ex.type, ex.well, sub.id order by sub.id asc)
    as innerResult WHERE innerResult.distinctNuclei >= 3
) GROUP BY nuc.id, ex.name, ex.well,ex.type)
as mainneurite group by expname, wellname, typeid
order by expname,typeid, wellname
```

Supplementary Figure S.5. *SQL statement for extracting neurite counts and total numbers of branching points per neuron.*

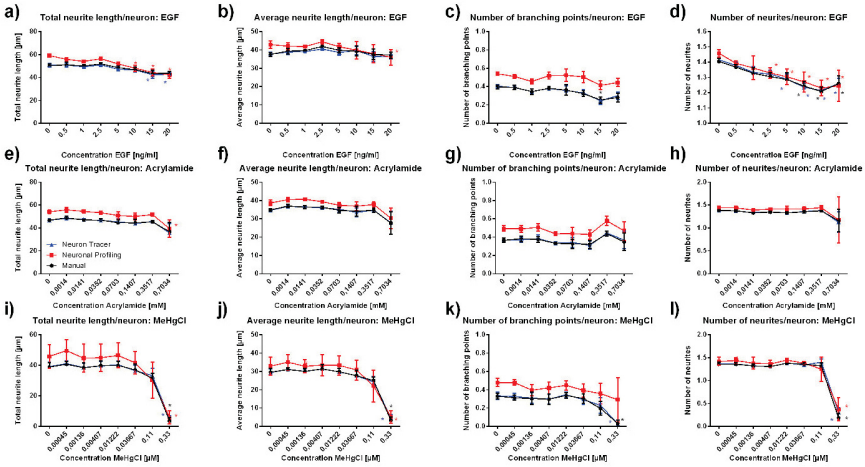

Supplementary Figure S.6. *Neuronal morphology. a-l)*: Total neurite length, average neurite length, number of branching points and number of neurites derived from the identified starting points by the manual evaluation and the two automated methods for all three model substances. Data are presented as mean±SEM. Significant differences among one method are indicated as *.

Supplement S.4 Determining extended analysis endpoints.

S.4.1 Determining migration area and migration distance

The outer boundary of the migration area is determined by generating a density matrix B_C of the nuclei coordinates with a subsequent seed fill operation using the same procedure as for determining the boundary of the neurosphere-core and its center point C from the density matrix C_I. The migration area, defined as the area between the two calculated boundaries, can now be described as the binary matrix $B_M = B_C - C_I$. The Matrix B_M is subdivided further into 64 circular wedges $W_1, \ldots, W_{64}$ with center point $(C(x_C, y_C))$. For each wedge W_j the point $I_j = (x_j^I, y_j^I)$ with the furthest distance from C is determined spanning the outer rim of the migration distance. The inner border is determined in a nested loop procedure in which for each wedge W_j the point $F_j = (x_j^F, y_j^F)$ is determined with the furthest distance from C still located within the area of the neurosphere-core (C_I). The circular polygon $I_1, \ldots, I_{64}, I_1$ and $F_1, \ldots, F_{64}, F_1$ can now be transformed back into original pixel coordinates, where it spans the *migration area*. Having identified the migration area, we can now compute the distance between F_j and the edge of the neurosphere-core I_j in W_j for each segment j, measuring the "furthest migration in segment j". Taking the average of all segmental migration finally yields the *average migration distance*. In order to account for washing artifacts and removed parts of the migration area during immuncytochemical staining, only directions with a minimal length of 33% of the longest measured distance in j were taken into account for the average migration distance. Furthermore, those W_j where the sphere migrated across the image boundary were not taken into account.

S.4.2 Neuronal density distribution

In order to quantify the distribution of neurons in different migration radii around the neurosphere-core, we compute *neuronal density distributions* as follows: Each segment W_j is further subdivided into ten rings $R_{1,j}, \ldots, R_{10,j}$, where $R_{k,j}$ covers all points in W_j whose distance lies within the range $(i-1) \cdot L_j/k$ and $i \cdot L_j/k$, where L_j denotes the distance between the edge of the neurosphere-core and F_j. Neuronal densities (% of neurons, i.e. number of neurons/number of nuclei) within each ring are further normalized to the average neuronal density within the entire migration area in order to account for decreasing neuron number with increased substance concentrations. Normalized neuronal densities within a given ring can be calculated according to

$$\overline{\delta_k} = \frac{\sum_j (R_{k,j} \cap X) / \sum_j (R_{k,j} \cap N)}{\sum_{\ell,j} (R_{\ell,j} \cap X) / \sum_{\ell,j} (R_{\ell,j} \cap N)}$$

Being X the neuron matrix and N the nuclei matrix. Obtained neuronal density functions are shown in Supplementary Fig. S.7, S.8, S.9 .

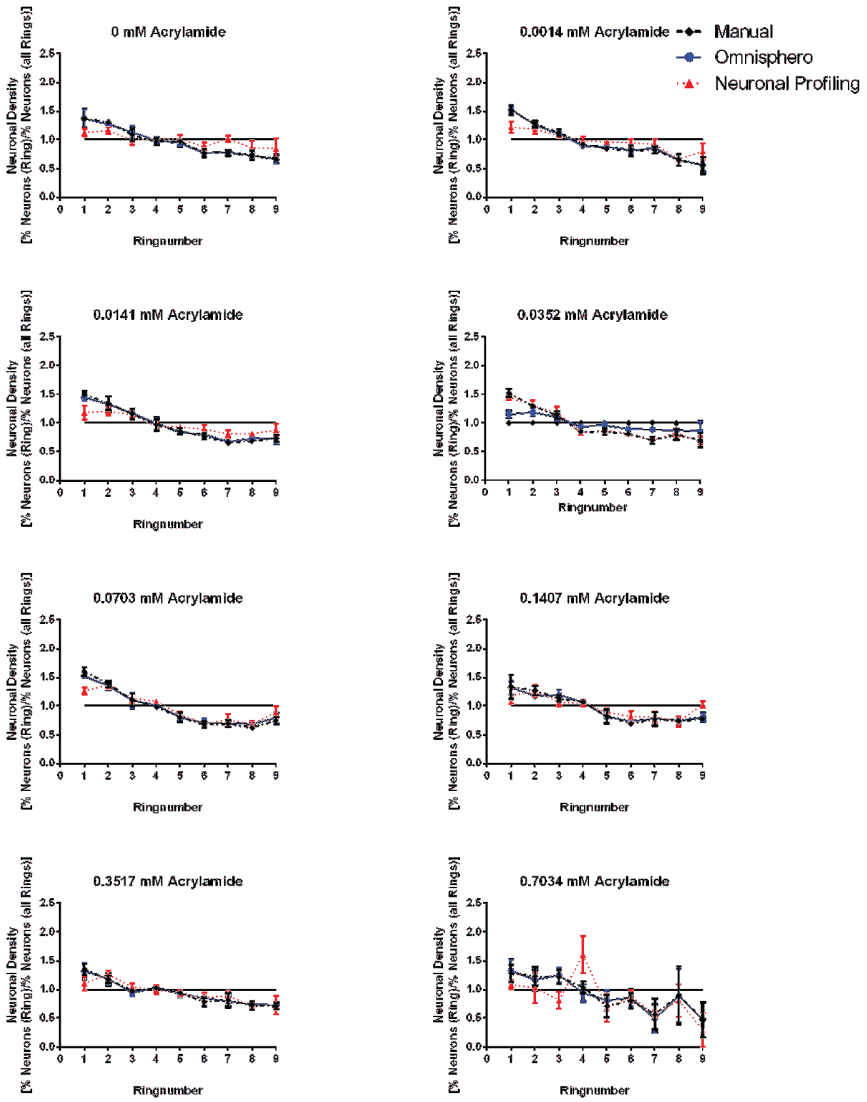

Supplementary Figure S.7. *Neuronal density distribution of acrylamide.* Neuronal density distributions of increasing acrylamide concentrations are assessed by dividing the migration area into 10 rings. In each ring, the ratio between the number of neurons and cell nuclei is normalized to the ratio within the entire migration area resulting in a distance-dependent neuronal density function. Results are obtained from four independent experiments with three technical replicates per concentration and are presented as mean±SEM.

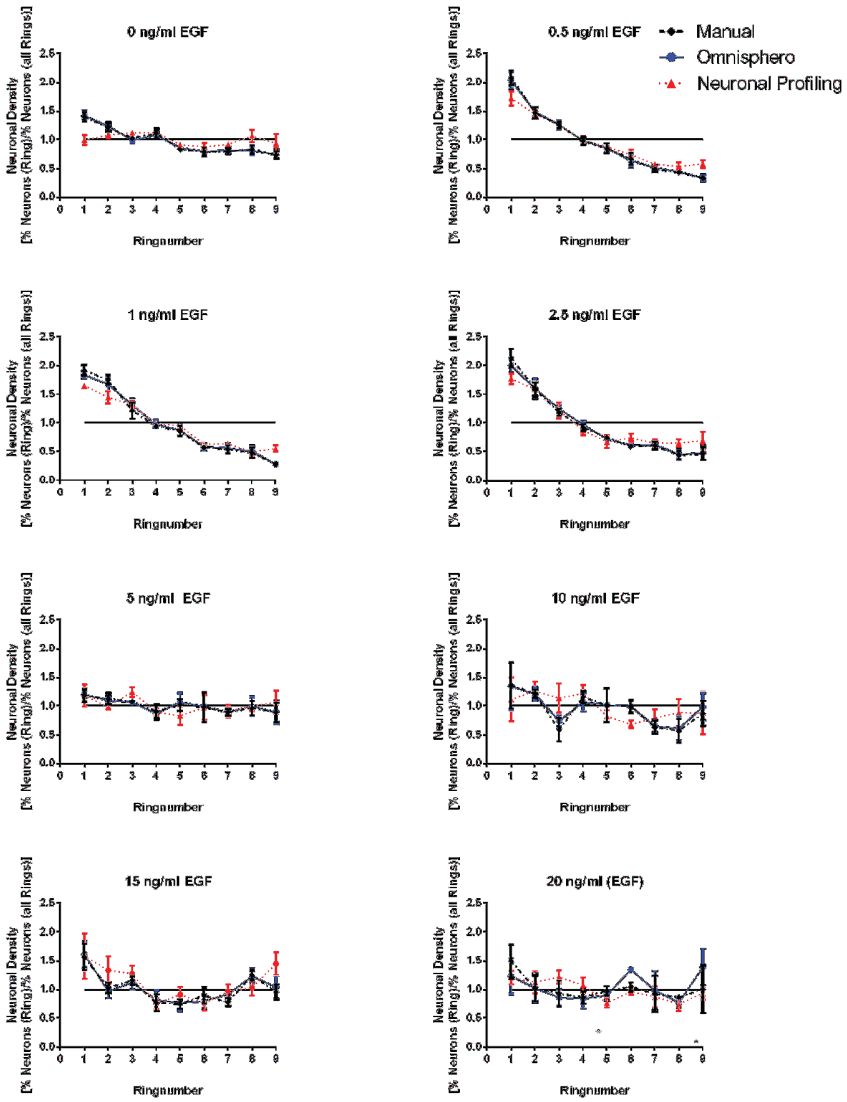

Supplementary Figure S.8. *Neuronal density distribution of EGF.* Neuronal density distributions of increasing EGF concentrations are assessed by dividing the migration area into 10 rings. In each ring the ratio between the number of neurons and cell nuclei is normalized to the ratio within the entire migration area resulting in a distance-dependent neuronal density function. Results are obtained from four independent experiments with three technical replicates per concentration and are presented as mean±SEM.

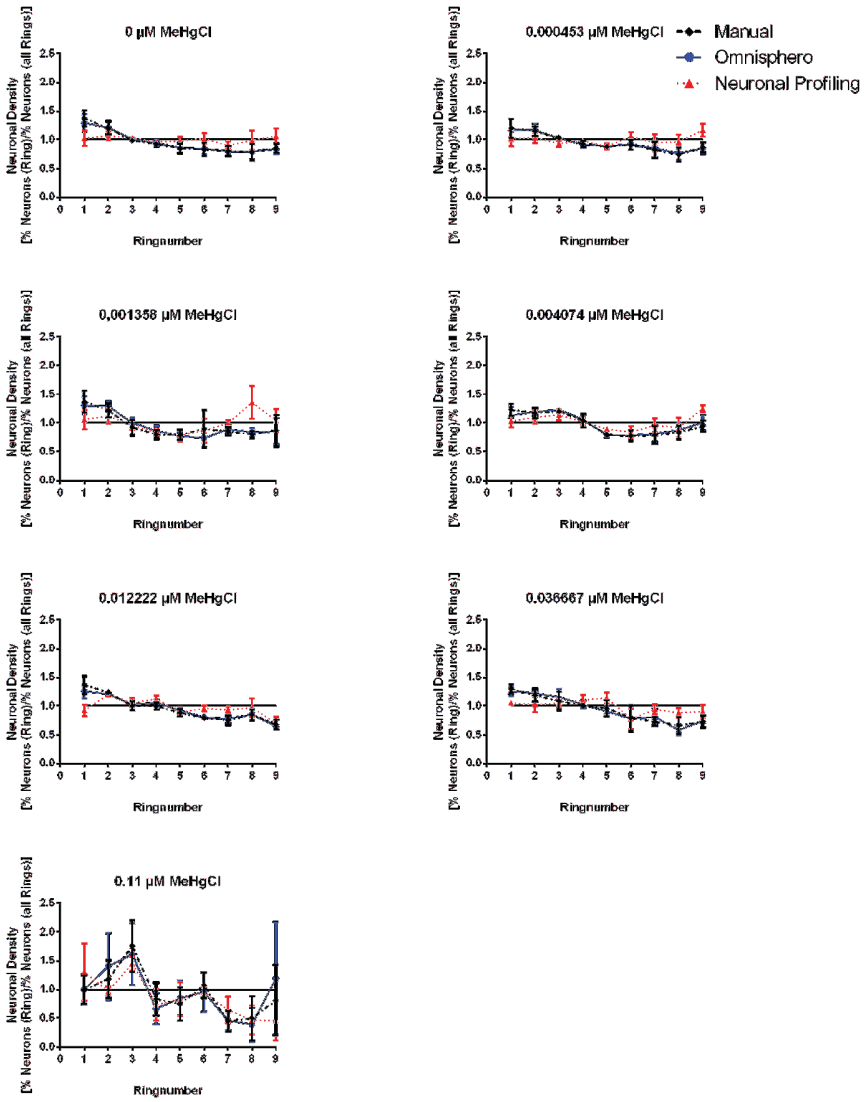

Supplementary Figure S.9. *Neuronal density distribution of MeHgCl.* Neuronal density distributions of increasing MeHgCl concentrations are assessed by dividing the migration area into 10 rings. In each ring the ratio between the number of neurons and cell nuclei is normalized to the ratio within the entire migration area resulting in a distance-dependent neuronal density function. Results are obtained from four independent experiments with three technical replicates per concentration and are presented as mean±SEM.

Supplement S.5 Parameter Optimization

S.5.1 Methods

Our parameter optimization is based on a dataset with manually annotated neuronal nuclei. As both detection power (DP) and false positive rate (FPR) should be accounted we optimize the DP without increasing the FPR above a user defined value. This value was defined as 15%, due to previous reports which revealed an average interindividual difference among experimentators of 11–19% (Schmuck *et al.*, 2014; Sciarabba *et al.*, 2009). In order to obtain the maximal DP without exceeding the user defined FPR, a so-called *Quality index* (QI) was introduced as the target value to be optimized. The QI assigns weights to different FPRs according to a piecewise linear function. FPR below 10% are not weighted in the QI, while FPR bigger than 15% are weighted a 100%. The weight for FPR between 10 and 15% within the QI is linearly interpolated.

Optimization is accomplished by an iterative interval method that starts with a user defined parameter interval calculating QIs for the lower $QI(Pl_0)$ and higher $QI(Ph_0)$ interval border. Subsequently, the interval border with the lower QI is shifted by $1/4$ of the difference between the higher and the lower interval border in the direction of the other interval border. This procedure is repeated until the difference between Ph_i and Pl_i is below a fixed threshold, set for every parameter individually.

S.5.2 Results

While the different computational analyses steps involve several parameters, we proposed a parameter optimization scheme in *Omnisphero* to calibrate these parameters based on a small annotated reference data set. The parameter optimization delivers comparable values for the DP, FPR and QI compared to manual parameter adjustment. In order to validate this optimization approach, we utilized a training set consisting of 17648 manually annotated neurons derived from full images from three experiments (one from each substance). In a first *complete* setting, we automatically optimized parameters on the complete manually annotated data set. As it turns out, we obtained a QI that was slightly higher compared to manually adjusted parameters (70.7% compared to 70.6%, Supplementary Fig. S.10*a*). The complete manual annotation, however, requires an manual annotation time of roughly 12 hours, which is not practicable for normal laboratory workflows. Therefore we tested the robustness of this method by using a *reduced* setting, where the data set used for optimization contained only a subimage of each image limited to the dimension of 1200×800 pixels (24 filters per experiment). The filter was placed vertical to the axis of the neurosphere-core in order to cover different regions of cell densities. This lowered the total number of annotated neurons to 2705 (see Supplementary Fig. S.10*b*). Therefore, total evaluation time decreased to roughly one hour. We observed only minor effect on the resulting DP, FP and QI (manual: DP=82.4%; FP=11.8%; QI=70.6% and reduced optimized: DP=81.0%; FP=13.8%; QI=67.2%). In a last step a *min.* setting using only nine filters containing a total of 950 annotated neurons were used for parameter optimization, reducing the evaluation time to 40 min but at the same time also reducing DP (76.7%) and QI (61.0%) and increasing the FPR (15.7%) (see Supplementary Fig. S.10*c*). Supplemen-

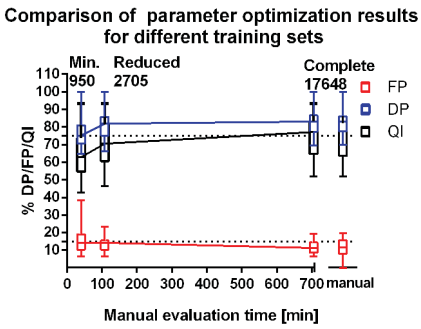

Supplementary Figure S.10. *Parameter optimization:* Relation between manual evaluation time, resulting values for DP, FP and QI and size of the training set for three reference data sets. Results are obtained from one experiment per substance (EGF, acrylamide, MeHgCl) with three technical replicates per experiment resulting in a total of three independent experiments. Data is presented in a box-plot diagram and corresponding means are connected via straight lines.

tary Fig. S.10 shows the relation between size of the training set, manual evaluation time and results for QI, DP and FP.

References

Bai, X., *et al.* (2007). Skeleton pruning by contour partitioning with discrete curve evolution. *IEEE Transactions on Pattern Analysis and Machine Intelligence*, **29**(3), 449–462.

Baumann, J., *et al.*, 2014. Comparative human and rat "neurosphere assay" for developmental neurotoxicity testing. *Current protocols in toxicology*, **59**, 12.21.1–12.21.24.

Schmuck, M., *et al.* (2014). Automatic counting and positioning of 5-bromo-2-deoxyuridine (BrdU) positive cells in cortical layers of rat brain slices. *Neurotoxicology*.

Sciarabba, M., *et al.* (2009). Automatic detection of neurons in large cortical slices. *Journal of neuroscience methods*, **182**(1), 123–40.

Wang, C., *et al.* (2013). An image skeletonization-based tool for pollen tube morphology analysis and phenotyping. *Journal of integrative plant biology*, **55**(2), 131–41.

Omnisphero: A novel computational approach for high content image analyses (HCA) of organoid neurosphere cultures *in vitro*

M. Schmuck*, T. Temme*, D. de Boer, A. Mosig, E. Fritsche

* Shared first authors

Journal:	Bioinformatics
Impact factor:	4.981
Contribution to the manuscript:	50% Designing and performing of all experiments, development of algorithms, writing and reviewing of the manuscript
Type of authorship:	First authorship
Status of manuscript:	Submitted 10.11.2015

2.2. Automatic counting and positioning of 5-bromo-2-deoxyuridine (BrdU) positive cells in cortical layers of rat brain slices.

M. Schmuck*, T. Temme*, S. Heinz, C. Baksmeier, A. Mosig, M.T. Colomina, M. Barenys, E. Fritsche

* Shared first authors

Neurotoxicology (Volume 43, July 2014, Pages 127–133)

Bromdesoxyuridin (BrdU) immunhistologische Färbungen werden häufig zur Untersuchung der Formierung der Schichten der Großhirnrinde bei der Gehirnentwicklung von Säugetieren verwendet. Diese Methode erlaubt die Quantifizierung von neu entstandenen Zellen, was die quantitative Untersuchung von Effekten von Xenobiotika oder genetischen Faktoren auf Proliferation, Zelltod und Migration erlaubt. Diese Endpunkte werden generell mittels zeitaufwändiger, manueller Evaluierung bewertet. In der vorliegenden Arbeit stellen wir eine neue Applikation zur Identifizierung und Quantifizierung von $BrdU^+$-Zellen vor, welche die kommerziell erhältliche vHCS-Scan V.6.3.1 Software zur Identifikation von $BrdU^+$-Zellkoordinaten sowie das neue Programm 'BrdeLuxe' zur Definition von Großhirnrindenschichten und die Zuordnung identifizierter $BrdU^+$-Zellen zu diesen Schichten verwendet. Diese Applikation wurde von zwei unabhängigen Wissenschaftlern mit der $BrdU^+$-Zell-Quantifizierung der Freeware 'ImageJ' im Bezug zur manuellen Evaluierung verglichen. BrdeLuxe weist eine hohe Genauigkeit und Präzision für die totale Quantifizierung von $BrdU^+$-Zellen im Vergleich zur manuellen Evaluierung auf, die von ImageJ nicht erreicht wird. Die Genauigkeit und Präzision für die prozentuale Verteilung von $BrdU^+$-Zellen innerhalb der Großhirnrindenschichten von BrdeLuxe ist ebenfalls höher als für ImageJ. Im Hinblick auf die Analysezeit, ist BrdeLuxe die schnellste der drei Methoden, was es für die Verwendung für Analysen multipler Gehirnschnitte qualifiziert.

NeuroToxicology 43 (2014) 127–133

Contents lists available at ScienceDirect

NeuroToxicology

Automatic counting and positioning of 5-bromo-2-deoxyuridine (BrdU) positive cells in cortical layers of rat brain slices

Martin Schmuck [a,1], Thomas Temme [a,b,1], Sabrina Heinz [a], Christine Baksmeier [a], Axel Mosig [b], M. Teresa Colomina [c], Marta Barenys [a,2], Ellen Fritsche [a,2,*]

[a] IUF – Leibniz Research Institute for Environmental Medicine, Auf'm Hennekamp 50, 40225 Düsseldorf, Germany
[b] Bioinformatics Group, Department of Biophysics, Ruhr-Universität Bochum, 44780, Germany
[c] Laboratory of Toxicology and Environmental Health/NEUROLAB, Department of Psychology, Universitat Rovira i Virgili, Campus Sescelades, 43007 Tarragona, Spain

ARTICLE INFO

Article history:
Received 31 October 2013
Accepted 14 February 2014
Available online 23 February 2014

Keywords:
Histopathology
Image analysis
Immunohistochemistry
Cortical development
BrdU
Automated evaluation

ABSTRACT

5-Bromo-2-deoxyuridine (BrdU) staining is often used to evaluate cortical layer formation during mammalian brain development. This method allows the quantification of newly generated cells and therefore the study of the effects of xenobiotics or genetic factors on proliferation, cell death and migration behavior in a quantitative manner. However, these endpoints are generally assessed by time-consuming manual evaluation. In the present work, we introduce a novel procedure to identify and quantify BrdU$^+$ cells within cortical layers, using the commercially available vHCS-Scan V.6.3.1 software to identify BrdU$^+$ cell coordinates and the novel program 'BrdeLuxe' to define cortical layers and quantitatively assign BrdU$^+$ cells to them. This procedure is compared to BrdU$^+$ cell counting with the freeware 'ImageJ' in respect to the manual evaluation, all by two different researchers. BrdeLuxe shows high accuracy and precision for the determination of total number of BrdU$^+$ cells compared to the manual counting, while ImageJ does not reach such results. Accuracy and precision are also higher for employing the BrdeLuxe program to evaluate the percentage of BrdU$^+$ cells per brain layer compared to ImageJ. In terms of running time, BrdeLuxe is the fastest method of the three making it more suitable for multiple brain slices analyses.

1. Introduction

During mammalian brain development, cortical layers are formed in an inside-out fashion, in which early-generated neurons occupy deeper layers, and later-generated ones locate to more superficial layers. This process is delicately guided by a variety of molecular signals and alterations of this molecular interplay produce organ malfunction with resulting behavioral deficits (reviewed in Aboitiz et al., 2001; Gupta et al., 2002). Such complex brain layer formation encompasses several biological processes: neural stem/progenitor cell (NPC) proliferation, migration and differentiation ensuring allocation of newly generated cells to their appropriate position. Besides genetic alterations (reviewed in Gupta et al., 2002), also exogenous noxae can interfere with cortical layer formation. Such compounds include MeHgCl (Kakita et al., 2002), gamma-irradiation (Inouye et al., 1993) and ethylnitrosourea (Oyanagi et al., 2001). These are thought to interfere with one or more of the processes necessary for proper cortical layer formation by perturbing cell adhesion, guidance cues, motogenic factors, stop and detachment signals or the cytoskeleton (Manent et al., 2011).

Safety evaluations for identifying compounds with such destructive potential or gene targeting in rodents to identify genes and pathways contributing to cortical layer formation utilize the common strategy of histology and immunohistochemistry in offspring brains to measure relative sizes of cortical layers (OECD 426, 2007; EPA OPPTS 870.6300, 1998; Tsuji and Crofton, 2012). This is often combined with the labeling of newly generated cells by 5-bromo-2-deoxyuridine (BrdU) incorporation. This method labels freshly divided NPCs and thus enables tracking of newborn cells to their final positions. Moreover, cell generation can be studied in a quantitative way by also counting the total number of BrdU$^+$ cells. These analyses are generally performed manually by

* Corresponding author at: IUF – Leibniz Research Institute for Environmental Medicine, Auf'm Hennekamp 50, 40225 Düsseldorf, Germany.
Tel.: +49 211 3389217.
E-mail address: ellen.fritsche@uni-duesseldorf.de (E. Fritsche).
[1] These authors contributed equally to this work.
[2] These authors contributed equally to this work.

http://dx.doi.org/10.1016/j.neuro.2014.02.005
0161-813X/

cell-to-cell evaluation of stained brain slices (Inouye et al., 1993; Kakita et al., 2002; Oyanagi et al., 2001). The total number of $BrdU^+$ cells in a brain area is a measure of NPC proliferation and the positioning within the layers reveals proper cell migration. This method bears two caveats. For one, manual counting of nuclei in numerous images is time-consuming and is therefore usually performed only in one image per brain. Even though the most time consuming step would be the animal experiment itself, analysis of multiple brain slices is limited by the manual evaluation. Secondly, a researcher bias is prone to be introduced.

There are several freely available applications for extracting cellular structures from images of histological slices (Mulrane et al., 2008). Other software is even able to reconstruct neuronal dendritic trees and axonal projections in 3D (Sciarabba et al., 2009). Such applications are specifically designed to extract a variety of information on, e.g., cell morphology, staining intensity, cell size or spatial information. However, to the best of our knowledge, there is so far no program available, that quantifies and positions $BrdU^+$ cells in brain slices.

The automatic program presented in this article, named 'BrdeLuxe', is specially designed to quantify the density of $BrdU^+$ cells in cortical layers of stained brain slices by assigning coordinates of $BrdU^+$-cells to certain brain layers. Therefore any Spot detector which is able to export coordinates of identified $BrdU^+$-cells would be suitable. In this approach, the Spot Detector V.4 bioapplication, which is part of the vHCS-Scan V.6.3.1 software (Thermo Scientific), is used for the identification of $BrdU^+$ cells. A suitable Spot detector has to meet several criteria, which are well fulfilled by the vHCS-Scan V.6.3.1 software. For one, the program has to extract such $BrdU^+$ events from the surrounding tissue through a background correction, differentiate them from bright staining artifacts like bubbles, holes, dirt particles, pieces of meninges, blood vessels or tissue foldings and has to acquire the position of each $BrdU^+$ cell within the slice. This positional information is then used by BrdeLuxe to associate each $BrdU^+$ cell to a certain cortical layer. To allow medium or high-throughput image analyses, the Spot Detector V.4 bioapplication even identifies $BrdU^+$ cells in non-perfect focusing conditions. In the present work, we describe the BrdeLuxe program in detail. Moreover, we compare the accuracy and precision of this method to conventional manual counting and to quantification with the open source software ImageJ.

2. Materials and methods

2.1. Animals

The *in vivo* experimental protocol was approved by the Animal Care and Use Committee of the "Rovira i Virgili" University, where all the *in vivo* experiments were performed. Sprague Dawley timed pregnant rats (Harlan InterfaunaIberica; Barcelona, Spain) were kept at a constant dark–light cycle of 12–12 h and maintained at a temperature of 22 ± 2 °C and humidity of $50 \pm 10\%$. The animals had free access to standard food (Panlab, Barcelona) and tap water and were monitored daily for general health during gestation and development.

2.2. BrdU administration

On gestational day (GD) 16, 8 Sprague-Dawley dams received one BrdU (Sigma–Aldrich) dose of 50 mg/kg b.w. intraperitoneally.

2.3. Brain sample collection and tissue sectioning

On post-natal day (PND) 28 one male and one female per litter (16 in total) were anesthetized with 2% tribromoethanol (0.15 ml/10 g body weight, i.p.) and perfused through the heart first with saline solution and then with 4% paraformaldehyde (PFA). Brains were removed, post-fixed in 4% PFA for 48 h at 4 °C and transferred into a 30% sucrose/phosphate-buffered saline (PBS) for 48 h at 4 °C. Brains were fast frozen in isopentane and dry ice at −80 °C for 30 s and stored at −20 °C until sectioning in 40 μm coronal sections with a cryostat (Leica CM 1850, Leica Microsystems). Brain slices of each animal were serially divided in six batches, each one containing slices with an interspace of 240 μm. One of the batches was used for the subsequent immunohistochemical analyses.

2.4. Immunohistochemical staining

Free floating coronary sections were washed two times for 5 min in TBS (tris buffered saline) and then the DNA was denatured with 2 M HCl for 30 min at 37 °C. After neutralizing for 10 min in 0.1 M sodium borate buffer (pH = 8.5) the slices were washed six times for 5 min again in TBS. Brain slices were permeabilized with TBS-plus (TBS containing 1% triton-X 100 and 3% goat serum) for 30 min and then incubated with a rat anti BrdU Monoclonal Antibody (AbDSerotec, Oxford, UK; # MCA2060) 1:500 diluted in TBS-plus over night at 4 °C. On the next day slices were washed two times for 5 min in TBS and then the Cy3-coupled secondary antibody (Dianova, Hamburg, Germany; # 712-165-153) 1:250 diluted in TBS-plus was applied for 2 h at room temperature (RT). Slices were washed six times for 5 min in TBS in order to remove non-specifically bound secondary antibody.

Subsequently, the same brain sections were permeabilized with PBS-Triton (PBS-T) [PBS containing 0.1% Triton X-100] for 10 min. Sections were placed in baskets with 400 μl of 1:100 fluorescent dye dilution (NeuroTrace® Fluorescent Nissl stain; Molecular Probes®, # N-21 480) in PBS each in a well of a 24-well plate and were incubated for 20 min at RT while shaking. The sections were again washed with PBS five times for 2 min. Finally, the sections were washed in PBS for 2 h at RT (or alternatively over night at 4 °C), placed into 0.1 M PBS phosphate buffer, transferred to microscope slides (Superfrost®, Menzel GmbH & Co KG) and mounted in mounting medium (Aqua Poly Mount, Polysciences Inc.).

2.5. Picture acquisition

The perirhinal area and the dorsolateral entorhinal area of the coronal sections were imaged using an inverted fluorescence microscope (Paxinos and Watson, 2009). Both areas were imaged at a 100x magnification at two positions with two channels each, one for Nissl (green: excitation: 470 nm, emission: 509 nm) and one for BrdU (red: excitation: 558 nm, emission: 583 nm). For all regions, both pictures were overlapped using the automated fotomerge function of Adobe Photoshop S3 (Fig. 1, (1) and (2)).

2.6. Image pre-processing

Images of the BrdU channel were scanned using the bioapplication SpotDetector (V.4) of the vHCS-Scan (V. 6.3.1) software (Thermo Fisher). Therefore, the BrdU channel images were pre-processed in three steps. First, the BrdU channel images were converted to 8-bit pictures using a batch function of ImageJ. In the following step a self-written program was used to scale pictures to 1024×1024 pixels, thereby saving scaling factors separately in a comma-separated values file (CSV-file) (Fig. 1, (3)). This program also renamed the pictures with a plate identity code, which can be recognized by the vHCS-Scan software. As the last step, images were scanned separately by using a fixed threshold, which resulted in the identification of $BrdU^+$ nuclei (Fig. 1, (4)). Afterwards, $BrdU^+$ cell coordinates on the rescaled picture were exported as a second

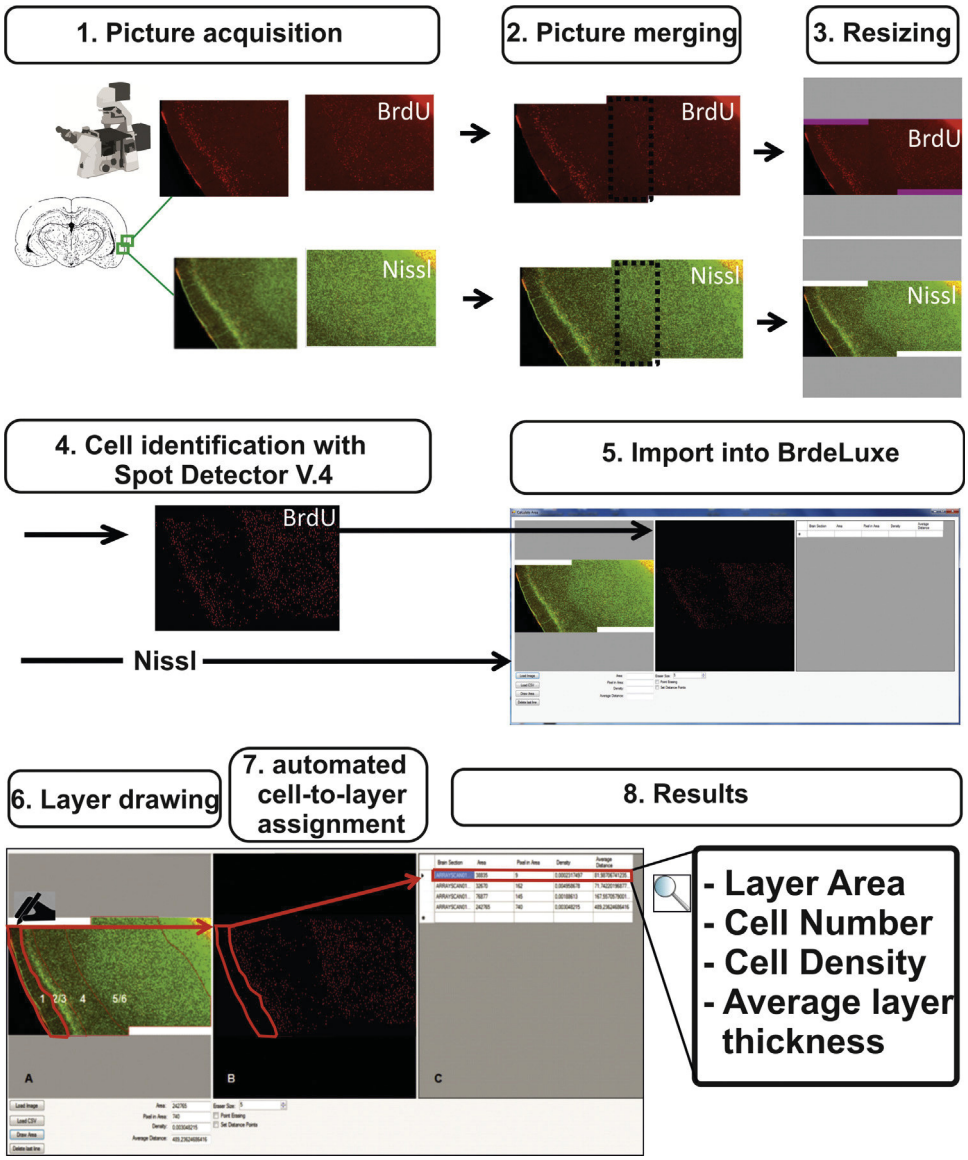

Fig. 1. Workflow of the evaluation of the number of BrdU$^+$ cells in cortical layers. Two pictures per brain area are taken (1) and merged (2). The red channel BrdU picture is converted to 8-bit and both, the BrdU channel and the Nissl channel picture, are rescaled to 1024 × 1024 pixels (3) and renamed. The BrdU channel picture is then analyzed with the vHCS-Scan V.6.3.1 software (Spot Detector V.4 bioapplication) (4). BrdU$^+$ cell coordinates are exported as a CSV-file (comma-separated values file). The Nissl picture and the CSV are imported to the BrdeLuxe user interface (5). The layers are marked manually in the Nissl picture (red lines in (6)). The resulting polygon is overlaid on the BrdU$^+$-cell coordinates to assign cells to the marked region (7). Results of BrdU$^+$ cell number, layer area, cell density and average layer thickness are shown in (8). (For interpretation of the references to color in this figure legend, the reader is referred to the web version of this article.)

CSV-file. Two color images were resized without converting them to 8-bit.

2.7. 'BrdeLuxe' program description

Our novel 'BrdeLuxe' software uses the coordinates of the identified BrdU$^+$ cells to calculate their number in a given brain layer. Within the BrdeLuxe user interface, the resized original two channel pictures (Fig. 1, (5)) and their corresponding CSV-files for BrdU$^+$ cell coordinates (Fig. 1, (5)) are loaded. An erasing tool is implemented in the program to manually erase the remaining staining artifacts after background correction if necessary. Within the left part of the BrdeLuxe users interface cortex layers have to be manually drawn following the green Nissl staining (Fig. 1, (6)). Thereby, only the upper and lower lines need to be sketched for the first layer because the program automatically completes the polygon by connecting the ends of both lines with the shortest possible distance along the edges of the picture. For cases in which layers are disrupted by holes, the area of the holes is calculated and subtracted from the area marked by the polygon automatically. Holes are identified as regions with a much lower intensity compared to the brain slice. For the second layer, only the non-adjacent line has to be drawn. This prevents a possible overlap of two polygons and ensures that the polygon covers the entire area. In the screen were the CSV-file is displayed, the layer area is automatically determined using a floodfill algorithm (Fig. 1, (7)). After all layers are marked, the total BrdU$^+$ cell number, the layer area, the density of cells (number of cells per μm^2) and the average layer thickness are automatically calculated and visualized in a table (Fig. 1, (8)).

2.8. BrdU$^+$ cell counting evaluation

A total of ten images, five from the perirhinal area and five from the dorsolateral entorhinal area belonging to two different brains were evaluated by two researchers independent of each other or the automated counts using three different methods: manual

counting, BrdeLuxe and ImageJ. Manual evaluation was performed first to avoid introduction of a counting bias by the results from the automated assessments. Then images were examined using the BrdeLuxe program as described in Section 2.7 and ImageJ, an open source image processing software developed at the National Institutes of Health of the United States (Rasband, 1997). When using ImageJ, the red channel BrdU pictures were background corrected using the rolling ball method (Sternberger, 1983). Afterwards, a threshold was chosen from the 'Auto threshold' function of ImageJ. Particles were subsequently evaluated in each layer by defining a ROI (region of interest) which met the layer borders and by running the 'Analyze particles' function. For all methods, the absolute numbers of $BrdU^+$ cells were counted for each individual layer.

2.9. Statistical analyses

Statistical analyses were used to examine differences in-between the three different evaluation methods (manual counting, BrdeLuxe and ImageJ) and between performances of the two evaluators for each method.

For comparing the accuracy of the two automated methods, the mean value from manual countings of the total number of $BrdU^+$ cells from both researchers (x_1 and x_2) was calculated for each picture (x_{manual}). As all pictures had different numbers of $BrdU^+$ cells, x_{manual} values were set to 100% and used as the standard value for comparative analysis. The total number of $BrdU^+$ cells assessed for the same pictures with the two automated methods, BrdeLuxe and ImageJ, for both researchers were then normalized to x_{manual} and compared. Variances were compared one by one for the manual versus each automatic program using the Bartlett's test. The significance threshold was set to $p < 0.05$ and is represented as #, while p values <0.01 are represented by ##. For not statistically significant differences in the variances (homogeneous parameters), means of manually and automatically counted images each were compared using the parametric one-way ANOVA test. In cases of statistically significant variances (non-homogeneous parameters), means were compared using the non-parametric Kruskal–Wallis test. Statistically significant differences among means were represented as * for $p < 0.05$ and as ** for $p < 0.01$.

To evaluate the inter-individual differences of the two different investigators across the three different methods, the mean values were also assessed for the two automated methods ($x_{BrdeLuxe}$ and x_{ImageJ}). Subsequently, the numbers of $BrdU^+$ cells determined by the researchers (e.g. $x_{BrdeLuxe1}$ and $x_{BrdeLuxe2}$) were divided by the respective mean value for each picture and method (e.g. $x_{BrdeLuxe}$). In case there was no difference in counting between the two evaluators, $x_{BrdeLuxe1}/x_{BrdeLuxe} = x_{BrdeLuxe2}/x_{BrdeLuxe} = 1$. Inter-individual differences were analyzed for each method by applying the Bartlett's test. The same procedures as for the total number of $BrdU^+$ cells/slice were also performed to evaluate the percentages of $BrdU^+$ cells per cortical layer. Results of the method and inter-individual comparisons are presented as box and whiskers graphs including outlayers (□) as defined by the Tukey method (Hoaglin et al., 1983).

To determine the time needed for image analyses across the three methods, evaluation time for each image with each method was recorded. The mean time needed for both researchers to evaluate the pictures with the three methods was compared using the Kruskal–Wallis test as the variances of the groups were significantly different from the Bartlett's test.

3. Results and discussion

The aim of this study was to evaluate how a novel, automated method for quantification of $BrdU^+$ cells in brain slices (BrdeLuxe) performs in comparison to ImageJ with regard to manual counting in slice evaluation. Moreover, reproducibility of the three methods across two independent investigators was assessed. For these studies, manual counting was set as the reference value because this is currently the most common method for quantification of $BrdU^+$ cells in brain slices. With these comparative investigations, accuracy and precision of the different image analysis methods was assessed. Thereby, these were defined as the closeness toward the defined true value, which is the manual counting, and as the variance of the individual data points, respectively.

Quantification of $BrdU^+$ cells in brain slices by utilizing BrdeLuxe comprises eight individual steps (Fig. 1). (1) Images are taken by a fluorescent microscope, (2) merged and the red channel pictures of the BrdU staining are converted to 8-bit. (3) Both, the Nissl picture and the BrdU picture, are rescaled to 1024 × 1024 pixels and renamed. (4) The BrdU picture is analyzed with the vHCS-Scan V. 6.3.1 (Spot Detector bioapplication V.4). $BrdU^+$ cell coordinates are exported as a CSV-file and the Nissl picture and the CSV-file are imported into the BrdeLuxe user interface (5) where individual layers are marked manually (red lines in 6) and the resulting polygon is transferred to the $BrdU^+$ cell coordinates to assign all cells to the marked area (7). Results of cell number, average layer thickness and density are then automatically determined and shown in (8).

When the total number of $BrdU^+$ cells was determined by the three different methods, manual counting, BrdeLuxe and ImageJ, the mean number of positively evaluated $BrdU^+$ cells did not significantly differ between BrdeLuxe and the manual counting. However, ImageJ identified significantly less $BrdU^+$ cells in the defined total cortical area (27%) than the manual counting ($p < 0.01$; Fig. 2a). BrdeLuxe thus achieved a higher accuracy than ImageJ reflecting systematic errors in the application of the latter. Next, the variances of each automatic method were compared to the variance of the manual method (standard deviation: SD = 13%). While there was no significant difference in variance between the manual and the BrdeLuxe evaluations (SD = 19%), ImageJ showed a significantly higher variance (SD = 27%) than the manual counting ($p < 0.01$; Fig. 2a). These results demonstrate that quantification of $BrdU^+$ cells in brain slices with BrdeLuxe is as precise as counting manually, while the same evaluations performed with ImageJ are significantly less precise.

In a following analysis, we evaluated the inter-individual differences in counting total numbers of $BrdU^+$ cells for each method. The variation between researchers using the manual method was in accordance with the published literature (SD = 11%, Sciarabba et al., 2009). There were no statistically significant differences between the variances of any method (Fig. 2b), showing that multiple researchers can use the automatic tools without introducing more variance than by counting manually.

An automatic program, which is able to accurately and precisely count total numbers of $BrdU^+$ cells in whole cortical areas is useful in cases where proliferation and/or cell death of NPCs are measured. This is the case when malformations of cortical development included in Group I of the Barkovich classification are assessed (Barkovich et al., 2012). Nevertheless, when evaluating alterations encompassed in Group II of the Barkovich classification, which cover malformations due to alterations in the migration pattern of cells, the quantitative distribution of $BrdU^+$ cells across cortical layers is required. In case one wants to involve automatic image analyses techniques into such evaluations, it is indispensable to ensure that the automatic program is identifying the number of $BrdU^+$ cells in cell rich versus cell poor layers or in layers with artifacts correctly. Manual counting of $BrdU^+$ cells revealed that on average 2% of the total $BrdU^+$ cells are in layer I, 34% in layer II/III, 35% in layer IV and 29% in layer V/VI (Fig. 3a). In all pictures, the percentages of $BrdU^+$ cells were much

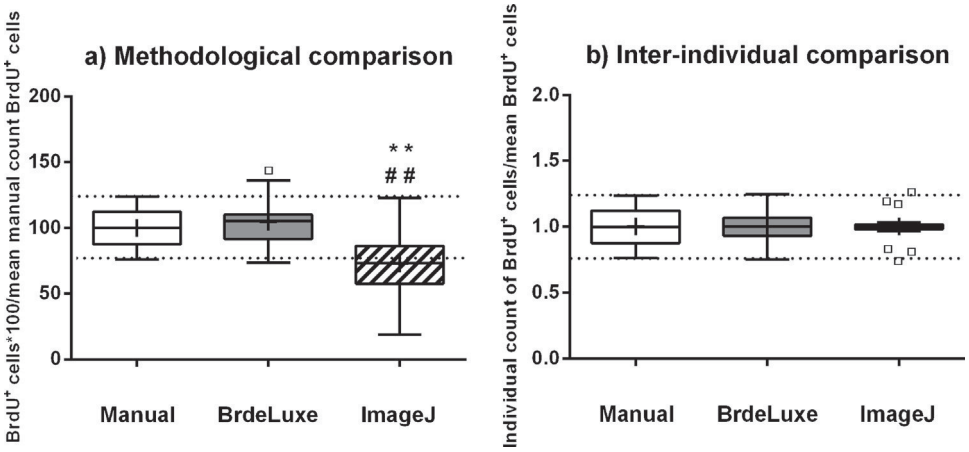

Fig. 2. Comparison of three methods for the determination of the total number of BrdU$^+$ cells. (a) Methodological comparison of the mean and the variance of the automatic methods in comparison to the manual evaluation. The total number of BrdU$^+$ cells counted by each researcher for each picture is expressed in percentage of the manual mean of the corresponding picture. (b) Inter-individual comparison of two researchers across the three methods. The total number of BrdU$^+$ cells counted by each researcher for each method in each picture is divided by the mean value of the respective method and picture. Symbols: *, ** = significantly different means respect to the manual group; #, ## = significantly different variances respect to the manual group; □ = outlayer.

higher in layers II–VI than in layer I. The distribution of BrdU$^+$ cells across layers corresponded to the published literature for the age of the animals (PND28), BrdU administration day (GD16) and areas evaluated (Bayer, 1990). Such raw percentages of BrdU$^+$ cell distribution do not allow a statistical comparison of the BrdeLuxe and ImageJ programs to the manual evaluation in terms of accuracy and precision of the methods because in each picture the percentages of BrdU$^+$ cells per layer was different (Fig. 3a). To define accuracy and precision of identified BrdU$^+$ cells in individual brain layers with the automated methods in comparison to the manual counting, all layer counts were set in relation to the mean manual count of the same layer in each image and were then statistically compared (Fig. 3b). Quantification of stained BrdU$^+$ cells in layers I–VI with the BrdeLuxe program did not reveal any significant differences between manual and BrdeLuxe evaluations in any layers. For ImageJ, quantified means were significantly higher in layer I (700%) and significantly lower in layer V/VI (79%). Layer I contains on average only 2% of the total number of BrdU$^+$ cells but usually holds many artifacts due to unspecific stainings of the meninges. With BrdeLuxe, the researchers were able to minimize those artifacts because the program – in contrast to ImageJ – includes an erasing tool. Although the results of ImageJ for layer I were seven times higher than the manual ones on average, this increase had no significant impact on the total number of BrdU$^+$ cells because the absolute BrdU$^+$ cell numbers in this layer were very low. Contrarily, the significant percentage of BrdU$^+$ cells (21%) that ImageJ missed in layer V/VI had a major influence on the total number of BrdU$^+$ cells as presented in Fig. 2a, because this layer contributes to approximately 30% of the total number of BrdU$^+$ cells. These data indicate that BrdeLuxe counts BrdU$^+$ cells in individual brain layers with a high accuracy compared to manual counting, while ImageJ does not perform as good due to generation of false-positive and false-negative data.

For analyses of method precision, variances of methods with regard to layer-specific BrdU quantification were gauged. The variance of the results obtained by BrdeLuxe was significantly higher than the manual one in layers I and II/III, while for ImageJ it was significantly higher in layers I, II/III and IV. This result indicates a lower precision of the automated methods in the evaluation of these layers than manual counting, which might be explained by program-generated random errors. In layer I these errors are possibly introduced by the presence of artifacts when using ImageJ and by the use of the erasing tool when using BrdeLuxe. In the subsequent layers, the random error would be more related to the layer drawing process or to the threshold selection when analyzing the picture. A shared limitation of all methods is that the researchers need to know how to define the cortical layers, as none of the programs is doing it automatically. Nevertheless, marking brain layers was more convenient for BrdeLuxe compared to ImageJ as only two borders per layer had to be drawn. This prevented an overlap of areas because the lower border from the previous layer was used by the program as the top border of the new layer. Taken together, accuracy and precision indicate that the BrdeLuxe method is superior over ImageJ, but still BrdeLuxe does not reach precision levels of manual counting.

Regarding the inter-individual performance of all methods for brain layer-specific quantification of BrdU$^+$ cells, there were no statistically significant differences between the variances of the manual percentages and the BrdeLuxe percentages in any layer (Fig. 3c) showing again that several researchers can use BrdeLuxe without introducing more variation by the automated method than by manual counting. For ImageJ there was only a significant higher variance in layer V/VI. When counting with the automatic methods, main inter-individual variances are introduced by the selection of different thresholds by the researchers themselves during the image segmentation step. The 'Auto threshold' function of ImageJ offers 16 possible fixed thresholds, which differ very much in background subtraction because they use different algorithms. In this study researchers could freely choose amongst them and it was found that the most applicable algorithms were Otsu (Otsu, 1979) and Triangle (Zack et al., 1977), whereas the other 14 algorithms were not suitable for the desired analyses in our image set. With Spot Detector V.4 the researchers were allowed to choose a manual threshold value per picture and judge in real time the mask of object identification within the picture. As the researchers could select more carefully among manual thresholds instead of applying two fixed options, the variance among them became lower, and the selection of the particles more exact.

While counting each picture, the employed time was recorded and the mean time needed for image evaluation of each method compared (Fig. 3d). These measurements demonstrated that both automated methods were significantly faster than manual counting. In this regard it has to be considered that within the recorded time, the manual evaluation gives only the result for the BrdU$^+$ cell number and extra time would be needed for the

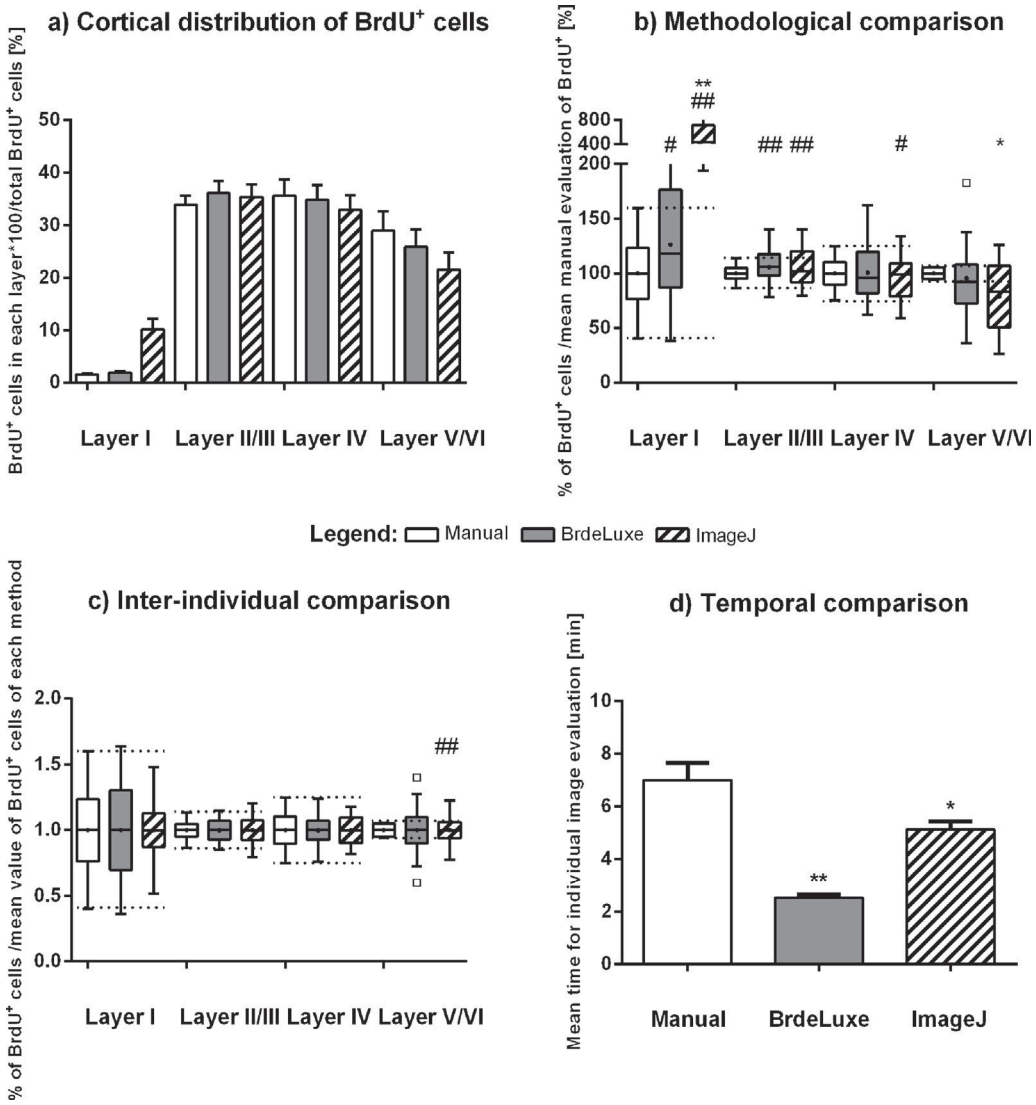

Fig. 3. Comparison of the three methods for determination of the percentage of BrdU$^+$ cells in each cortical layer. (a) Mean percentage of BrdU$^+$ cells in the ten evaluated pictures by two researchers with the standard error (SEM). No statistical analysis is performed on this data, since methodological comparison required data normalization as presented in graph b. (b) Methodological comparison of the mean and the variance of the automatic methods in comparison to the manual evaluation for all cortical layers. The percentage of BrdU$^+$ cells per layer obtained by each researcher for each picture is divided by the manually determined mean percent of the corresponding picture. (c) Inter-individual comparison of two researchers within the three methods for all cortical layers. The percentage of BrdU$^+$ cells per layer obtained by each researcher for each method in each picture is divided by the mean value of the respective layer and method. (d) Comparison of the time needed to evaluate one picture with each method in minutes. Symbols: *, ** = significantly different means compared to the manual group; #, ## = significantly different variances compared to the manual group; □ = outlayer.

measurement of the areas of the counted regions. In the reported mean times of both automatic methods, the area measurement is included as this is automatically done while counting the particles. The time needed to select the fixed threshold for ImageJ or the manual threshold for BrdeLuxe was also included in the reported times. Between the two automated methods, BrdeLuxe was the fastest, making it more suitable for multiple brain slices screening. The relevance of the speed stands out when large *in vivo* neurodevelopmental studies need to be performed, where several litters per dose have to be examined and if multiple pictures per animal have to be evaluated. In previously published work, BrdU$^+$ cell analyses were performed manually, and the evaluation of only one slice per animal (Oyanagi et al., 2001) or two slices per animal (Inouye et al., 1993) was included. With the BrdeLuxe method approximately 20 pictures can be evaluated in one hour, offering the possibility to assess complete areas in the brain through the evaluation of several seriated slices in less time.

As a summary, the advantages and disadvantages of the three methods are displayed in Table 1. Considering the evaluated criteria, it is concluded that BrdeLuxe is a fast, accurate and precise tool to count the number of BrdU$^+$ cells in cortical slices. This automatic application will be useful for neurodevelopmental toxicity studies and for physiological evaluations on the genetic mechanisms implied in cortical development. Therefore, misplacement of cells could in addition be assed via cell identity by using layer-specific markers, which could be analyzed by BrdeLuxe in the same fashion. Regarding future studies, it is important to remark that this approach offers the possibility to scan entire brain slices with an ArrayScan device (Thermo Scientific), enabling the evaluation of several brain regions. In this case, extra time is saved, as the ArrayScan device is able to take pictures of brain slices automatically and thus no manual microscopic picture taking and overlapping is needed. Hence, automated brain slice evaluation for quantitative analysis of BrdU$^+$ cells with the BrdeLuxe program is a feasible alternative to manual counting.

Table 1
Advantages and disadvantages of manual versus automated methods for $BrdU^+$ cell evaluation in brain slices.

Manual	BrdeLuxe	ImageJ
Advantages		
Best pattern recognition	Fastest method	No need of scaled pictures
No layer overlapping	No layer overlapping	Open source software
No need for scaled pictures	High accuracy	Faster than manual
	High precision	
	Same inter-individual differences than with manual counting	
Disadvantages		
Slowest method	No open source software	Slower than BrdeLuxe
Not suitable for medium/high-throughput	Less precise than manual method for layers I and II/III	Layers overlapping
		Low accuracy
		Low precision
		More inter-individual difference than in manual evaluation

Conflicts of interest

The authors declare that they have no conflicts of interest.

Appendix A. Supplementary data

Supplementary data associated with this article can be found, in the online version, at http://dx.doi.org/10.1016/j.neuro.2014.02.005.

References

Aboitiz F, Morales D, Montiel J. The inverted neurogenetic gradient of the mammalian isocortex: development and evolution. Brain Res Brain Res Rev 2001;38:129–39.

Barkovich AJ, Guerrini R, Kuzniecky RI, Jackson GD, Dobyns WB. A developmental and genetic classification for malformations of cortical development: update 2012. Brain 2012;135:1348–69.

Bayer SA. Development of the lateral and medial limbic cortices in the rat in relation to cortical phylogeny. Exp Neurol 1990;107:118–31.

Environmental Protection Agency. Health Effects Test Guidelines OPPTS 870.6300 Developmental Neurotoxicity Study. 1998 EPA 712-C-98-239.

Gupta A, Tsai LH, Wynshaw-Boris A. Life is a journey: a genetic look at neocortical development. Nat Rev Genet 2002;3:342–55.

Hoaglin D, Mosteller F, Tukey J. Understanding robust and exploratory data analysis. New York: John Wiley & Sons; 1983.

Inouye M, Hayasaka S, Sun XZ, Yamamura H. Disturbance of neuronal migration in mouse cerebral cortex by low-dose gamma-radiation. J Radiat Res 1993;34:204–13.

Kakita A, Inenaga C, Sakamoto M, Takahashi H. Neuronal migration disturbance and consequent cytoarchitecture in the cerebral cortex following transplacental administration of methylmercury. Acta Neuropathol 2002;104:409–17.

Manent JB, Beguin S, Ganay T, Represa A. Cell-autonomous and cell-to-cell signalling events in normal and altered neuronal migration. Eur J Neurosci 2011;34:1595–608.

Mulrane L, Rexhepaj E, Penney S, Callanan JJ, Gallagher WM. Automated image analysis in histopathology: a valuable tool in medical diagnostics. Expert Rev Mol Diagn 2008;8:707–25.

OECD Test Guideline 426. OECD guideline for the testing of chemicals: Developmental Neurotoxicity Study. Paris: OECD; 2007 Available: http://www.oecd-ilibrary.org/environment/test-no-426-developmental-neurotoxicity-study_9789264067394-en.

Otsu N. A threshold selection method from gray-level histograms. IEEE Trans Syst Man Cybern 1979;9:62–6.

Oyanagi K, Kakita A, Kawasaki K, Hayashi S, Yamada M. Expression of calbindin D-28k and parvalbumin in cerebral cortical dysgenesis induced by administration of ethylnitrosourea to rats at the stage of neurogenesis. Acta Neuropathol 2001;1:375–82.

Paxinos G, Watson C. The rat brain in stereotaxic coordinates. compact 6th ed. China: Elsevier; 2009.

Rasband WS. ImageJ. Bethesda, MD, USA: U.S. National Institutes of Health; 1997–2013 Available: http://imagej.nih.gov/ij/.

Sciarabba M, Serrao G, Bauer D, Arnaboldi F, Borghese NA. Automatic detection of neurons in large cortical slices. J Neurosci Methods 2009;182:123–40.

Sternberger S. Biomedical image processing. In: IEEE Computer. January; 1983.

Tsuji R, Crofton KM. Developmental neurotoxicity guideline study: issues with methodology, evaluation and regulation. Congenital Anomalies 2012;52:122–8.

Zack GW, Rogers WE, Latt SA. Automatic measurement of sister chromatid exchange frequency. J Histochem Cytochem 1977;25:741–53.

Automatic counting and positioning of 5-bromo-2-deoxyuridine (BrdU) positive cells in cortical layers of rat brain slices.

M. Schmuck*, T. Temme*, S. Heinz, C. Baksmeier, A. Mosig, M.T. Colomina, M. Barenys, E. Fritsche

* Shared first authors

Journal:	Neurotoxicology
Impact factor:	3.379
Contribution to the manuscript:	40%
Type of authorship:	First authorship
	Development of algorithms, writing and
reviewing	of the manuscript
Status of manuscript:	Published (Neurotoxicology ,Volume 43, July 2014, Pages 127–133)

2.3. Developmental Neurotoxicity of Epigallocatechin Gallate (EGCG) Is Triggered by Interference with β1-Integrin Function in Human Neural Progenitor Cells.

M. Barenys*, K. Gassmann*, C. Baksmeier, S. Heinz, I. Reverte, M. Schmuck, T. Temme, F. Bendt, T. C. Zschauer, T. D. Rockel, K. Unfried, W. Wätjen, S. M. Sundaram, H. Heuer, M. T. Colomina, E. Fritsche

Environmental Health Perspectives (submitted 08.09.2015)

Hintergrund: Nahrungsergänzungsmittel auf Pflanzenbasis werden immer häufiger während der Schwangerschaft als Teil eines Präventivansatzes eingenommen. Die Annahme, dass diese Nahrungsergänzungsmittel sicher und gesund sind, ist dabei tief im Bewusstsein der generellen Bevölkerung verankert, obwohl diese nicht denselben strengen Sicherheitsvorschriften wie Medikamente unterliegen.

Ziele: Ziel dieser Studie ist die Charakterisierung von Spezies-spezifischen Effekten des im Grüntee enthaltenen Catechins EGCG, welches kommerziell als hochdosiertes Nahrungsergänzungsmittel erhältlich ist, auf Entwicklungsprozesse des Nervensystems.

Methoden: In dieser Studie wird der 'Neurosphären Assay' verwendet um zum einen die Effekte von einer EGCG Behandlung auf sich entwickelnde humane NPCs und NPCs der Ratte *in vitro* zu untersuchen und zum anderen die zugrunde liegenden molekularen Mechanismen zu identifizieren. *In vivo* Effekte von EGCG auf die Entwicklung des Nervensystems werden mittels Immunzytochemie von Gehirnschnitten EGCG-behandelter Ratten untersucht.

Ergebnisse: EGCG beeinträchtigt die Entwicklung von NPCs in Mensch und Ratte *in vitro* und in Ratte *in vivo*. *In vitro* vermindert EGCG die Migrationsdistanz, verändert das Migrationsmuster und reduziert die Kerndichte von NPCs von Ratte und Mensch, die als Neurosphären kultiviert wurden. Diese funktionellen Beeinträchtigungen werden durch die Bindung von EGCG an das extrazelluläre Matrix-Glykoprotein Laminin hervorgerufen, wodurch die Bindung der β1-Integrin Untereinheit an EGCG verhindert wird. Dies resultiert in einer verminderten Zelladhäsion, welche zu einer veränderten Gliazell-Orientierung und einer verminderten Zahl von migrierten jungen Neuronen führt. Weiterhin konnten wir die *in vivo* Relevanz dieser Beobachtungen in Ratte bestätigen, da eine Exposition von EGCG

während der Entwicklung zu einer Verminderung der Bromdesoxyuridin positiven Zellen führte.

Schlussfolgerungen: Unsere Daten werfen begründete Bedenken für die Einnahme von hochdosierten EGCG Nahrungsergänzungsmitteln während der Schwangerschaft auf, da die normale Gehirnentwicklung in Menschen beeinträchtigt sein könnte.

08-Sep-2015

Dear Schmuck:

A manuscript titled Developmental Neurotoxicity of Epigallocatechin Gallate (EGCG) Is Triggered by Interference with β1-Integrin Function in Human Neural Progenitor Cells. (15-10728-ART) has been submitted by n/a to Environmental Health Perspectives.

You are listed as a co-author for this manuscript. The online peer-review system, Manuscript Central, automatically creates a user account for you. Your USER ID and PASSWORD for your account is as follows:

Site URL: https://mc.manuscriptcentral.com/ehp
USER ID: Martin.Schmuck@iuf-duesseldorf.de
PASSWORD: For security reasons your password is not contained in this email. To set your password click the link below.

https://mc.manuscriptcentral.com/ehp?URL_MASK=62c79b3c4eb141a8b821f2a69700c46d

You can use the above USER ID and PASSWORD (once set) to log in to the site and check the status of papers you have authored/co-authored. If necessary, please log in to https://mc.manuscriptcentral.com/ehp to update your account information via the edit account tab at the top right.

Thank you for your participation.

Sincerely,

Environmental Health Perspectives Editorial Office

Title page

Full title: Developmental Neurotoxicity of Epigallocatechin Gallate (EGCG) Is Triggered by Interference with β1-Integrin Function in Human Neural Progenitor Cells.

Short title: EGCG Induces Neurodevelopmental Toxicity.

Marta Barenys[1]*, Kathrin Gassmann[1]*, Christine Baksmeier[1], Sabrina Heinz[1], Ingrid Reverte[2], Martin Schmuck[1], Thomas Temme[1], Farina Bendt[1], Tim-Christian Zschauer[1], Thomas Dino Rockel[1], Klaus Unfried[1], Wim Wätjen[3], Sivaraj Mohana Sundaram[1], Heike Heuer[1], Maria Teresa Colomina[2], Ellen Fritsche[1]

1: IUF – Leibniz Research Institute for Environmental Medicine. Auf'm Hennekamp 50, 40225 Düsseldorf, Germany.

2: Laboratory of Toxicology and Environmental Health / NEUROLAB, Department of Psychology, Universitat Rovira i Virgili, Campus Sescelades, 43007 Tarragona, Spain.

3: Institute of Agricultural and Nutritional Sciences, Martin-Luther-Universität Halle-Wittenberg, Weinbergweg 22, 06120 Halle/Saale, Germany.

* Both authors contributed equally to this work.

Corresponding author

Prof. Ellen Fritsche, M.D.

IUF - Leibniz Research Institute of Environmental Medicine

Auf'm Hennekamp 50, 40225 Düsseldorf, Germany

Tel.: 00492113389217; Fax: 00492113190910

Ellen.Fritsche@uni-duesseldorf.de

Acknowledgments

M.B. received a Leibniz-DAAD Research Fellowship. K.G. was supported by the DFG (GRK1427).

Financial interests declaration

The authors declare that there are no conflicts of interest.

Abstract

Background: Food supplements based on herbal products are widely used during pregnancy as part of a self-care approach. The idea that such supplements are safe and healthy is deeply seated in the general population, although they do not underlie the same strict safety regulations than medical drugs.

Objectives: We aimed to characterize the species-specific effects of the green tea catechin EGCG, which is now commercialized as high-dose food supplement, on neurodevelopment.

Methods: We used the "Neurosphere Assay" to study the effects and unravel underlying molecular mechanisms of EGCG treatment on human and rat neural progenitor cells (NPCs) development *in vitro*. *In vivo* EGCG effects on neurodevelopment were assessed by brain immunohistochemistry in rats.

Results: EGCG alters human and rat NPC development *in vitro* and in rats *in vivo*. *In vitro*, EGCG disturbs migration distance, migration pattern and nuclear density of rat and human neural progenitor cells growing as neurospheres. These functional impairments are initiated by EGCG binding to the extracellular matrix glycoprotein laminin, preventing its binding to β1-integrin-subunits and thereby prohibiting cell adhesion and resulting in altered glia alignment and decreased number of migrating young neurons. Furthermore, we confirm the *in vivo* relevance of these findings in rats, where developmental exposure to EGCG reduces 5-bromo-2-deoxyuridine positive cells in brain cortical layers.

Conclusions: Our data raise the concern that intake of high-dose EGCG food supplements during pregnancy might disrupt normal brain development in humans.

Keywords: food supplements, extracellular matrix, adhesion, migration, neurospheres, DNT.

Introduction

Food supplements freely available as pills or liquids contain high amounts of plant extracts or their pure ingredients. Although general toxicities of such food supplements, like lethal doses killing 50 % of rodents are commonly known, specific toxicities concerning more subtle endpoints are in many cases understudied. One of these endpoints is developmental neurotoxicity, which has recently been recognized as a major threat for society by academia and regulators (Bal-Price et al. 2015; EFSAPPR 2013; Grandjean and Landrigan 2014). In this regard it is important to note that consumers consider herbal-based food supplements as healthy and safe and thus use them during pregnancy (Bishop et al. 2011; Forster et al. 2006; Moussally et al. 2009; Nordeng and Havnen 2004). However, they are not regulated to the same degree as pharmaceutical drugs (Abdel-Rahman et al. 2011).

The flavonoid epigallocatechin gallate (EGCG) is the most abundant catechin in green tea (Rothwell et al. 2013). EGCG has been drawing remarkable scientific attention for its potential health benefits in preventing and treatment of several chronic diseases including cancer (Hollman et al. 1999; Singh et al. 2011; Yang et al. 2009). It has also been preclinically tested for the prevention of the neurodevelopmental adverse effects related to the fetal alcohol syndrome (Long et al. 2010; Tiwari et al. 2010). Various cellular targets are discussed to promote the beneficial health effects of EGCG, which contribute to its actions on cell proliferation, adhesion and migration (Mineva et al. 2013; Shankar et al. 2008; Singh et al. 2011; Suzuki and Isemura 2001), but such cellular processes are also substantial for brain development (Holmes and McCabe 2001). The potential of EGCG to cause developmental neurotoxicity when taken at high doses far exceeding natural occurrence in tea, is yet not known.

Therefore, in this study, we evaluated if concentrations reached after maternal supplement EGCG intake pose a threat to the developing central nervous system (CNS). We report that *in*

vitro migration of rat and human neural progenitor cells (NPCs) growing as neurospheres is disturbed by EGCG displaying a specific 'arborized' phenotype. We provide evidence that EGCG (i) binds to the extracellular matrix (ECM) glycoprotein laminin, which (ii) prevents laminin binding to NPCs β1-integrin-subunits and thereby (iii) prohibits NPC adhesion resulting in (iv) altered glia alignment and reduction of the number of migrating young neurons. Accordingly, developmental exposure of rats to EGCG reduced 5-bromo-2-deoxyuridine (BrdU) positive cells in brain cortical layers *in vivo.*

Methods

Reagents. EGCG (>98 %) was purchased from TransMIT PlantMetaChem (Giessen, Germany). All other chemicals used (unless otherwise noted) were purchased from Sigma–Aldrich (Munich, Germany) and were of the highest purity available.

Cell culture. Human NPCs (Lonza Verviers SPRL, Belgium; gestational week 16 to 20) from 5 individuals were thawed and timed-matched rNPCs from PND 5 pups (Clancy et al. 2007) were isolated as previously described (Baumann et al. 2014). NPCs were cultured as floating neurospheres in "proliferation medium" [Dulbecco´s modified Eagle medium (DMEM) and Hams F12 (3:1) supplemented with B27 (Invitrogen GmBH, Karlsruhe, Germany), 20 ng/mL EGF (Biosource, Karlsruhe, Germany), 20 ng/mL recombinant human FGF (R&D Systems, Wiesbaden-Nordenstadt, Germany) or 20 ng/mL recombinant rat FGF (R&D Systems), 100 U/mL penicillin, and 100 µg/mL streptomycin] at 37 °C in a humidified 5% CO_2 incubator.

Assay conditions and chemical exposure. Migration, adhesion and differentiation studies were performed under differentiation conditions, consisting in withdrawal of growth factors and culture of neurospheres on a poly-D-lysine (0.1 mg/mL) and laminin (5 µg/mL) coated chamber slide or multiwell-plate. Differentiation medium composition was: DMEM and

Hams F12 (3:1) supplemented with N2 (Invitrogen), 100 U/mL penicillin, and 100 µg/mL streptomycin. Proliferation analysis was performed under proliferating conditions, consisting of free-floating neurospheres in "proliferation medium". A detailed description of assay conditions and the endpoint specific positive controls used to ensure proper assay performance is given in (Baumann et al. 2014).

Migration. ***Migration distance.*** Mean migration distance was analyzed after 24 or 48 h in culture as described in (Baumann et al. 2014; Moors et al. 2007). Briefly, neurospheres were exposed to EGCG or blocking antibody against β1-integrin (hamster IgM anti-rat CD29, BD Pharmingen, San Diego, CA, USA) or against β4-integrin (mouse IgG anti-human CD104, Millipore, Billerica, MA, USA) RGD peptide (GRGDS, Calbiochem, Darmstadt, Germany) or the respective isotype controls (hamster IgM isotype standard anti-trinitrophenol, BD Pharmingen; mouse IgG negative control clone 1E2.2, Millipore) and RAD control peptide (GRADSP, Calbiochem). A 1 h pre-incubation of floating spheres was applied to all experiments implying antibodies. ***Migration pattern.*** The corona of migrating cells around a sphere was evaluated by manual measurement of the angles covered by cells after 48 h in culture in 4 independent experiments and expressed in percentage of the total corona. Spheres were fixed with PFA 4% and stained with Hoechst to count the number of nuclei/µm² within the migration area using the "Analyze Particle" macro of ImageJ software (Rasband 1997-2013). The homogeneity of nuclei distribution was automatically evaluated using an algorithm implemented in Omnisphero software (www.Omnisphero.com) which subdivides the image into small boxes and counts the number of cells in each box. The mean differences (gradient) among adjacent boxes of the migration area are determined using the Matlab command imgradient (100 x solvent control gradient/ treatment gradient). ***Viability.*** Cell viability was evaluated by means of Alamar Blue metabolization using the CellTiter-Blue assay (CTB) (Promega, Mannheim, Germany) as described in (Baumann et al. 2014).

Western Blot Analyses. A detailed description of Western Blot Analyses is given in SI Methods.

Adhesion. Human neurospheres were dissociated by chopping to 0.1 mm squares and gently pipetting, re-suspended in differentiation medium and plated on PDL/laminin coated 96-well plates in presence or absence of flavonoids. After 1 h incubation at 37 °C and 5% CO_2, medium was aspirated and wells were washed with PBS+Ca^{2+}/Mg^{2+} (Gibco, Invitrogen). Adherent cells were quantified using the CTB assay.

Laminin-β1-integrin binding. Human neurospheres were incubated for 1 h in differentiation media containing 5 µg/mL laminin and increasing concentrations of EGCG in non-coated 96-well plates. Wells were washed with PBS+Ca^{2+}/Mg^{2+}, incubated for 1 h at 37°C and 5% CO_2 with hamster anti-β1-integrin antibody or isotype control (BD Pharmingen), washed, and incubated 1 h with FITC labeled anti-hamster antibody (BD Pharmingen). After final washing, fluorescence was measured (490/525 nm; Tecan) in three wells per concentration containing ten neurospheres each.

Immunocytochemistry and $GFAP^+$-processes angle measurement. A comprehensive description of the method applied is given in SI Methods.

Proliferation. A detailed description of the methods used to evaluate proliferation is given in SI Methods.

RNA Preparation, cDNA Synthesis, and Real-Time RT-PCR. A detailed description is given in SI Methods.

***In vivo* protocol.** The *in vivo* protocol was approved by the Universitat Rovira i Virgili (Tarragona, Spain) Animal Welfare and Ethics Committee. Sprague Dawley timed pregnant rats (Harlan Interfauna Iberica; Barcelona, Spain) were housed under standard conditions and daily monitored for general health during gestation and weaning. From GD 12 to 20, 7 and 8

pregnant rats received daily doses of 1g/kg body weight (b.w.) EGCG dissolved in distilled water by gavage or only distilled water, respectively. EGCG doses were adjusted to b.w. and freshly prepared daily. On GD 16, all dams received 50 mg/kg b.w. of BrdU intraperitoneally. On PND 0 all litters were culled to 6 pups, 3 males and 3 females. ***Brain samples collection and tissue sectioning.*** On PND 28 one male and one female per litter were anesthetized with 2% tribromoethanol (0.15 mL/10 g b.w. i.p.) and perfused with 4% paraformaldehyde (PFA). Brains were removed, post-fixed in 4% PFA for 48 h at 4°C and transferred into 30% sucrose/PBS for 48 h at 4 °C. Brains were fast frozen in isobutene at -80 °C and stored at -20 °C until sectioning. Serial-coronal 40 µM sections were cut with a cryostat (Leica CM 1850, Leica, Wetzlar, Germany*)*.

Immunohistochemistry and fluorescent image analysis. Brain slices from 5 control pups and 8 EGCG treated pups were evaluated. One out of 6 coronal sections (240 µm interspace) were used for $BrdU^+$ cells immunohistochemistry and Nissl fluorescent staining as detailed in SI Methods. Image analysis was performed in 10 images/animal and per area (PRh and DLEnt) on average, using the 'BrdeLuxe' tool for automatic counting and positioning of $BrdU^+$ cells in cortical layers of rat brain slices as previously described (Schmuck et al. 2014).

Statistics. All *in vitro* results are presented as mean ± SEM in % of solvent control (sc; DMSO 0.1%) of at least 3 independent experiments. To calculate effective concentration 50 (EC_{50}) data were fitted to a nonlinear sigmoidal concentration-response curve with GraphPad Prism 6 software. Data were analyzed by one-way ANOVA and Bonferroni's or Dunnett's post-hoc test for one factor analyses, two-way ANOVA and Bonferroni's post-hoc test for multifactor analyses. *In vivo* results were analyzed with Student's t test.

Results

EGCG disturbs migration of rat and human NPCs *in vitro* by interacting with the ECM glycoprotein laminin.

The cerebral cortex forms through tightly regulated processes, including proliferation of NPCs and migration of newly generated cells to reach their final destinations in cortical layers (Manent et al. 2011). One way of investigating specific NPC functions is the "neurosphere assay", which mimics neurodevelopmental processes *in vitro* (Baumann et al. 2014; Moors et al. 2007; Moors et al. 2009). This approach has the advantage that one can study compound's molecular and functional effects on NPC development across species (Baumann et al. 2014; Gassmann et al. 2010), because neurospheres are available from humans and rodents and their timing of development can be matched (Clancy et al. 2007).

EGCG did not affect rat (r) or human (h)NPC proliferation (S1A Fig), but reduced migration distance significantly without affecting viability (Fig 1A). In addition to the shortened migration distance, EGCG induced a unique, irregular migration pattern containing gaps in the migration corona in both species (inserts in Fig 1A). The presence of gaps was manually evaluated in hNPCs by quantification of gaps within the corona of migrating cells around a sphere (Fig 1B), and verified by an automatic evaluation of the homogeneity of nuclei distribution, indicating in both cases a concentration-dependent alteration of the migration pattern (Fig 1B). As a result of the decreased migration distance and the gaps/homogeneity alteration in the migration area, EGCG decreased the nuclear density of the hNPC migration area *in vitro* (Fig 1C).

To elucidate the molecular mechanisms underlying the disturbance of migration in hNPCs, we tested if the effects were related to EGCG's well-described antioxidant properties. This was not the case as hNPCs correctly migrated in presence of two other known antioxidants, vitamin C and trolox, (S1B Fig). Next, we assessed if EGCG interfered with normal migration by affecting MAP-kinase ERK1/2 phosphorylation (pERK1/2) as one described target of

EGCG (Yang et al. 2009) necessary for hNPC migration (Moors et al. 2007). Western blots indicated no change in pERK1/2 of EGCG-exposed hNPCs (S1C Fig). An involvement of the aryl hydrocarbon receptor was ruled out, as it is not present in human neurospheres (Gassmann et al. 2010). In addition to intracellular signaling pathways, we tested the hypothesis that EGCG might operate through interaction with the ECM protein laminin, which is one of the major brain ECM proteins necessary for NPC migration (Chen et al. 2009) and thus the regular coating protein employed in the neurosphere assay. We evaluated hNPC migration with three different EGCG exposure scenarios: exposure of the spheres and the ECM, exposure of the spheres only or exposure of the ECM only. EGCG disrupted migration of NPCs only in those scenarios where the ECM was exposed (Fig 1D). As EGCG has the ability of laminin binding (Suzuki and Isemura 2001), we postulated that it inhibits hNPC migration by prohibiting laminin-cell surface receptor interaction resulting in disturbed cell adhesion. In support of this assumption, increasing amounts of extracellular laminin antagonized EGCG-induced decreased migration and gap formation in the hNPC migration corona (Fig 1E).

EGCG and structurally related catechins inhibit hNPC adhesion to laminin.

To confirm that EGCG affects migration via impairment of cell adhesion, adhesion assays were performed. EGCG decreased adhesion of dissociated hNPCs plated in presence of EGCG for 1 h in a concentration-dependent manner (S2A Fig, S2B Fig). To gain further insight into structure-activity relationships of laminin-dependent adhesion inhibition, we studied flavonoids, which were structurally related to EGCG. Flavonoids containing either a galloyl group (epicatechingallate; EC**G**) or a pyrogallol group (epigallocatechin; E**G**C) impaired hNPC adhesion, but less potently than the E**G**C**G** containing both groups.

Flavonoids without these two residues, i.e. epicatechin (EC), hesperetin (H) and kaempherol (K) did not inhibit hNPC adhesion (S2B Fig).

Because cell migration requires cell adhesion as well as cell motility, we next studied by time-lapse microscopy over a time-course of 18 h if EGCG also affects NPC movement. The movie clearly shows that even 10 µM EGCG did not affect hNPC motility (S2C Fig and S1 Movie). These results indicate that EGCG decreases hNPC migration by interfering with cell-ECM adhesion, but not motility, due to the presence of its galloyl/pyrogallol residues.

EGCG prevents laminin binding to β1-integrin.

NPC adhesion to laminin primarily depends on integrins, a family of α/β heterodimeric transmembrane receptors (Hynes 2002). Most laminin-binding integrin dimers contain a β1- or, more rarely, a β4-subunit (Barczyk et al. 2010; Humphries et al. 2006). In agreement with Flanagan et al. (Flanagan et al. 2006) RT-PCR analyses revealed mRNA expression of these *β1*- and *β4-integrin* subunits in differentiated hNPCs (Fig 2A). Functional blocking antibodies against β1-integrin (Fig 2B) decreased hNPC migration and induced an irregular migration pattern with gaps in the migration corona just like the neurosphere phenotype observed after EGCG exposure (Fig 2C). This gap-bearing phenotype seems to be specific for neurosphere adhesion defects as compounds disturbing pathways involved in migration during development *in vivo,* methylmercury chloride (MeHgCl) and the src-kinase inhibitor PP2 (Moors et al. 2007), decreased hNPC migration distance *in vitro*, yet without inducing gaps in the migration corona (Fig 2D) (Moors et al. 2007). In contrast to the β1-integrin blocking antibody, functional blockage of β4-integrin by a blocking antibody or the RGD tripeptide did not interfere with hNPC migration (S1D,E Fig). The lack of effect of the RGD peptide on laminin-dependent migration was expected, as β1-containing integrin heterodimers recognize

the RGD peptide sequence of fibronectin, but not laminin (Barczyk et al. 2010; Humphries et al. 2006). Additional evidence that EGCG indeed binds to laminin thereby prohibiting β1-integrin binding was provided by the observation that EGCG increased immunofluorescent labeling of β1-integrin when spheres were incubated for 1 h in a solution containing laminin (Fig 2E).

We next wondered about the nature of the rat-human species difference in sensitivity towards EGCG-induced reduction in cell migration (Fig 1A). Real-time RT-PCR analyses revealed that *β1-integrin* subunit transcript levels are approximately 50% lower in hNPCs than in rNPCs (Fig 2F). We propose that this difference accounts for the roughly two-fold higher susceptibility of human vs rat neurospheres towards EGCG adhesion/migration inhibition (Fig 1A).

EGCG causes defective GFAP$^+$/Nestin$^+$ processes *in vitro* and decreases the number of βIII-tubulin$^+$ migrated cells.

A previous study by Graus-Porta et al. (Graus-Porta et al. 2001) reported on neurodevelopmental abnormalities of β1-integrin CNS conditional knockout mice. In particular, BrdU$^+$ cells labeled at gestational day (GD) 15.5 of such transgenic animals achieved appropriate positions in cortical layers, but cell bodies in the layers were "less tightly packed" (Graus-Porta et al. 2001). The authors attributed this defective cortical layer formation to faulty cortical radial glial processes not forming correct glia end-feet and meandering chaotically (Belvindrah et al. 2007). Therefore, we next studied if -similar to β1-integrin-deficient glia cells- EGCG also causes chaotic orientation of GFAP$^+$ processes in differentiated hNPCs. GFAP$^+$ processes of control human neurospheres were mainly oriented between 0° and ±30° angles towards the reference axis (Fig 3A and arrows in Fig 3B). In contrast, 24 h EGCG exposure caused a chaotic orientation of processes with a significantly

increased percentage of cells between ±30° and ±60° angles (Fig 3B,C). To study if the chaotic orientation of radial processes had consequences on the migration of a particular kind of differentiated cell, the fate of the cells in the migration area was evaluated every 24 h in a time-course study with neurospheres exposed to EGCG for 5 days (Fig 3D). Counting of the different cell types confirmed EGCG's adverse effects on the radial glia cell population as mainly the number of undifferentiated $Nestin^+$ cells was reduced. EGCG also reduced the $\beta III\text{-}tubulin^+$ cell population in the migration area but these effects appeared later in culture (after 72 h of exposure) and were less potent, while the $O4^+$ cell population was not significantly affected after 5 days of exposure (Fig 3D). Masking laminin by EGCG and thereby blocking β1-integrin-laminin binding thus produced an altered glia phenotype in the neurosphere assay and resulted in a consecutive reduced migration of young neurons *in vitro*.

Developmental exposure to EGCG *in vivo* reduces the number of $BrdU^+$ cells/μm^2 in two cortical areas of rat brain.

To confirm the *in vivo* relevance of these EGCG neurodevelopmental effects observed *in vitro*, pregnant rats were exposed for 9 days (GD 12-20) to EGCG and injected a single dose of BrdU i.p. on GD16. EGCG did not affect gestation length, litter size, sex ratio, pup weight, and pup survival, thereby confirming previous studies that did not reveal any general embryo-fetal toxicity or teratogenicity after EGCG exposure (Isbrucker et al. 2006). Cortical development of the offspring was evaluated by quantification of BrdU labeled cells on postnatal day (PND) 28 in two brain areas: the perirhinal cortex (PRh) and the dorsolateral entorhinal cortex (DLEnt) (Bayer 1990). An automated, unbiased BrdU-immunoreactive cell count (Schmuck et al. 2014) revealed that developmental exposure to EGCG significantly decreased the total number of $BrdU^+$ cells/μm^2 in PRh and DLEnt (Fig 4A,C) without altering the gross cortical structure or distribution of $BrdU^+$ cells among cortical layers (Fig 4B).

Discussion

The idea that herbal supplements are safe and healthy products is deeply seated in the general population; however, these products do not undergo the same strict research safety and effectiveness requirements than medical drugs (Abdel-Rahman et al. 2011), their growing use in general population has already been related with increasing adverse outcomes (Ekor 2013; Navarro et al. 2014), and their safety during the developmental period is currently understudied (reviewed by (Barenys et al. 2015)). We show here that EGCG alters neurodevelopment in human and rat NPCs *in vitro* by binding to the ECM protein laminin and in rats *in vivo*.

Human exposure and kinetics determine risk for neurotoxicity of compounds (Dorman et al. 2001). EGCG oral supplements offered for sale over the Internet contain up to 0.1 g EGCG/mL resulting in a 3 g dose when two spoons (15 mL/spoon) are ingested. Extrapolating from pharmacokinetic data of clinical studies in humans consuming 1.6 and 2 g EGCG/d result in maximum plasma concentrations of 7.4 and 8.7 μM, respectively [calculated from (Ullmann et al. 2003) and (Shanafelt et al. 2009)]. Considering that pregnant women weigh between 43 and 80 kg (Deeluea et al. 2013; Emanuel et al. 2004), maximum concentrations of EGCG achieved in pregnant women's plasma would range from 11.9 to 22.2 μM. The major EGCG metabolites, glucuronidated and sulfated EGCG conjugates, do not exceed 6-16% in maternal plasma (Wang et al. 2008) and therefore also not in the fetus as fetal liver contains only 23% of maternal glucuronidation. In contrast, fetal liver contains 53% of maternal β-glucuronidase capacity (Soucy et al. 2006) thus favoring the EGCG aglycone. Total EGCG is found at approximately 8 times lower concentrations in the fetus compared to maternal plasma when administered to pregnant rats and is well measurable in fetal brain (Chu et al. 2006). Assuming similar pharmacokinetics in pregnant rats and humans, which is

supported by comparable EGCG kinetics in non-pregnant individuals of different species (Chu et al. 2006; Shanafelt et al. 2009; Suganuma et al. 1998; Ullmann et al. 2003; Zini et al. 2006), EGCG concentrations in human fetal brain after a 3 g oral dose are expected to be around 1-3 μM. These concentrations are in the range of our observed LOAEC for disturbance of migration, adhesion and $GFAP^+$ process orientation. Thus, there is a strong indication that high-dose EGCG supplement intake during pregnancy might disturb human brain development.

EGCG decreases NPC migration distance and produces a specific "arborized" phenotype with alterations of the migration pattern resulting in decreased nuclear density in the hNPC migration area (Fig 1A-C). These migration defects observed in the neurospheres are caused by EGCG's interaction with the ECM glycoprotein laminin (Fig 1D, E). Such binding affinity of catechins, and specifically EGCG to laminin *in vitro* was founr to disturb cell adhesion in melanoma cells (Bracke et al. 1987; Suzuki and Isemura 2001) and rat NPCs (Chen et al. 2003). Here, to the best of our knowledge, we show for the first time, that EGCG affects hNPC adhesion (S2A, B Fig), but not motility (S2C Fig; S1 Movie) by direct interaction with laminin (Fig 1E, 2E). The moieties governing this EGCG-laminin binding seem to be galloyl/pyrogallol groups because catechins lacking these residues do not disrupt hNPC adhesion (S2B Fig). Cell adhesion to the ECM protein laminin in developing brains is mainly enabled by the laminin binding transmembrane proteins integrins and the 67-kDa-laminin receptor (LR-67) (Flanagan et al. 2006; Humphries et al. 2006; Nelson et al. 2008; Schmid and Anton 2003). Our data shows that EGCG disturbs NPC development by prohibiting laminin β1-integrin binding as: the (i) functional blocking β1- but not the β4-integrin antibody produced a neurosphere phenotype similar to EGCG treatment: shortened migration distance with gaps in the corona of migrating cells (Fig 2B-D) and (ii) EGCG antagonized soluble laminin binding to β1-integrin (Fig 2E). That the LR-67 was not involved in EGCG-induced

358 disturbance of hNPC adhesion was already excluded by the lack of direct EGCG-effect on the
359 spheres sparing matrix exposure (Fig 1B), because LR-67 is a cell surface EGCG receptor
360 (Umeda et al. 2008).

361 Developmental functions of β1-integrin have been studied in rodents. One of the
362 histopathological findings in mice lacking the β1-integrin subunit in neural precursor cells
363 (CNS-(nestin-Cre)-β1-integrin-deficient mice) is disturbed cortical development. These mice
364 develop faulty cortical radial glial processes not forming correct glia endfeet and meandering
365 chaotically through parts of the developing brain. As a consequence, cells are 'less tightly
366 packed' in cortical layers (Graus-Porta et al. 2001) and this glial phenotype is still maintained
367 *ex vivo* (Belvindrah et al. 2007). Because we unraveled that EGCG interferes with NPC
368 migration by disturbing β1-integrin-lamnin binding, we expected similar glial phenotype in
369 the "Neurosphere Assay" in presence of EGCG. Indeed, the polar plots in Fig 3 demonstrate
370 that in contrast to the untreated controls, $GFAP^+$ process orientation in EGCG exposed NPCs
371 revealed a significant and concentration-dependent increase in chaotic orientation (Fig 3B, C)
372 similar to the defective developing glia structure observed in CNS-(nestin-Cre)-β1-integrin-
373 deficient mice *ex vivo* (Belvindrah et al. 2007) and resulted in a consecutively reduced
374 migration of young neurons *in vitro* (Fig 3D).

375 Finally, in a proof-of-concept study we showed that prenatally EGCG-exposed rats present
376 less $BrdU^+$ nuclei/μm^2 in cortical layers than controls (Fig 4A). Tthe cellular distribution
377 among layers, however, was not affected (Fig 4B). These data confirms the *in vivo* relevance
378 of the *in vitro* observation that EGCG decreased the nuclear density in the hNPC migration
379 area (Fig 1C). With this *in vitro – in vivo* comparison we thus might be able to help predicting
380 developmental pathology by a neurosphere phenotype in a species-specific manner. For
381 prediction of hazards to humans, such species-specific susceptibilities based on molecular
382 signatures are of high relevance because there is increasing evidence -especially from

experiences in the drug development field- that human responses towards compounds can qualitatively or quantitatively differ from rodents (Leist and Hartung 2013). Here, we detected an approximately 2-fold higher sensitivity of human compared to rat NPCs towards EGCG-induced disturbance of NPC migration (Fig 1A), which might be due to the approximately 50% lower *β1-integrin* mRNA expression in hNPCs compared to rNPCs (Fig 2F). Implementing such data into the safety assessment process will help protecting human health.

Conclusions

In conclusion, we have shown that the use of high concentrated EGCG supplements during pregnancy should not be considered safe, as it is suspected to cause developmental neurotoxicity. Before new high-dose, EGCG-based therapeutic or preventive strategies are developed for pregnant women further *in vivo* comprehensive evaluation of the neurodevelopmental safety of this compound is clearly needed.

In addition, the endpoint adhesion/migration might be a valuable add-on to a potential *in vitro* testing strategy assessing compounds' effects on brain development.

References

Abdel-Rahman A, Anyangwe N, Carlacci L, Casper S, Danam RP, Enongene E, et al. 2011. The safety and regulation of natural products used as foods and food ingredients. Toxicol Sci 123:333-348.

Bal-Price A, Crofton KM, Leist M, Allen S, Arand M, Buetler T, et al. 2015. International stakeholder network (istnet): Creating a developmental neurotoxicity (dnt) testing road map for regulatory purposes. Arch Toxicol 89:269-287.

Barczyk M, Carracedo S, Gullberg D. 2010. Integrins. Cell Tissue Res 339:269-280.

405 Barenys M, Masjosthusmann S, Fritsche E. 2015. Is intake of flavonoid-based food
406 supplements during pregnancy safe for the developing child? A literature review. Curr Drug
407 Targets:In press.
408 Baumann J, Barenys M, Gassmann K, Fritsche E. 2014. Comparative human and rat
409 "neurosphere assay" for developmental neurotoxicity testing. Curr Protoc Toxicol:12.21. 11-
410 12.21. 24.
411 Bayer SA. 1990. Development of the lateral and medial limbic cortices in the rat in relation to
412 cortical phylogeny. Exp Neurol 107:118-131.
413 Belvindrah R, Graus-Porta D, Goebbels S, Nave K-A, Müller U. 2007. B1 integrins in radial
414 glia but not in migrating neurons are essential for the formation of cell layers in the cerebral
415 cortex. J Neurosci 27:13854-13865.
416 Bishop JL, Northstone K, Green J, Thompson EA. 2011. The use of complementary and
417 alternative medicine in pregnancy: Data from the avon longitudinal study of parents and
418 children (alspac). Complement Ther Med 19:303-310.
419 Bracke ME, Castronovo V, Van Cauwenberge RM, Coopman P, Vakaet Jr L, Strojny P, et al.
420 1987. The anti-invasive flavonoid (+)-catechin binds to laminin and abrogates the effect of
421 laminin on cell morphology and adhesion. Exp Cell Res 173:193-205.
422 Chen C-N, Liang C-M, Lai J-R, Tsai Y-J, Tsay J-S, Lin J-K. 2003. Capillary electrophoretic
423 determination of theanine, caffeine, and catechins in fresh tea leaves and oolong tea and their
424 effects on rat neurosphere adhesion and migration. J Agric Food Chem 51:7495-7503.
425 Chen Z-L, Haegeli V, Yu H, Strickland S. 2009. Cortical deficiency of laminin γ1 impairs the
426 akt/gsk-3β signaling pathway and leads to defects in neurite outgrowth and neuronal
427 migration. Dev Biol 327:158-168.
428 Chu KO, Wang CC, Chu CY, Chan KP, Rogers MS, Choy KW, et al. 2006. Pharmacokinetic
429 studies of green tea catechins in maternal plasma and fetuses in rats. J Pharm Sci 95:1372-
430 1381.

Clancy B, Finlay BL, Darlington RB, Anand K. 2007. Extrapolating brain development from experimental species to humans. Neurotoxicology 28:931-937.

Deeluea J, Sirichotiyakul S, Weerakiet S, Arora R, Patumanond J. 2013. Fundal height growth curve for underweight and overweight and obese pregnant women in thai population. ISRN Obstet Gynecol 2013.

Dorman DC, Allen SL, Byczkowski JZ, Claudio L, Fisher JE, Jr., Fisher JW, et al. 2001. Methods to identify and characterize developmental neurotoxicity for human health risk assessment. Iii: Pharmacokinetic and pharmacodynamic considerations. Environ Health Perspect 109 Suppl 1:101-111.

EFSAPPR. 2013. Scientific opinion on the developmental neurotoxicity potential of acetamiprid and imidacloprid. EFSA Journal 11:47.

Ekor M. 2013. The growing use of herbal medicines: Issues relating to adverse reactions and challenges in monitoring safety. Front Pharmacol 4.

Emanuel I, Kimpo C, Moceri V. 2004. The association of maternal growth and socio-economic measures with infant birthweight in four ethnic groups. Int J Epidemiol 33:1236-1242.

Flanagan LA, Rebaza LM, Derzic S, Schwartz PH, Monuki ES. 2006. Regulation of human neural precursor cells by laminin and integrins. J Neurosci Res 83:845-856.

Forster DA, Denning A, Wills G, Bolger M, McCarthy E. 2006. Herbal medicine use during pregnancy in a group of australian women. BMC Pregnancy Childbirth 6:21.

Gassmann K, Abel J, Bothe H, Haarmann-Stemmann T, Merk HF, Quasthoff KN, et al. 2010. Species-specific differential ahr expression protects human neural progenitor cells against developmental neurotoxicity of pahs. Environ Health Perspect 118:1571-1577.

Grandjean P, Landrigan PJ. 2014. Neurobehavioural effects of developmental toxicity. Lancet Neurol 13:330-338.

Graus-Porta D, Blaess S, Senften M, Littlewood-Evans A, Damsky C, Huang Z, et al. 2001. B1-class integrins regulate the development of laminae and folia in the cerebral and cerebellar cortex. Neuron 31:367-379.

Hollman PC, Feskens EJ, Katan MB. 1999. Tea flavonols in cardiovascular disease and cancer epidemiology. Proc Soc Exp Biol Med 220:198-202.

Holmes G, McCabe B. 2001. Brain development and generation of brain pathologies. Int Rev Neurobiol 45:17-41.

Humphries JD, Byron A, Humphries MJ. 2006. Integrin ligands at a glance. J Cell Sci 119:3901-3903.

Hynes RO. 2002. Integrins: Bidirectional, allosteric signaling machines. Cell 110:673-687.

Isbrucker RA, Edwards JA, Wolz E, Davidovich A, Bausch J. 2006. Safety studies on epigallocatechin gallate (egcg) preparations. Part 3: Teratogenicity and reproductive toxicity studies in rats. Food Chem Toxicol 44:651-661.

Leist M, Hartung T. 2013. Inflammatory findings on species extrapolations: Humans are definitely no 70-kg mice. Arch Toxicol 87:563-567.

Long L, Li Y, Wang YD, He QY, Li M, Cai XD, et al. 2010. The preventive effect of oral egcg in a fetal alcohol spectrum disorder mouse model. Alcohol Clin Exp Res 34:1929-1936.

Manent JB, Beguin S, Ganay T, Represa A. 2011. Cell-autonomous and cell-to-cell signalling events in normal and altered neuronal migration. Eur J Neurosci 34:1595-1608.

Mineva ND, Paulson KE, Naber SP, Yee AS, Sonenshein GE. 2013. Epigallocatechin-3-gallate inhibits stem-like inflammatory breast cancer cells. PLoS One 8:e73464.

Moors M, Cline JE, Abel J, Fritsche E. 2007. Erk-dependent and-independent pathways trigger human neural progenitor cell migration. Toxicol Appl Pharmacol 221:57-67.

Moors M, Rockel TD, Abel J, Cline JE, Gassmann K, Schreiber T, et al. 2009. Human neurospheres as three-dimensional cellular systems for developmental neurotoxicity testing. Environ Health Perspect 117:1131-1138.

Moussally K, Oraichi D, Bérard A. 2009. Herbal products use during pregnancy: Prevalence and predictors. Pharmacoepidemiol Drug Saf 18:454-461.

Navarro VJ, Barnhart H, Bonkovsky HL, Davern T, Fontana RJ, Grant L, et al. 2014. Liver injury from herbals and dietary supplements in the us drug-induced liver injury network. Hepatology.

Nelson J, McFerran N, Pivato G, Chambers E, Doherty C, Steele D, et al. 2008. The 67 kda laminin receptor: Structure, function and role in disease. Biosci Rep 28:33-48.

Nordeng H, Havnen GC. 2004. Use of herbal drugs in pregnancy: A survey among 400 norwegian women. Pharmacoepidemiol Drug Saf 13:371-380.

Rasband WS. 1997-2013. Imagej. Bethesda, md, USA: U.S. National institutes of health

Rothwell JA, Perez-Jimenez J, Neveu V, Medina-Remón A, M'Hiri N, García-Lobato P, et al. 2013. Phenol-explorer 3.0: A major update of the phenol-explorer database to incorporate data on the effects of food processing on polyphenol content. Database (Oxford) 2013.

Schmid RS, Anton E. 2003. Role of integrins in the development of the cerebral cortex. Cereb Cortex 13:219-224.

Schmuck M, Temme T, Heinz S, Baksmeier C, Mosig A, Colomina MT, et al. 2014. Automatic counting and positioning of 5-bromo-2-deoxyuridine (brdu) positive cells in cortical layers of rat brain slices. Neurotoxicology.

Shanafelt TD, Call TG, Zent CS, LaPlant B, Bowen DA, Roos M, et al. 2009. Phase i trial of daily oral polyphenon e in patients with asymptomatic rai stage 0 to ii chronic lymphocytic leukemia. J Clin Oncol 27:3808-3814.

Shankar S, Ganapathy S, Hingorani SR, Srivastava RK. 2008. Egcg inhibits growth, invasion, angiogenesis and metastasis of pancreatic cancer. Front Biosci 13:440-452.

506 Singh B, Shankar S, Srivastava R. 2011. Green tea catechin, epigallocatechin-3-gallate
507 (egcg): Mechanisms, perspectives and clinical applications. Biochem Pharmacol 82:1807-
508 1821.
509 Soucy NV, Parkinson HD, Sochaski MA, Borghoff SJ. 2006. Kinetics of genistein and its
510 conjugated metabolites in pregnant sprague-dawley rats following single and repeated
511 genistein administration. Toxicol Sci 90:230-240.
512 Suganuma M, Okabe S, Oniyama M, Tada Y, Ito H, Fujiki H. 1998. Wide distribution of
513 [3h](-)-epigallocatechin gallate, a cancer preventive tea polyphenol, in mouse tissue.
514 Carcinogenesis 19:1771-1776.
515 Suzuki Y, Isemura M. 2001. Inhibitory effect of epigallocatechin gallate on adhesion of
516 murine melanoma cells to laminin. Cancer Lett 173:15-20.
517 Tiwari V, Kuhad A, Chopra K. 2010. Epigallocatechin-3-gallate ameliorates alcohol-induced
518 cognitive dysfunctions and apoptotic neurodegeneration in the developing rat brain. Int J
519 Neuropsychopharmacol 13:1053-1066.
520 Ullmann U, Haller J, Decourt J, Girault N, Girault J, Richard-Caudron A, et al. 2003. A single
521 ascending dose study of epigallocatechin gallate in healthy volunteers. J Int Med Res 31:88-
522 101.
523 Umeda D, Yano S, Yamada K, Tachibana H. 2008. Green tea polyphenol epigallocatechin-3-
524 gallate signaling pathway through 67-kda laminin receptor. J Biol Chem 283:3050-3058.
525 Wang J-S, Luo H, Wang P, Tang L, Yu J, Huang T, et al. 2008. Validation of green tea
526 polyphenol biomarkers in a phase ii human intervention trial. Food Chem Toxicol 46:232-
527 240.
528 Yang C, Wang X, Lu G, Picinich S. 2009. Cancer prevention by tea: Animal studies,
529 molecular mechanisms and human relevance. Nat Rev Cancer 9:429-439.
530 Zini A, Rio DD, Stewart AJ, Mandrioli J, Merelli E, Sola P, et al. 2006. Do flavan-3-ols from
531 green tea reach the human brain? Nutr Neurosci 9:57-61.

532

533

534

535

536

537

538

539

540

541

542

543

544

545

546

547

548

549

550

Figure Legends

Fig 1. EGCG disturbs migration of rNPCs and hNPCs by interacting with laminin. (A) Rat and human neurospheres were cultured for 24 h with increasing concentrations of EGCG. Migration distance (black circles) and viability (by means of Alamar Blue metabolization; blue triangles), were measured in 5 neurospheres/concentration in 3 (rNPCs) and 5 (hNPCs) independent experiments. Results presented as mean ± SEM in % of solvent control (sc; DMSO 0.1%) and fitted to a nonlinear sigmoidal concentration-response curve with GraphPad Prism 6 to calculate EC_{50} values. *: $p<0.05$ vs. sc. Image inserts: representative neurospheres exposed to 10 µM EGCG. (B) Human neurospheres were exposed to increasing concentrations of EGCG. The corona of migrating cells around a sphere was evaluated after 48 h of exposure by manual measurement of the angles covered by cells in at least 5 neurospheres/concentration in 4 independent experiments and expressed in percentage of the total corona (mean ± SEM). *:$p<0.05$ vs. sc. The homogeneity of nuclei distribution was automatically evaluated after 24 h of exposure using Omnisphero software in 5 neurospheres/concentration in 4 independent experiments. Results expressed as mean ± SEM of 100 x sc / treatment. (C) Human neurospheres were exposed to increasing concentrations of EGCG for 48 h. The number of migrated nuclei of at least 5 spheres/concentration was counted and divided by the mean migration area occupied by control neurospheres in µm². Results expressed as mean ± SEM in % of sc of 3 independent experiments. (D) Representative microscopic phase-contrast images of hNPCs under conditions described on each picture row. Scale bar = 300 µm. (E) Migration distance in µm of hNPCs after 48 h exposure to increasing EGCG and laminin concentrations. Mean ± SEM of at least 3 independent experiments (5 spheres/condition). *: $p<0.05$ vs. respective sc. Image insert: representative neurospheres exposed to 5 µM EGCG at 50 µg/mL of laminin.

Fig 2. EGCG prevents laminin binding to integrin-β1. (A) RT-PCR of 48 h differentiated human neurospheres showed that they express *integrin-β1* and *-β4* mRNA (n.c.: negative control; p.c.: positive control, *β-actin*). (B) Human neurospheres were exposed to integrin-β1 antibody or isotype control antibody 1 h prior differentiation and during differentiation for 48 h (5 neurospheres/concentration). Mean ± SEM of at least 3 independent experiments in % of respective control. *:$p<0.05$ vs. respective isotype control. (C) Human neurospheres were exposed to increasing integrin-β1 antibody or isotype control antibody for 48 h. EGCG results presented in Figure 1B are included here for comparison. The corona of migrating cells around a sphere was measured in percentage in at least 5 spheres/concentration in 4 independent experiments. *:$p<0.05$ vs. sc; *:$p<0.05$ vs. respective isotype control antibody. (D) Representative images of human neurospheres exposed for 48 h to sc, EGCG (1 and 5 µM), the positive control PP2 (10 µM; src kinase inhibitor), the neurodevelopmental toxic compound MeHgCl (0.1 µM) or integrin-β1 antibody (20 µg/mL; scale bar = 300 µm). (E) Human neurospheres were incubated 1h in a 5 µg/mL solution of laminin with increasing concentrations of EGCG (3 wells/condition, 10 neurospheres/well). Integrin-β1 free subunits were immunofluorescently labeled with a FITC-antibody. Mean ± SEM of 3 independent experiments in % of control. (F) Human and rat control neurospheres were incubated for 48 h. Real-time q-PCR shows that basal mRNA expression of *integrin-β1* subunit is higher in rat neurospheres than in human neurospheres.

Fig 3. EGCG causes chaotic orientation of GFAP$^+$ processes *in vitro* and decreases the number of βIII-tubulin$^+$ migrated cells. (A) Schematic representation of the measurement of GFAP$^+$ processes orientation angle in a neurosphere migration area, showing the sphere core, the complete migration area, the GFAP$^+$ processes angle measurement area (area inside the black dotted lines), the reference axis (black arrow = 0°), three examples of GFAP$^+$ processes (red arrows) and the angle measurement (red arrows vs. black arrow). (B) Human neurospheres were exposed to increasing concentrations of EGCG for 24 h, fixed and immunostained for GFAP (red) and stained for Hoechst (blue). Representative pictures of the migration area showing the GFAP$^+$ processes angle measurement area (area inside the white dotted lines) and five examples of GFAP$^+$ processes angle orientation (white arrows; scale bar = 100 μm). (C) Color coded polar plot displaying the orientation of GFAP$^+$ processes in relation to the reference axis after exposure of human neurospheres to increasing concentrations of EGCG during 24 h. Horizontal angles (blue: -30 to 30°), oblique angles (yellow: 31° to 60° and -31° to -60°) or vertical angles (red: 61° to 90° and -61° to -90°). Results expressed in percentage of total angles measured (percentage axis in logarithmic scale from inner to outer ring). Data representing 3 to 4 independent experiments, where the angle of 350 GFAP$^+$ processes/concentration and experiment was measured on average. *, *: $p<0.05$ vs. respective sc angle group. (D) Human neurospheres were exposed to increasing concentrations of EGCG for 5 days, fixed and immunostained for βIII-tubulin, O4 and Nestin and counterstained for Hoechst. The total number of nuclei was automatically counted using the Spot Detector bioapplication V.4 of the vHCS-software (6586, Thermo Fischer) and the number of βIII-tubulin and O4 positive cells were manually counted using Omnisphero software. Cell counts of 5 spheres/concentration in 4 independent experiments are presented in absolute numbers combining all cell types, or in percentage of solvent control for single cell types. *: $p<0.05$ vs. solvent control.

Fig 4. Developmental exposure to EGCG in rats decreases the number of BrdU$^+$ cells in two brain cortical areas. 8 and 7 pregnant rats were exposed from GD 12 to 20 to 0 or 1000 mg/kg b.w. EGCG respectively and received 50 mg/kg b.w BrdU on GD 16. Offspring brains were collected on PND 28 and immunostained for BrdU and Nissl. (A) Number of BrdU$^+$ cells/μm^2 in perirhinal cortex (PRh) and dorsolateral entorhinal cortex (DLEnt). (B) Mean percentage of BrdU$^+$ cells per cortical brain layer in PRh and DLEnt. Results representing 10 pictures per animal and per area on average in 5 control and 8 EGCG treated pups. (C) Representative pictures of one control and one EGCG exposed PRh area.

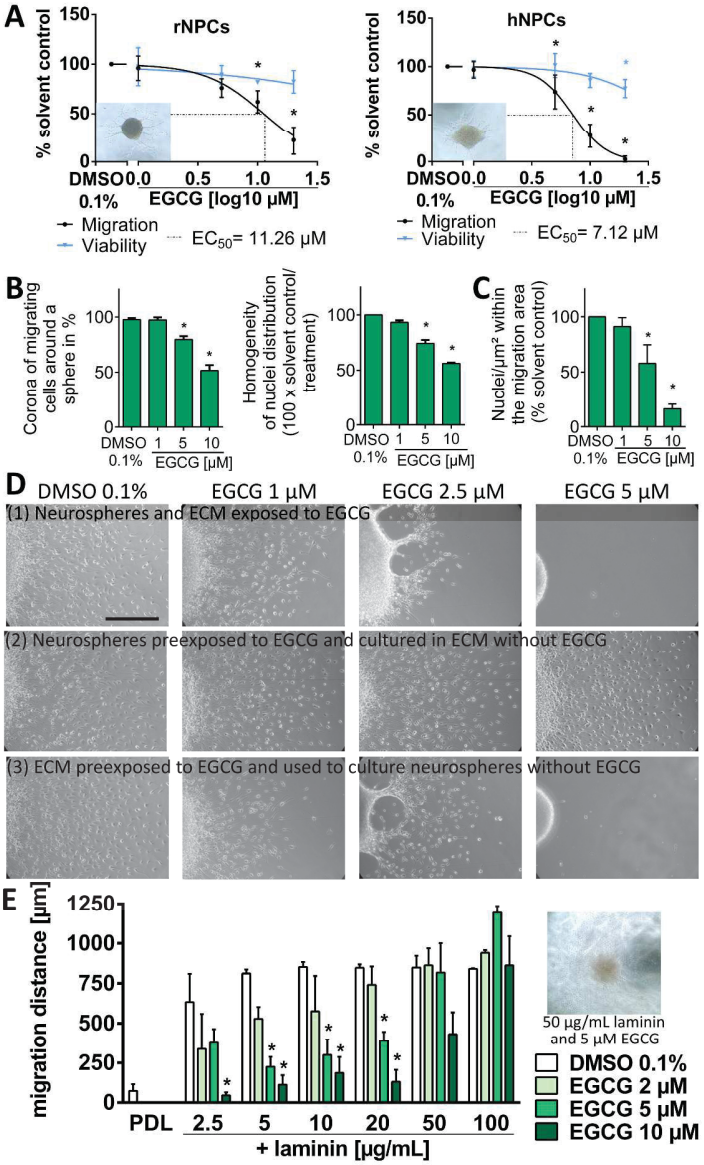

143x239mm (600 x 600 DPI)

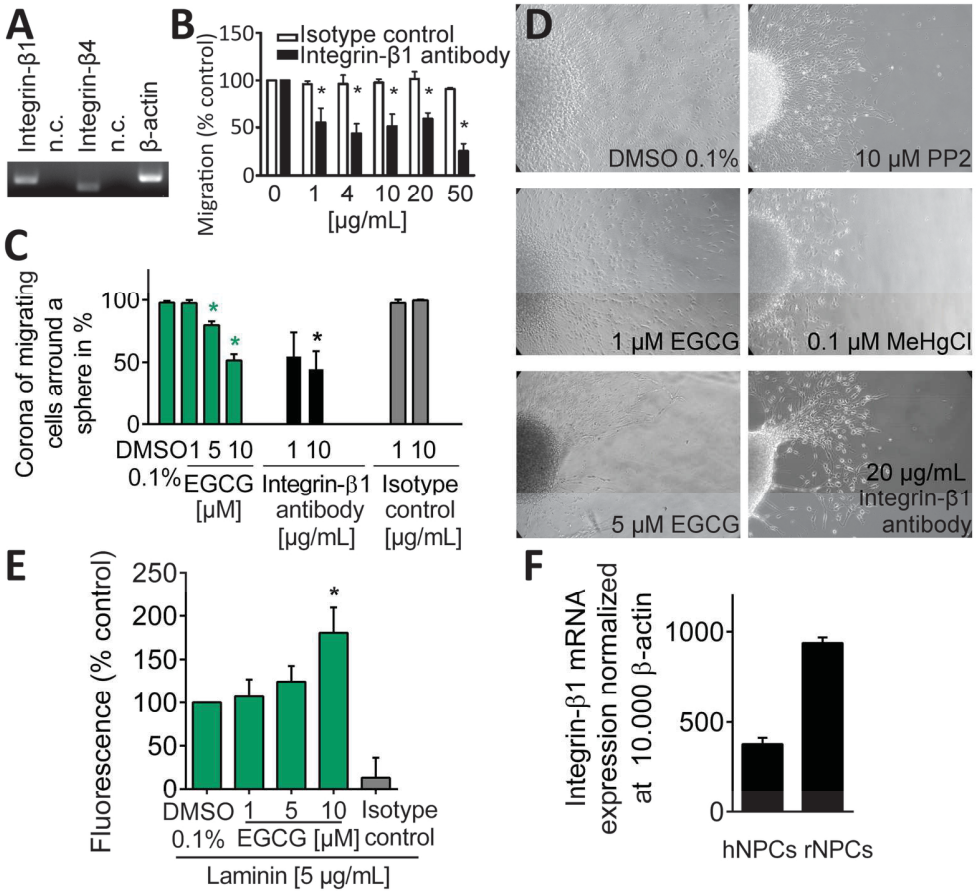

80x73mm (600 x 600 DPI)

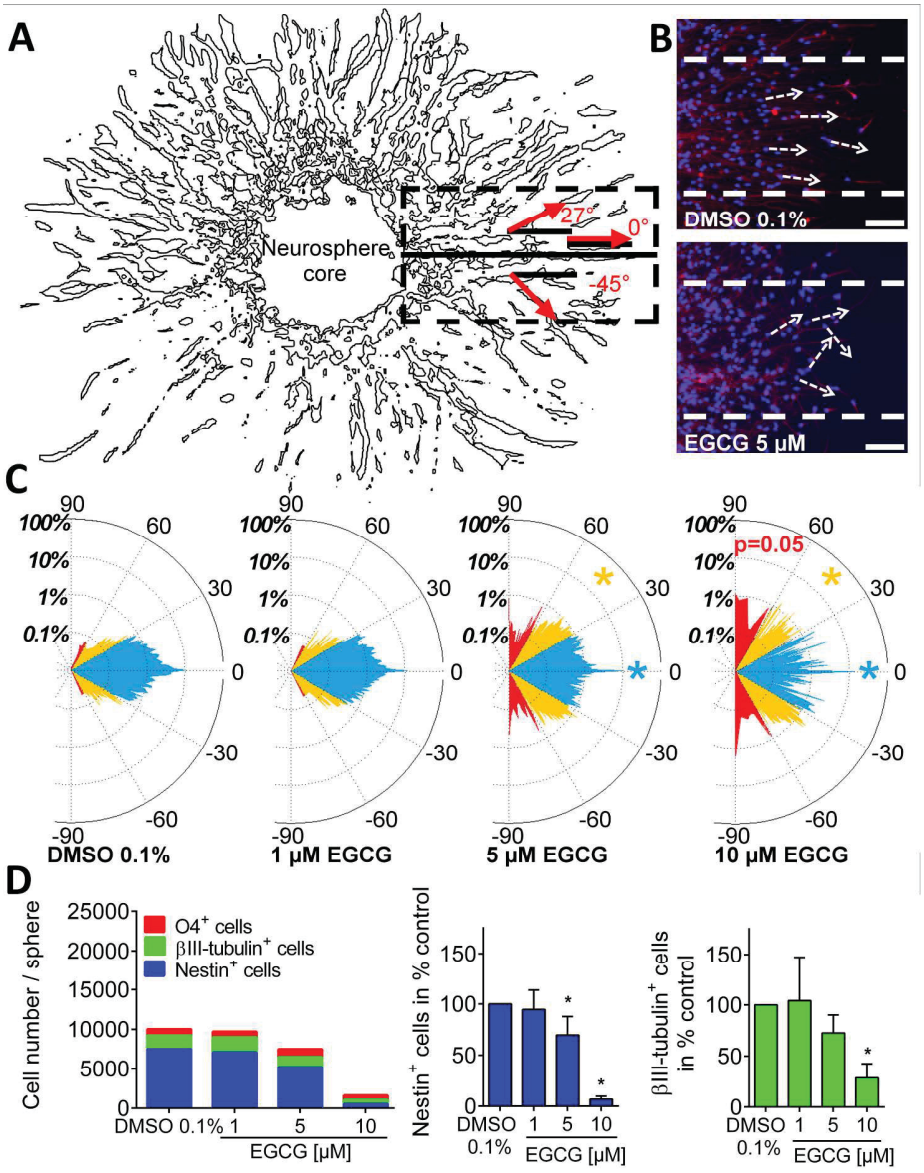

110x140mm (600 x 600 DPI)

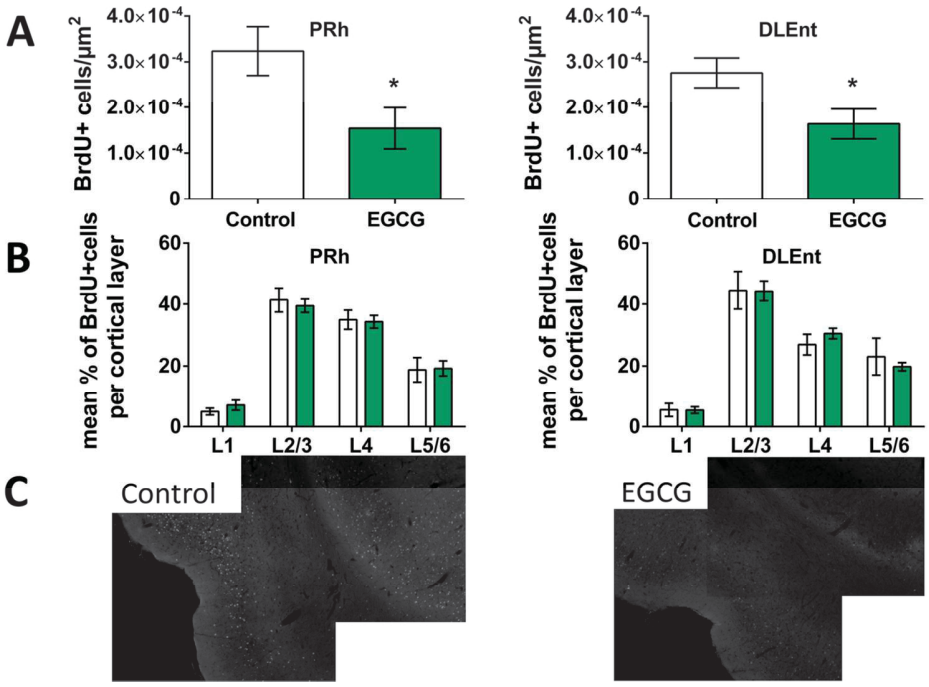

59x41mm (600 x 600 DPI)

Supporting information

Supporting figures captions

S1 Movie. Representative movie of a human neurosphere cultured for 18 h under differentiation conditions in presence of EGCG (10 μM) showing NPC motility.

S1 Fig. Lack of significant effects of EGCG on proliferation and intracellular signaling in NPCs and lack of significant effects of integrin-β4 antibody on hNPC migration. (A) Proliferation of rat and human neurospheres cultured with increasing concentrations of EGCG was measured by means of diameter increase (black circles; 7 d in culture) and BrdU incorporation (blue triangles; 3 d in culture), in 6 neurospheres/concentration in 3 (diameter increase) and 7 (BrdU incorporation) independent experiments. Results are presented as mean ± SEM in % of solvent control (DMSO 0.1%) and fitted to a nonlinear sigmoidal concentration-response curve with GraphPad Prism software. Data analyzed with one-way ANOVA and Bonferroni's posthoc test. **(B)** Human neurospheres were exposed to increasing concentrations of trolox and vitamin C for 48 h. Data represent mean migration in % control ± SEM of 3 independent experiments (with 5 spheres/condition each). Statistical analysis: one-way ANOVA and Bonferroni's posthoc test. **(C)** Human neurospheres were exposed to 10 μM EGCG or solvent control (DMSO 0.1%) for 24 h. Whole cell lysates were analysed for ERK1/2 activation by western blot. P-ERK1/2 analyses were normalized to GAPDH expression and expressed relative to control levels as mean ± SEM. of three independent experiments. **(D and E)** Human neurospheres were exposed to increasing concentrations of integrin-β4 antibody or isotype control antibody, RGD or RAD as control peptide, for 1 h prior differentiation and during differentiation on laminin coated slides for further 48 h (5 neurospheres/concentration). Data represent the mean ± SEM of at least 3 independent experiments as % of respective control. Statistical analysis performed with two-way ANOVA and Bonferroni post-hoc test.

S2 Fig. EGCG and structure related catechins inhibit hNPCs adhesion to laminin. (A) Human neurospheres were mechanically dissociated and exposed for 1 h to increasing concentrations of EGCG (6 wells/concentration). Representative microscopic phase-contrast images showing the remaining adherent cells after 1 h of exposure and washing step (scale bar = 100 μm). **(B)** Adhesion was measured by means of Alamar Blue metabolization after 1 h of exposure at increasing concentrations of EGCG and other flavonoids. Adhesion expressed in % of sc and presented as mean ± SEM of at least 3 independent experiments (6 wells/concentration). *: $p<0.05$ vs. respective sc; #: $p<0.05$ vs. respective EGCG concentration. EGCG: epigallocatechingallate; ECG: epicatechingallate; EGC: epigallocatechin; EC: epicatechin; H: hesperetin; K: kaempherol. **(C)** Human neurospheres were exposed to increasing concentrations of EGCG for 18 h. Representative images of four time-points of a neurosphere exposed to 10 μM EGCG showing cell movement (black arrows). See S1 Movie covering the complete incubation period (scale bar = 200 μm).

Supporting information Methods

Real-time PCR. Total RNA was isolated from 48h differentiated rat or human neurospheres using the RNEasy® Mini Kit, (Qiagen, Hilden, Germany) according to the manufacturer's instructions. RNA samples were reverse transcribed at 42 °C for 30 m and the reaction was inactivated at 95°C for 3 m. Real-time PCR was performed by using the Rotor-Gene Q Thermocycler (Qiagen) the PCR mix consisted of 7.5 µL of QuantiTect SYBR green PCR Master Mix (Qiagen), 4 µM solutions of each primer, 3 µL of cDNA, and 2.5 µL DEPC water. The application started with an initial incubation step of 15 m at 95°C to activate the DNA polymerase. The conditions for PCR amplifications were 50 cycles of 20 s at 95°C for denaturation, 20 s at 56°C for primer annealing and 20 s at 72°C for elongation and fluorescence detection. PCR-primer sequences for human and rat homologue integrin-β1, integrin-β4, and β-actin are given in the Supplementary Table 1. PCR products were quantified using the Rotor Gene Q 1.7 (Qiagen) software and calculated from fragment-specific standard curves prepared using 1.5 × 102 to 1.5 × 106 complementary DNA copies per µl and amplified as described above. For qualitative determinations, fragments were separated on a 2% agarose gel containing midori green (Nippon Genetics, Düren, Germany) and visualized under ultraviolet light.

Immunohistochemistry and fluorescent image analysis. For every animal brain slices with an interspace of 240 µm were used for immunohistochemical analysis. Free floating coronary sections were washed two times for 5 m in Tris buffered saline (TBS) and incubated with 2 M HCl for 30 m at 37 °C to denaturize DNA. After neutralizing for 10 m in 0.1 M sodium borate buffer (pH = 8.5) sections were permeabilized with TBS-plus (TBS containing 1 % Triton-X 100 and 3 % goat serum) for 30 m and incubated overnight at 4°C with a rat anti BrdU Monoclonal Antibody (1:500; AbD Serotec, Oxford, UK) diluted in TBS-plus. On the next

92 day, sections were incubated for 2 h at RT with a Cy3-coupled secondary antibody (Dianova,
93 Hamburg, Germany) 1:250 dilution in TBS-plus, permeabilized with PBS-Triton (PBS-T;
94 PBS containing 0.1% Triton X-100) for 10 m and incubated for 20 m at RT with a 1:100
95 fluorescent dye (NeuroTrace Fluorescent Nissl stain; Life Technologies, Darmstadt,
96 Germany) dilution in PBS. Finally, sections were washed in PBS over night at 4°C, placed in
97 0.1 M PBS, transferred to microscope slides (Superfrost, Menzel GmbH & Co KG,
98 Braunschweig, Germany) and mounted in mounting medium (Aqua Poly Mount, Polysciences
99 Inc, Eppelheim, Germany).

100

101 **Proliferation.** Proliferation was assessed using two different methods. Diameter increase.
102 Neurosphere diameter was microscopically determined every 2-3 days for a 7 d period under
103 proliferation conditions. Neurospheres cultured without growth factors served as negative
104 control (Moors et al., 2009). At the end, cell viability was measured using a CTB assay. BrdU
105 incorporation. For quantification of NPC proliferation the Cell Proliferation ELISA, BrdU
106 (chemiluminescent, Roche, Mannheim, Germany) was used according to the manufacturer's
107 instructions with a BrdU incubation period of 16 h, as described in (Baumann et al., 2014).

108 Western Blot Analyses. Proteins were isolated from hNPC differentiated for 0 m, 30 m, 1 h, 2
109 h, 4 h, 6 h, 9 h, 12 h, 18 h and 24 h in presence of 10 µM EGCG as described in Moors et al.
110 (Moors et al., 2007). Whole-cell lysates were separated by 10% SDS-PAGE and transferred to
111 an Amersham Hybond-P-membrane (GE Healthcare, Chalfont St. Giles, UK). The membrane
112 was blocked in Tris-buffered saline containing 0.01% Triton (v/v) and 5% (w/v) nonfat dry
113 milk for 1 h at RT, followed by incubation in the same buffer containing a rabbit anti-P-
114 ERK1/2 antibody (1:1,000; Biosource) or an anti-GAPDH antibody (1:200,000; Biozol,
115 Eching, Germany) overnight at 4°C. As secondary antibodies we used enhanced
116 chemiluminescence (ECL) anti-rabbit IgG or ECL anti-mouse IgG horseradish peroxidase–

linked antibodies (both 1:5,000; GE Healthcare). Chemiluminescence signals were detected with X ray film. Bands were scanned and quantified with the programme QuantityOne (BioRad, Munich, Germany).

Immunocytochemistry and GFAP$^+$-processes angle measurement. After differentiation for 24 h, human neurospheres were fixed for 30 m at 37°C in 4% PFA and stored in PBS at 4°C until immunostaining was performed as follows: neurospheres were incubated for 1 h at 37°C with a rabbit IgG anti-GFAP antibody (1:100; Sigma-Aldrich) in PBS-T (PBS containing 0.1% Triton X-100), followed by a 30 m incubation at 37°C with Hoechst 33258 (1:100; Sigma-Aldrich) and Alexa Fluor 546 anti-rabbit secondary antibody (1:100; Life Technologies) in PBS. The orientation angle respect the perpendicular direction from the sphere core was measured for at least 75 GFAP+-processes per neurosphere. Cell type analysis was performed every 24 h in human neurospheres differentiated for 5 days. Neurospheres were fixed for 45 m at 37°C in 4% PFA and immunostained as follows: spheres were incubated overnight at 4°C with a mouse IgM Oligodendrocyte Marker O4 MAb (1:200; Clone O4), in PBS, followed by a 30 m incubation at 37°C with Hoechst 33258 and Alexa Fluor 488 goat anti-mouse secondary antibody (1:250) in PBS. After a second fixation of 45 m in 4% PFA, neurospheres were incubated for 1 h at 37°C with a rabbit anti-βIII-tubulin antibody (1:200; Sigma Aldrich), followed by a 30 m incubation at 37°C with Hoechst and Alexa Fluor 546 goat anti-rabbit secondary antibody (1:200) in PBS. Neurospheres were incubated overnight at 4°C with a mouse anti-human-nestin antibody conjugated with Alexa 647 (1:20; BD Bioscience) in PBS. Cell type quantification of four independent experiments was performed with the Omnisphero software (www.Omnisphero.com). Cell types were quantified within two extracts of the migration area with a manual counting tool. The total number of cells for each cell type was calculated by the program using the automatically

142 counted total number of nuclei and the number of cells manually quantified within the two
143 extracts.

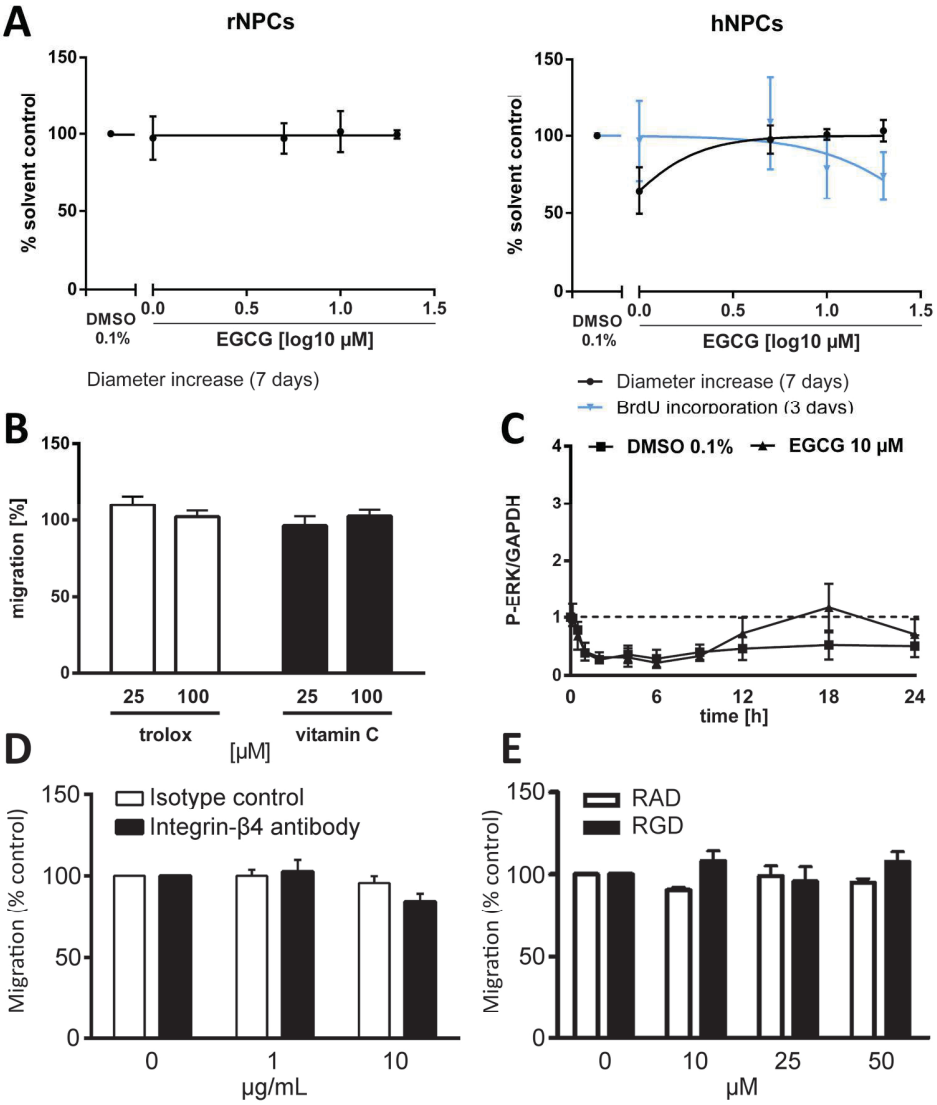

99x114mm (600 x 600 DPI)

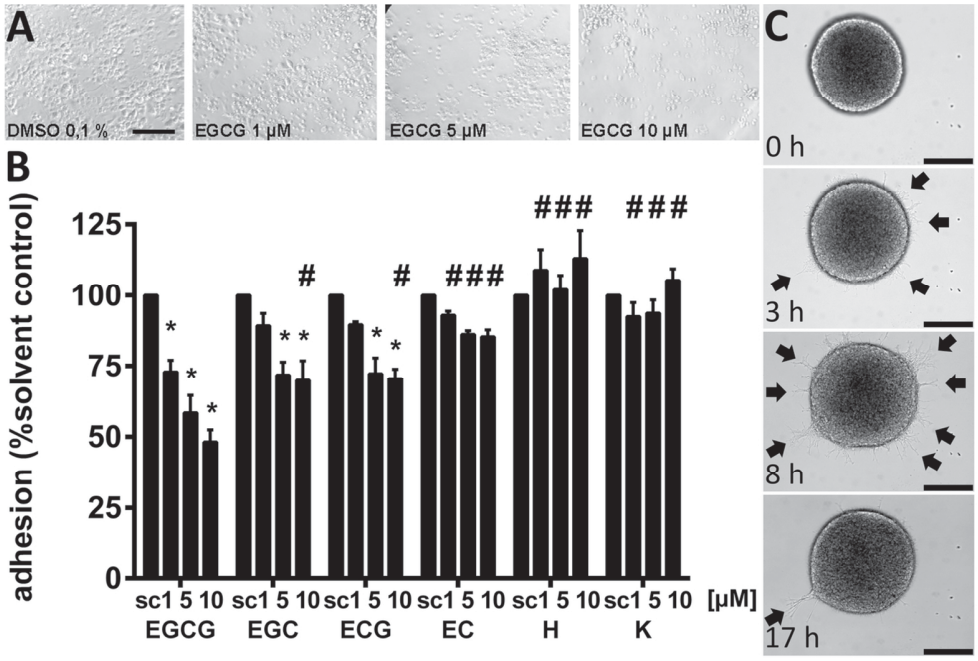

58x39mm (600 x 600 DPI)

Developmental Neurotoxicity of Epigallocatechin Gallate (EGCG) Is Triggered by Interference with β1-Integrin Function in Human Neural Progenitor Cells.

M. Barenys*, K. Gassmann*, C. Baksmeier, S. Heinz, I. Reverte, M. Schmuck, T. Temme, F. Bendt, T. C. Zschauer, T. D. Rockel, K. Unfried, W. Wätjen, S. M. Sundaram, H. Heuer, M. T. Colomina, E. Fritsche

* Shared first authors

Journal:	Environmental Health Perspectives
Impact factor:	7.98
Contribution to the manuscript:	15% Conduction of experiments involving triple stainings, image analyses, development of algorithms for assessment of migration pattern, review of the manuscript
Type of authorship:	co-author
Status of manuscript:	Submitted on: 08.09.2015

3. Discussion

Developmentally neurotoxic substances present a serious risk for society making testing of any kind of registered chemical indispensable. Therefore, stakeholders from academia, industries and governments recently agreed on the importance of toxicological safety testings for DNT (Bal-Price et al. 2015a). However, out of thousands of chemicals, which are already on the market, 214 are known to be neurotoxic and only 12 to be DNT compounds (Grandjean and Landrigan 2014). This lack of data - especially on compounds' abilities to interfere with brain development - can be attributed to the fact that DNT risk assessment for humans according to the OECD testing guideline 426 and the U.S. EPA guideline OPPTS 870.6300 (OECD 2007; USEPA 1998) requires animal experiments with large numbers of animals resulting in a tremendous time effort and high cost and are thus rarely performed (Crofton et al. 2012). To lower the time effort, the costs for general toxicological safety testing and to help priorizing substances for further animal testing a new toxicity testing paradigm was introduced based on *in vitro* systems in combination with novel technologies (Collins et al. 2008; NRC 2007). The outcome of such screenings is crucially dependent on the applied *in vitro* systems and should therefore reflect the human *in vivo* situation as closely as possible (Gibb 2008). In this regard neurospheres consisting of primary NPCs are a promising *in vitro* system for DNT testing because they are able to mimic basic processes of brain development, consist of a heterogeneous population of cells, which seem to equal the physiological distribution in the brain (Baumann et al. 2014) and have a 3D architecture which to some extent reflects the tissue environment (Pampaloni et al. 2007). In order to perform safety and efficacy substance screenings within those *in vitro* systems novel technologies like HCA are required to screen for alterations of relevant endpoints and/or critical toxicity pathways. However, screening of chemicals utilizing 3D neurospheres by employing HCA requires advanced scanning and evaluation processes which is due to characteristic features of the culture: 1) A 3D sphere core, which leads to unfocused images, 2) a variable cell density within the migration area, 3) a heterogonous cell population of neurons and glia cells and 4) neurosphere-specific endpoints. Therefore, the scope of this thesis was the establishment of medium throughput HCA workflows for DNT testing with the Neurosphere Assay. This requires the establishment of staining protocols in 96-well plates for all relevant cell types, scanning protocols and development of HCA algorithms. HCA algorithms have to cover classical endpoints like neuronal quantification and neuronal morphology in high density heterogeneous cell populations as well as the identification of endpoints involving the spatial distribution of cells within the entire well, like migration distance and neuronal density distributions. Furthermore, it is desirable to also assess endpoints like NPC distributions *in vivo* with HCA algorithms to facilitate *in vitro* and *in vivo* effect comparisons of compounds.

3.1. HCA for medium throughput DNT substance screening in the Neurosphere Assay

The development of an alternative, mechanism-based testing paradigm for DNT testing comparable to those described in Tox21 is highly desirable to lower costs and improve compound throughput (Crofton et al. 2012). One method to achieve this goal are HCA substance screenings. Thereby, the scientific information level of HCA DNT screenings is crucially dependent on critical factors: (a) The applied *in vitro* system, (b) robust sample preparation procedures and image acquisition and (c) reliable HCA algorithms for analyses of relevant endpoints.

a) Choosing an appropriate *in vitro* system:

The relevance of the extracted information from HCA medium throughput DNT substance testing is directly linked to the type of investigated *in vitro* system. The applied *in vitro* system has to reflect the human *in vivo* situation and therefore has to fulfill several criteria: (I) it has to mimic DNT-relevant endpoints (Breier et al. 2010), (II) it should be well characterized in terms of sensitivity, specificity and predictivity (Crofton et al. 2011), (III) it has to be robust (Wilson et al. 2014) and (IV) the investigated *in vitro* system should be suitable for medium to high throughput screenings (Breier et al. 2010).

Currently, applied *in vitro* systems in neurotoxicty and DNT studies comprise transformed cell lines like human SH-SY5Y and rat PC12 cells (Radio et al. 2010; Wilson et al. 2014), primary neuronal cultures like primary rat cortical neurons (Harrill et al. 2013), transformed neural precursor cells like LUHMES cells (Krug et al. 2013), co-culture systems from primary hippocampal neurons and astrocytes (Anderl et al. 2009), stem-cell-derived neural progenitor cells (Breier et al. 2010) and embryonic stem cell (ESC)-derived hN2^{TM} cells (Harrill et al. 2010; Wilson et al. 2014).

While every model serves useful purposes, all have some significant drawbacks as models of the developing nervous system (Coecke et al. 2007). Most systems can only mimic limited number endpoints and the complexity of some systems will lower substance throughput. Both, PC12 and SH-SY5Y possess neurite outgrowth, so that chemical effects on this process can be studied (Das et al. 2004; Påhlman et al. 1984). With these tumor cell lines (Greene and Tischler 1976; Påhlman et al. 1984), HCA assessment of neurite outgrowth is routinely performed (Radio and Mundy 2008; Radio et al. 2010; Wilson et al. 2014). However, the obtained neuronal phenotypes are often different from those found *in vivo* and only the SH-SY5Y cells form functional synapses and are therefore potentially suitable to study late fetal developmental endpoints such as synaptogenesis and electrical network

formation (Påhlman et al. 1990). However, due to lack of glia cells in such cultures, also physiological synapse formation is limited (Ullian et al. 2001). Differentiation *in vivo* requires cell cross-talk in addition to differentiation factors resulting in a differentiation into either the glia or neuronal lineage. Therefore, these *in vitro* systems do most likely not accurately describe the physiological processes of early fetal development like proliferation and neuronal as well as glial differentiation. In addition, the fact that different neuroblastoma cell lines show distinct susceptibilities towards the same chemicals already indicates the challenge in interpreting results from such models (Radio and Mundy 2008). Primary rodent cell cultures represent an excellent *in vitro* system to study neurite outgrowth and functional network activity (Harrill et al. 2011a, 2011b, 2013), but contain in many cases populations of post-mitotic neurons and are therefore missing the developmental endpoints of proliferation and differentiation. Furthermore, due to their rodent origin, an extrapolation towards the human *in vivo* situation might be difficult (Abbott et al. 1999; Gassmann et al. 2010; Leist and Hartung 2013). Co-culture systems from rodent primary hippocampal neurons and astrocytes are closer to the *in vivo* situation due to the presence of astrocytes, but still contain post-mitotic neurons (Anderl et al. 2009). ESCs and NPCs offer the possibility to study effects of substances on differentiation processes into any neuroectodermal cell type present in the brain and to perform a species comparison between humans and rodents (Baumann et al. 2015). However, ESCs like hN2^{TM} cells are cultured two dimensionally, which is not the ideal situation for cultured cells since cell physiology is significantly altered in 2D cultures compared to the 3D tissue architecture (Alépée et al. 2014; Cukierman et al. 2001; Yamada and Cukierman 2007). One example for a 3D *in vitro* system is the so called ‘neurosphere system’ consisting of primary NPCs. Such organoid cell clusters are able to mimic a variety of endpoints relevant for neurodevelopment *in vitro*: NPC proliferation, migration, differentiation into neurons, astrocytes and oligodendrocytes as well as apoptosis (Baumann et al. 2014; Breier et al. 2010; Fritsche et al. 2005, 2011; Moors et al. 2007, 2009, 2010). Applying such organoids in the Neurosphere Assay allows detection of disturbances of these processes *in vitro* (Gassmann et al. 2010; Moors et al. 2007, 2009; Schreiber et al. 2010). Due to the three dimensionality, the ability to differentiate into a heterogeneous cell population and the human origin, neurosphere cultures might reflect human physiology better than tumor, rodent, or cells grown in 2D (Breier et al. 2010; Yamada and Cukierman 2007). However, a significant drawback of primary *in vitro* cell systems is their limited availability and ethical concern going along with their use (Breier et al. 2010). Therefore, induced pluripotent stem cells (iPSCs) are a promising alternative as a source to generate NPCs overcoming the limitations of availability and ethical concerns (Barker and de Beaufort 2013). Furthermore the fact that these cells can be derived from patients with various

mutations will allow to generate progenitor cells with disease-specific phenotypes (Brannen and Sugaya 2000; Hossini et al. 2015; Kim et al. 2014).

Besides physiological relevance, the applied system has to be suitable for medium to high throughput and has therefore to be robust. The importance of medium to high throughput becomes evident by the fact that only a small part of the chemicals in circulation were tested for their DNT potential (Grandjean and Landrigan 2014). Many studies showed the advantage of automated plating and exposure of cells yielding a very high throughput (Reif et al. 2015). Beside the high substance throughput automated sample preparation and analysis have the advantage to eliminate experimenter-dependent factors like cell sorting, manual image analysis and manual pipetting of substances. In a case study by Reif et al. (2015) a high throughput screening using established HCA applications was conducted for the ToxCast I library for relevant DNT endpoints like proliferation in primary CX neural progenitor cells and neurite outgrowth in the immortalized PC12 cells. The clear advantage of these cell lines lies in their robustness, which makes them easy to handle in automated plating systems. Therefore, experiments showed a very low variance. In a study conducted by Wilson and co-workers (2014) three different neuronal *in vitro* systems, primary neural progenitor hN2^{TM} cells and the immortalized SH-SY5Y and PC12 cells, were tested in chemical screens for neurotoxicity each delivering different toxic profiles obtained by heatmaps and clustering analysis (Wilson et al. 2014). The physiologically more relevant hN2^{TM} cells were shown to be much more sensitive in handling compared to the SH-SY5Y and PC12 cells (Wilson et al. 2014). Whether the difficulties in handling of primary cell lines like hN2^{TM} can be outweighed by better prediction towards the human *in vivo* situation compared to the rat pheochromocytoma cell line PC12 or the human neuroblastoma line SH-SY5Y has to be studied by screening higher numbers of substances with different MOAs. However, all cell lines described above are 2D and can only mimic one or two of the relevant DNT endpoints. Therefore using 3D systems covering a larger set of relevant endpoints is highly desirable to reduce the number of assays, which have to be performed and to allow crosstalk between different cell types. An overview of a selection of different endpoints that can be measured with different cell systems is given in Table 1 (modified after Bal-Price et al. 2012).

Table 1: Overview of a selection of DNT-relevant endpoints assessible with different cell systems (modified after Bal-Price et al. 2012)

	Apoptosis	Proliferation	Differentiation	Neurite outgrowth	Migration	Synapto-genesis
SH-SY5Y (2D)	+	-*	(+)	+	-**	+
PC12 (2D)	+	-*	(+)	+	-**	-
Primary cortical neuron cultures (2D)	+	-	-	+	-**	+
Primary cortical neuron and astrocyte cultures (2D)	+	-	-	+	-**	+
LUHMES (2D)	+	-*	(+)	+	-**	+
ReNcell CX	+	+	+	+	-**	+
hN2^{TM} (2D)	+	+	+	+	-**	+
NPCs (3D)	+	+	+	+	+	+

Legend: +: endpoint can be assessed; -: endpoint cannot be assessed; (+): Induced differentiation by factors like nerve growth factors (NGF) and retinoic acid; *: Proliferation is generally assessable only for the undifferentiated tumor cell lines or v-myc-overexpressing LUHMES cells, not after induction of differentiation; **: Migration for all cell types can be studied by scratch assays, which however does not reflect the guided migration present in the 3D neurosphere system.

b) HCA workflow part I: Sample preparation and image acquisition

Besides choosing an adequate *in vitro* system, a suitable workflow has to be available to perform a medium to high throughput HCA screening. Robust sample preparation procedures and image acquisition require automated plating and exposure, cytotoxicity tests, reliable staining protocols and robust image acquisition algorithms.

HCA medium throughput DNT substance screenings in the 3D Neurosphere Assay require adjusted workflows (Fig. 8) due to the 3D architecture of the neurosphere core and the spatial distribution of cells within the entire well. The adjusted workflow starts with the sample preparation and initial quality controls. In case of 3D *in vitro* systems automated sorting and plating is much more challenging compared to their 2D counterparts. While there are some approaches for automated cell sorting using large particle sorters like the Copas Instrument (Union Biometrica; Gassmann et al. 2012), such automated plating still remains challenging and time consuming. The challenge of automated plating lies in correct positioning of neurospheres within a given well to ensure sufficient migration space (Fig. 8b). Therefore, this plating step is currently the time delimiting step in the workflow. Substance exposure can be achieved utilizing pipetting robots. In addition to the throughput increase another advantage of using automated systems is the avoidance of user introduced errors in cell sorting and in dilution series (Fig. 8c). In an initial step viability assessment is performed to monitor cell health status and to sort out samples with decreased viability in solvent controls (Fig. 8d). Since viability is determined via the CellTiter-Blue® Cell Viability Assay (Promega), which is based on fluorescence measures with standard plate readers, this assay is well suitable for high throughput screenings. Afterwards, staining of samples has to be performed (Fig. 8e). In contrast to conventional 2D cultures fixation and staining procedures have to be milder in order to avoid cell loss. Fixation and staining have therefore to be performed without complete exchange of the supernatant. We established a staining protocol, which uses concentrated stocks of fixation and staining reagents which are added directly into the medium. The detailed procedure is published in 2.3. These staining protocols deliver stable and reproducible results. Image acquisition and raw data generation is performed using the ArrayScan VTI (Thermo Fisher Scientific; Fig. 8f). We established suitable scanning protocols, which image complete wells of multi-well plates (196 images per well on a 96 well plate and 576 images per chamber on an 8-chamber cover-slip) and account for unfocussed images attributed to the 3D neurosphere core.

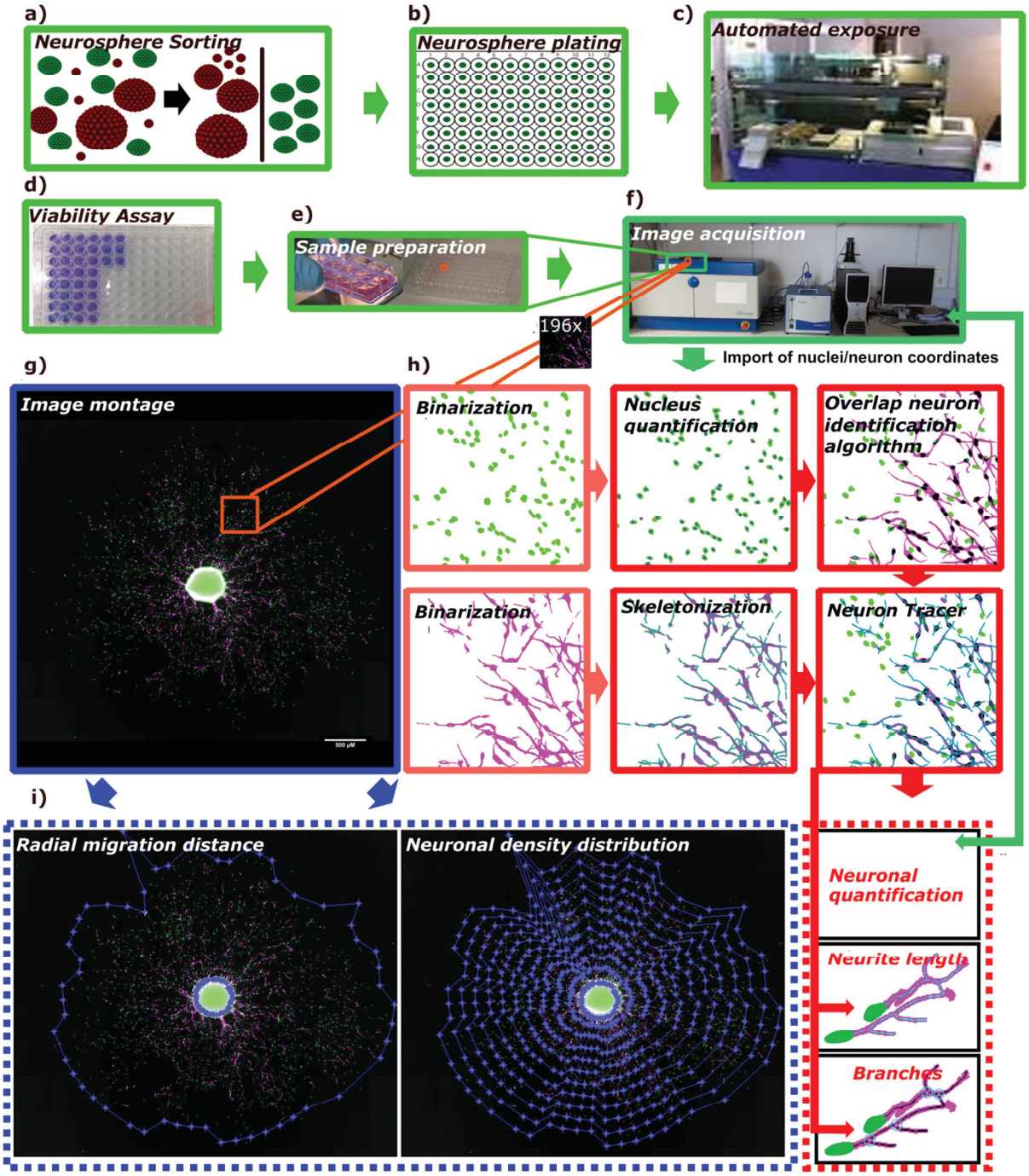

Fig. 8: Workflow for HCA medium throughput substance screening in the Neurosphere Assay: a) Neurospheres presorted utilizing large particle sorters, are manually plated into the multi-well plates (b). c) Substance exposure can be performed using pipetting robots allowing to avoid human errors in e.g. creating a dilution series. d) Directly after the exposure period a viability assay is performed to on the hand sort out plates showing unhealthy controls and to later distinguish specific substance effects from general cytotoxicity. In the next step samples are immunocytochemically stained (e) and automatically imaged utilizing the ArrayScan VTI device (f). Image analysis is simultaneously performed with the vHCS-Scan software. g) Omnisphero composes acquired images to an image montage, resulting images are binarized, and nuclei are identified using a watershed algorithm (h). Neurons are identified in an initial step as neuron candidates by employing the Overlap neuron identification algorithm, which is based on the overlap of intensity in the nucleus channel and the neuron channel. Obtained neuron candidates are verified with the Neuron Tracer algorithm which is based on a skeletonization algorithm. i) Omnisphero is able to assess classical endpoints like neuronal quantification and neuronal morphology and compares these data against a manual ground truth validation and the results obtained by the vHCS-software. Furthermore, Omnisphero comprises algorithms to assess neurosphere-specific endpoints like radial migration and neuronal density distributions.

In the final step quality criteria are examined in the samples to guarantee on the hand that the biology of endpoints is functional within the *in vitro* system and on the other hand that staining quality is sufficient. These quality controls include the endpoint specific migration

capacity, which is assessed by a minimum migration distance of untreated neurospheres and staining quality controls like signal to noise ratios of acquired images. The migration distance is automatically assessed by our software Omnisphero (manuscript 2.1) and the quality of the staining can be accessed via an automated isodata thresholding method (Ridler and Calvard 1978) also included in Omnisphero. Experiments not fulfilling these criteria have to be discarded without further analysis and therefore save automatic scanning and evaluation time for further analyses.

c) Workflow part II: Image analysis

In the final part of the workflow obtained images from paragraph 3.1 b) have to be automatically evaluated utilizing automated image analysis algorithms. Reliable HCA software has to identify all relevant endpoints of the investigated *in vitro* system, results have to show a high accuracy and precision and should be independent of user-bias. In this regard we compared our self-developed software Omnisphero and the commercially available Neuronal Profiling bio-application V4.1 with the manual evaluation as a gold standard (manuscript 2.1).

Image analysis is simultaneously performed with image acquisition utilizing the Neuronal Profiling bio-application V4.1 (Fig. 8f) which was used in many studies (Breier et al. 2008; Harrill et al. 2010, 2011a, 2011b, 2013; Radio and Mundy 2008). Images were analyzed for neuronal quantification and neuronal morphology and automated analyses of these endpoints were comparably precise than manual evaluation (Ramm et al. 2003). However, most studies including the Neuronal Profiling bio-application V4.1 were conducted in pure neuronal cell cultures and cell densities were adjusted to facilitate object discrimination (Dragunow 2008; Harrill et al. 2010). The neurosphere model substantially deviates from 2D cell cultures discussed above. For one, the migration comprises a heterogeneous cell population of neuronal and glia cells and adjustment of the cell density by plating different cell numbers/well is not possible, so that either existing algorithms have to be re-validated or new software approaches validated for their applicability to quantify relevant cellular parameters. Second, the spatial cell distribution within the entire well opens the opportunity to study additional endpoints like radial migration and neuronal density distributions, which require the development of novel algorithms.

As discussed before the Neuronal Profiling bio-application was designed for pure neuronal cultures with adjusted cell densities (Dragunow 2008; Harrill et al. 2010) and therefore its algorithms had to be re-validated for the neurosphere system. In order to assess accuracy and precision of the Neuronal Profiling bio-application V4.1 we compared it to a manual

ground truth validation and our self-developed software Omnisphero (Fig. 8g). Omnisphero is designed to quantify neuronal numbers and assess neuronal morphology also in high density, heterogeneous cell systems and to further assess endpoints unique for the neurosphere model (Fig. 8i). These unique endpoints involve spatial distribution of cells in the entire well, which is not covered by the Neuronal Profiling bio-application V4.1 as it analyzes cellular features on small image extracts of the well.

In order to compare automated methods amongst each other and to the manual ground truth validation, suitable endpoint measures have to be selected. A commonly calculated value for quantification of substance effects is the EC_{50}-value (Neubig et al. 2003). The EC_{50}-value defines the concentration that reduces a given endpoint to 50%. For a first quality assessment of automated methods we compared calculated EC_{50}-values of automated methods to the manual evaluation (manuscript 2.1). Although no significant difference was found for the obtained EC_{50}-values, the Neuronal Profiling bio-application V4.1 was always overestimating the EC_{50}-values compared to manual evaluation. In manuscript 2.1 we only assessed EC_{50}-values from three compounds all presenting steep concentration-response gradients but this overestimation might be of more concern for substances with slight concentration-response gradients. We attributed the overestimation of the EC_{50}-value of the Neuronal Profiling bio-application V4.1 to its underestimation of percentage of neurons for control and low concentrations. In case of concentration-response curves with slight slopes, this could lead to missing the effects in the low concentration range resulting in a significant higher EC_{50}-value.

A more sophisticated method to compare automated methods is the determination of the accuracy and precision of an automated method versus a gold standard, in our case the manual evaluation. The accuracy of an automated method is defined as the 'closeness of agreement between a measured quantity value and a true quantity value of a measurand' while the precision is defined as 'closeness of agreement between indications or measured quantity values obtained by replicate measurements on the same or similar objects under specified conditions' (JCGM 2008). Automated neuronal identification is done in a binary classification. Binary classification divides elements into two groups based on the classification rule. In our case these groups are represented by neuronal and non-neuronal cells. In order to evaluate the performance of a binary classification, different specific metrics have to be defined based on the specific data set created by the binary classification containing four types of data: true positives (TP), false positives (FP), true negatives (TN) and false negatives (FN; Fawcett 2006; Powers 2011). Two frequently used terms are the false positive rate (FPR) and true positive rate (TPR) or detection power (DP; Fawcett 2006). These values are defined by the proportion of either correctly identified neurons (DP) or

false identified neurons (FPR) divided by the number of all manual annotated neurons. Both values influence the accuracy and precision. However, a low accuracy or precision can be attributed to either a low DP, a high FPR or a combination of both. Therefore, studying the DP and FPR is a suitable tool to interpret calculated accuracy values. Therefore, Omnisphero (described in manuscript 2.1) was designed to compare manual assigned neuronal cell bodies to those of automated evaluation revealing an average DP of 41.9% for the Neuronal Profiling V4.1 bio-application and 83,8% for Omnisphero and an average FPR of 52,1% for the Neuronal Profiling V4.1 bio-application and 11,0% for Omnisphero. This analysis points to a much higher accuracy of the algorithms of Omnisphero compared to the Neuronal Profiling bio-application V4.1. Additionally, comparison of the variances of DP and FPR among different experiments and concentration ranges revealed a much higher variability of the Neuronal Profiling bio-application V4.1 indicating a lower precision compared to Omnisphero.

In order to figure out whether the overestimation of the EC_{50}-values of the Neuronal Profiling bio-application V4.1 is attributed to a systematic error, Bland Altman diagrams were plotted. The Bland Altman representation (Bland and Altman 1986) plots the difference between two paired values of two methods versus the mean of those values. The mean of the obtained differences denotes for the bias and the 95% confidence interval reveals the fluctuation margin. Both values enable to identify systematic or proportional errors and thereby the robustness of an automated algorithm. Bland Altman representation revealed a concentration-dependent proportional error for the Neuronal Profiling bio-application V4.1 for neuronal quantification, which leads to an increased EC_{50}-value. We showed in manuscript 2.1 that the overestimation of the EC_{50}-value derived from the Neuronal Profiling bio-application V4.1 is attributed to the low DP for low concentrations, which results in an underestimation in the % of neurons in the migration area.

The high FPR of the Neuronal Profiling bio-application V4.1 is attributed to the applied algorithm to identify neurons (Thermo_Fisher_Scientific 2010a). As described in paragraph 1.4, the Neuronal Profiling bio-application V4.1 identifies neurons based on intensity overlap information within a certain distance around the nucleus originating from the stained cell soma. However, also crossing neurites contribute to this intensity and especially in areas with high densities, where multiple neurites can pass or cross nuclei, this leads to falsely identified neurons (FPs). By increasing the overlap criteria this can be reduced to a certain level, but simultaneously leads to a decreased DP. Therefore, we used two algorithms in Omnisphero for the identification of neurons (Fig. 8h). The first algorithm is also based on overlap criteria and assigns neurons based on the overlap of βIII-tubulin staining and the nucleus. Comparable to the Neuronal Profiling V4.1 bio-application this leads to a high FPR.

Therefore, in a second approach, we verify identified neuronal coordinates or identify missing coordinates with a skeletonization algorithm. This algorithm assumes that each neurite has to have at least one assigned nucleus. Nuclei identified by the first algorithm lying on top of or at the ends of neurites are verified, those without a skeleton or a too short skeleton are discarded and for neurites without a corresponding nucleus the closest nuclei is searched from the end of the neurite. This allows to set the overlap-criteria less stringent since FPs are eliminated by the skeletonization algorithm resulting in a high DP without increasing the FPR.

In terms of evaluation speed the Neuronal Profiling bio-application V4.1 has a significant advantage over Omnisphero, due to the fact that image analysis is performed simultaneously with image acquisition, while Omnisphero starts image analysis after the scanning process. However, since neurosphere-specific endpoints require image montages of all 196 pictures across the entire well (Fig. 8g), only the endpoints neuronal quantification and neuronal morphology are assessed faster by the Neuronal Profiling bio-application V4.1 as this software does not have the ability to evaluate neurosphere-specific endpoints. Within the whole process of compound screening, it is obvious that neurosphere sorting and plating is the main bottleneck for the throughput of substance screenings (Fig. 8a,b).

In order to avoid the introduction of a user bias in automated image analysis, the software itself should perform the parameter optimization of the HCA algorithms. Conventional HCA software asks the user to adjust a huge set of parameters on sample images, which requires the user to have sophisticated knowledge on the meaning of each parameter. This might lead to a parameter set which is valid for the current image extract but fails to describe the remaining images. To avoid these issues, we implemented a supervised learning algorithm into the Omnisphero software as described in manuscript 2.1. This algorithm utilizes the user-defined coordinates to automatically determine optimal parameter settings. The user builds a training silo by manual annotation of cell types of interest. In manuscript 2.1 we demonstrated that a manual annotation time of roughly 1.5 hours is sufficient to set parameters for 5 days differentiated neurospheres stained for βIII-tubulin and Hoechst obtaining comparable results than by expert-determined parameter settings. Additionally, this procedure is much faster and much more robust than manual parameter optimization. The relevance of the time demand of parameter adjustment becomes evident by the fact that for each alteration in experimental design, like exposure time and immunocytochemistry, all parameters have to be re-adjusted. Furthermore, stable accuracy and precision within a constant experimental set-up have to be ensured by regular quality assessments. This can be achieved by the introduction of quality controls within the running screening to exclude changes in culture conditions or staining qualities. Quality control utilizes a min.-scale, multi-

parametric analysis as performed in manuscript 2.1. This min.-scale, multi-parametric analysis requires manual annotation of roughly 200-300 objects, which corresponds to 40 min of manual annotation time. This min.-scale, manual ground truth annotation is important as a quality assurance for stable image qualities.

As a last quality criterion the obtained values for untreated neurospheres and of endpoint-specific controls for a given time and endpoint have to be in a specific range derived from a complete characterization of the *in vitro* system. These endpoint-specific controls are mandatory to ensure the biological function of endpoints within the *in vitro* system. This characterization can be obtained from substance testings averaging the values for solvent controls and endpoint-specific controls (Crofton et al. 2011; Kadereit 2012). Only experiments matching these criteria can be used as valid experiments since potential cell culture or treatment artifacts are thereby ruled out. For endpoint-specific controls we use EGF to suppress neuronal differentiation (Ayuso-Sacido et al. 2010) and the Src-kinase inhibitor PP2 to inhibit NPC migration (Moors et al. 2007).

3.2. Phenotypic screening of NPCs to classify modes of action (MOA) for developmental neurotoxicity (DNT) *in vitro*

Within integrated approaches for testing and assessment (IATA) computational toxicology plays an indispensable role for the evaluation of existing data, the priorization of compounds (SAR based read across) and the modeling of MIEs and KEs for integrated AOPs (Tollefsen et al. 2014). Computational toxicology includes *in silico* methods, which predict human hazard based on structure–activity relationship (SAR) approaches to identify appropriate surrogates via a read-across approach (Wang et al. 2012). However, such *in silico* methods crucially rely on the availability of an adequate volume of data, especially human-relevant information. For some areas, like in the field of DNT with only 12 known human positive environmental compounds, such data are not available (Grandjean and Landrigan 2014). A recent study demonstrated impressively the high value of chemical ‘fingerprint’ libraries derived from primary human cell systems for assessing and classifying toxic and therapeutic properties of untested compounds and to disclose their modes of action (MOA; Kleinstreuer et al. 2014). Within this study 641 environmental compounds and 135 pharmaceuticals and failed drugs were screened in eight different primary cell lines conducting 87 endpoints resulting in specific chemical-response signatures/ fingerprints for each substance. This enables to cluster substances with comparable chemical signatures into groups with potential equal MOAs. Within the resulting clusters chemicals can be compared for structural similarity allowing to utilize them in *in silico* methods as potential surrogates with comparable

toxicological properties. In a final step this fingerprint library even enables to associate the fingerprint of an untested compound to a specific MOA. While there are extensive data sets available for certain organs like e.g. liver and skin, there is a lack of sufficient human *in vivo* and MOA data for DNT as described above. Therefore it will be of high value to build up a DNT fingerprint library that will enable to identify DNT compounds via their MOA - especially in the light of regulatory attention that this field has recently received (EFSA 2013). To fill the data gap in the area of DNT, especially with regards to human-relevant MOA, this thesis describes an interdisciplinary approach – from bioinformatics to molecular toxicology - to develop tools that enable creation of a fingerprint library for DNT utilizing the human Neurosphere Assay, which will allow associating a certain phenotypic fingerprint of a compound with a specific MOA. Relevant pathways for neural development and migration to study by e.g. screening of inhibitors of signaling pathways include e.g. Wnt/BMP-signaling (Lie et al. 2005), the Hesh1/mesh-pathway (Bertrand et al. 2002), TH-signaling (Bernal 2005), the Notch- (Kageyama et al. 2008), or the reelin pathway (Dulabon et al. 2000). Omnisphero is a promising tool for contributing to the generation of fingerprint libraries for DNT by analyzing relevant endpoints of the Neurosphere Assay.

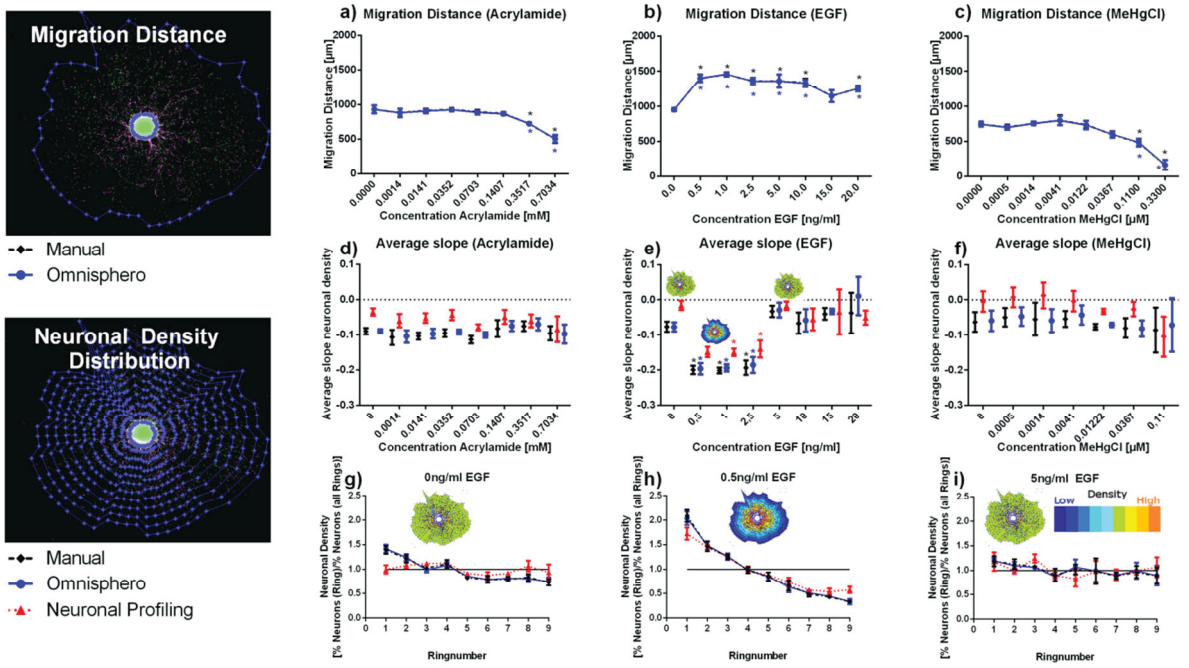

Fig. 9: 'Migration distance and neuronal density distributions. a-c) Migration distance obtained by manual and automated measurements of Omnisphero for the three model substances. d-f) Average slope of each neuronal density function obtained by manual evaluation, Omnisphero and NPBA for all three model substances and all concentrations. g) Neuronal density graphs of untreated samples and h,i) EGF treated samples (0.5 ng/ml and 5 ng/ml EGF). g,i) Equal distributions are indicated as homogeneous green colored migration areas and h) altered density distributions as color coded migration areas Results are obtained from four independent experiments with three technical replicates per condition and are shown as mean±SEM. Significant differences among one method are indicated as *. (from manuscript 2.1).'

We demonstrated Omnisphero's capability to assess specific neurosphere fingerprints by two case studies. In the first study (manuscript 2.1) effects of EGF on endpoints of the Neurosphere Assay were studied. EGF inhibits differentiation (manuscript 2.1) and induces cell migration (Ayuso-Sacido et al. 2010). By using Omnisphero we found that EGF inhibited

neuronal differentiation and induced NPC migration *in vitro* (Fig. 9b). In addition, low concentrations of EGF (0.5-2.5 ng/ml) altered neuronal density distributions (Fig. 9h): untreated neurospheres display a close to ideal equal distribution of neurons within the migration area (Fig. 9g). In presence of low EGF concentrations a high neuronal density was found in close proximity to the neurosphere core (Fig. 9h), which decreases towards the periphery of the migration area, while the whole radial migration distance is increased (Fig. 9b). This endpoint adds complexity to the neurosphere fingerprint of EGF by adding cell type-specific information of cell distribution, which is directly linked to the migration capacity of a single cell type. This is the first time that neuronal migration was linked to EGF in a concentration-dependent manner (manuscript 2.1). One possible explanation for the EGF-dependent altered neuronal migration density distribution might be a different sensitivity of glia cells and neurons towards EGF. If glia cells are more susceptible towards EGF, this would induce glia migration at low concentrations of EGF while neuronal migration stays unaffected and effectively cause a relative accumulation of neurons towards the center of the migration area (Fig. 9h). Puhringer et al. (2013) showed that EGF induces neuronal migration *in vitro* and that EGF-receptor knockout mice show decreased neuronal migration *in vivo*. In contrast to our work this group used high EGF concentrations of 20 - 100 ng/ml. We did not observe inhibition of neuronal migration at high EGF concentrations (5-20 ng/ml) but measured an equal neuronal distribution across the prolonged migration area (Fig. 9b,i). To obtain such an equal neuronal distribution across an increased total migration distance, also neuronal migration had to be stimulated. One molecular explanation for these migrational observations could be the involvement of cell type-specific pathways for different concentration ranges of EGF. Puhringer et al. (2013) demonstrated that EGF-dependent EGF-receptor (EGFR) transactivation was mediated via the Trk receptor. Direct EGF-stimulation of EGFR is the most common mechanism of EGF action (Jorissen 2003). If indeed different mechanisms are involved in cell type-specific EGF effects on migration, will in the future be studied by employing specific inhibitors for the EGFR and Trk receptor. Furthermore, more inhibitors could be used to identify pathways involved in glial as well as neuronal migration by using the Omnisphero software.

In our third manuscript (2.3) we identified and explained the unique neurosphere fingerprint of the green tea catechin EGCG with the underlying MOA. EGCG induces a characteristic arborized migration phenotype with gaps in the migration area. This migration phenotype is unique as other substances effecting migration, like MeHgCl (Baumann et al. 2014), decrease overall migration distance but do not introduce gaps in the migration area. Since EGCG has the ability to bind to the extracellular matrix (ECM) protein laminin (Suzuki and Isemura 2001), which is essential for proper cell adhesion, we studied, whether EGCG-laminin binding could be the explanation for this arborized neurosphere phenotype.

Therefore, experiments were performed, in which only the ECM and not the neurospheres themselves, only the neurospheres and not the ECM or both were exposed to EGCG. Only in cases of ECM exposure this specific migration phenotype was induced pointing to an interference of EGCG with ECM - cell adhesion proteins. An important protein family of α/β heterodimeric transmembrane receptors involved in laminin binding are the integrins (Barczyk et al. 2010; Humphries et al. 2006; Hynes 2002). Functional blocking antibodies against the laminin-binding β1-integrin induced the same specific arborized phenotype in neurospheres than EGCG suggesting that EGCG interferes with laminin- β1-integrin binding. Due to the EGCG-induced prohibited NPC adhesion to the ECM, also glia orientation was altered and the total number of migrated young neurons was decreased. Thus, we identified a specific neurosphere phenotype based on inhibition of cell adhesion. This study revealed the value of a fingerprint library of pathway-specific inhibitors to associate a neurosphere phenotype with a specific MOA, here with the example of cell migration. Furthermore, for compounds with unknown MOA, the advantage of organoid cell systems to evaluate multiple endpoints with HCA becomes evident since effects on the entire cell population, like decreased migration, lower cell densities and the introduction of gaps within the migration area, but also influences on single cell populations, like neurons, astrocytes or oligodendrocytes can be evaluated. Quantification of single cell types revealed that EGCG mainly reduced the astrocyte population but also decreased the neuronal population. Spatiotemporal analyses revealed that the reduced number of neurons seems to be a consequence of the prohibited adhesion of astrocytes, which makes sense since neurons migrate on top of astrocytes. Finally, this study demonstrates that observed phenotypes *in vitro* can also be compared to compounds' effects *in vivo*. Densities of cell nuclei and their distributions in rat brain cortical layers were determined utilizing $BrdU^+$ cell identification with the ArrayScan VTI (Thermo_Fisher_Scientific 2010b) and subsequently spatial analyses with the self-developed software BrdLuxe were performed. EGCG reduced the number of nuclei in cortical layers of rat brains. Thus, at least in some cases, HCA allow an *in vitro in vivo* comparison of effects which is of high relevance for validation of such *in vitro* data since legacy data from animals could be correlated with the results of the Neurosphere Assay.

These two examples already highlight the importance for building up an endpoint database for specific inhibitors or activators of relevant pathways to interpret chemical effects on neurodevelopmental key events (KE) and – by linking MOA to neurosphere phenotypes – will allow computational predictions of chemical effects in the future. Extension of this work might thus link *in silico* methods like SAR, QSAR and binding affinities to *in vitro* responses of cellular function based on toxicity pathways (Kleinstreuer et al. 2014).

In this thesis we established HCA methods for the neurodevelopmental KE neuronal differentiation, neuronal maturation, radial migration, migration pattern and neuronal migration/positioning. While neuronal differentiation, neuronal maturation and radial migration are endpoints already assessed in the Neurosphere Assay the description of the migration pattern and neuronal migration/positioning added two more endpoints to the endpoints repertoire. These additional endpoints will lead to a more specific phenotype description, which will result in a better discrimination of substance MOA (Kleinstreuer et al. 2014).

Within further projects, the KE portfolio will be extended towards glia cell (oligodendrocyte and astrocyte) differentiation. Therefore, algorithms will be established to specifically identify oligodendrocyte and astrocyte number, morphology and distribution in the migration area, which differentiate and migrate together with neurons. These algorithms will be implemented into the 'Omnisphero'-software leading the extended 'Omnisphero 1.1'. The additional glia endpoints will increase the number of KE within the fingerprint and thereby enhance their complexity without raising the number of experiments. Increasing the number of KE is crucial because the magnitude of data-richness of fingerprints will determine their ability to separate different compounds by MOA (Kleinstreuer et al. 2014). Secondly, for generating the MOA-based DNT fingerprint library a variety of specific signaling pathway modulators known to be crucial for brain development will be studied with the help of 'Omnisphero 1.1' in the Neurosphere Assay across all endpoints. These pathway-specific fingerprints will then be compared to fingerprints generated by testing of DNT compounds with 'Omnisphero 1.1'.

3.3. Integration of Omnisphero/BrdeLuxe into flexible software platforms for HCA image analysis of cell phenotypes

Recent advantages in automatic imaging techniques allow gathering thousands of images from organ-specific *in vitro* systems per day enabling HCA substance screenings (Reif et al. 2015). The automated analysis of such big and versatile image data sets requires the use of software platforms which have to fulfill certain criteria: 1) They have to comprise available algorithms for image analysis of various organ specific endpoints (Carpenter et al. 2006), 2) have to deliver an appropriate infrastructure for screening of huge image data sets (Swedlow et al. 2003), 3) have to be modular for the implementation of new algorithms from foreign software (Kamentsky et al. 2011) and 4) have to be capable to perform a direct comparison of algorithms assessing the same endpoints in regard of accuracy and precision. The most frequently used platform, called CellProfiler, was developed in 2006 by the group around

Anne E. Carpenter (Carpenter et al. 2006). The CellProfiler includes a large set of different algorithms for analyses of various organ-specific endpoints together with a suitable infrastructure to run those algorithms on large scale image sets. Furthermore this platform is built in a modular way to allow implementation of custom developed algorithms.

Prior to this approach, the only flexible, open-source biological image analysis package was ImageJ/NIH Image (Abràmoff et al. 2004). While ImageJ was used in many publications, its main application domain lies in the analysis of single images. Although macros are available for ImageJ for processing multiple images, adaption of those to other applications requires programming skills by the user. Beside ImageJ, other laboratories and companies even wrote their own image analysis software written in commercial or open source software (for example, MetaMorph, ImagePro Plus, MATLAB or Java) for automated image analysis like our self-developed software Omnisphero (manuscript 2.1; Matlab) and BrdeLuxe (publication 2.2; C-Sharp). These custom-made software enable the assessment of specific endpoints not available in standard image analysis software to enhance the portfolio for endpoint-specific screenings. The need of self-developed algorithms is attributed to the fact that biological questions are highly diverse and that the number of *in vitro* systems is constantly increasing which makes it illusory to design one single software approach to address all biological questions (Echeverri and Perrimon 2006).

Beside open source software platforms also commercial software is available covering a broad spectrum of bio-applications like the vHCS Scan software (Thermo Fisher). The clear advantage of this software is the capability to perform image analysis simultaneously with image acquisition, since the software is directly operating an automated scanning microscope. Furthermore, many endpoint-specific algorithms are combined in one software platform (e.g. Thermo_Fisher_Scientific 2010a, 2010b). However, significant drawbacks of these platforms are high costs and the missing opportunity to customize algorithms within the code, which is normally not editable by the user. Another significant drawback of such platforms is the lack of bio-applications for complex 3D *in vitro* systems like the neurospheres.

Self-developed and commercially available software often face the problem not to be modular, which makes inclusion of additional features from foreign software time-consuming. This is mostly attributed to the fact that software is developed using different programming languages making it complicated to include applications from one software into the other (Carpenter et al. 2006). Another drawback of self-developed and commercially available software is the limited accessibility for the full spectrum of researchers. Commercially available software is mostly connected to an automated scanning microscope like the Array

Scan VTI (Thermo Fisher) and is therefore highly expensive. Custom-made software is mostly maintained in one lab and often too complex to be used by untrained researchers (Carpenter et al. 2006). Therefore, gathering existing algorithms in one flexible software platform is desirable.

The CellProfiler opens the opportunity to implement novel endpoints assessed by either custom-made or commercially available software as modules. However, often more than one software approach investigates the same endpoint set (Carpenter et al. 2006) which raises the following question to the researcher: Which of the available software approaches is the most adequate, in terms of accuracy and precision, for the endpoint of interest in the applied *in vitro* system? In order to answer this question the results obtained from different software approaches have to be compared towards a gold standard, which is in most cases the manual evaluation. The accuracy and precision is routinely assessed qualitatively by judging the identification of objects in image extracts within the software (Harrill et al. 2010, 2011b; Radio and Mundy 2008). This bears several disadvantages. For one, adjusting the parameters only for image extracts might lead to parameter sets describing the image extracts accurately but fail to describe the entire image set, and second, sophisticated knowledge on the meaning of the parameters is required by the user to obtain robust results. However, quantitative estimations of the accuracy and precision of different algorithms require a one by one comparison of identified objects as described in paragraph 3.1. This is for most software not possible, since manual annotation is not implemented as a software tool. The only other possibility to judge whether the algorithm delivers data comparable to manual evaluations requires the user to manually go back to the images' raw data and to perform e.g. manual counting of objects. The obtained quantification can then be used to e.g. calculate EC_{50}-values of automated versus manual counting to compare both quantification methods. However, as described in 3.1, the comparison of EC_{50}-values is not a sufficient descriptor for accuracy and precision. Low accuracy and precision found for evaluation of neuronal endpoints within neurosphere samples with the Neuronal Profiling bio-application V4.1 would have been missed by simply judging the magnitudes of the EC_{50}-values. In manuscript 2.1 we demonstrated that high a FPR and low a DP caused an overestimation of morphological features, which would have been very difficult and time-consuming to detect manually.

The ability to judge accuracy and precision of algorithms quantitatively instead of purely qualitatively becomes more and more important since development of new algorithms is an emerging field. This is due to the fact that the key challenge remains in the development of accurate image analysis algorithms (Price et al. 2002). One major issue for automated image analysis software is how to deal with images containing high object densities.

Therefore, the cell density is often adjusted as a compromise between cell viability and the ability to discriminate between objects (Dragunow 2008; Harrill et al. 2010). This is a practice that cannot be operated in organoid cultures like neurospheres, since adjustment of cell density is impossible. Moreover, subpopulations of cells have to be reliably discriminated from the rest of the cell population. With Omnisphero (manuscript 2.1) we tackled theses challenges with new algorithms to perform neuronal quantification and morphological analysis with high accuracy and precision even in high-density, heterogeneous cultures. Omnisphero for the first time allows the researcher to compare different automated methods for the endpoints of neuronal quantification in terms of accuracy and precision against manual evaluation since it requires only the images and identified coordinates of nuclei and neurons. This is an essential tool since already several, mostly commercially available, software approaches exists (Harrill et al. 2010; Wang et al. 2010; Wilson et al. 2014) for evaluation of these endpoints, which perform with variable accuracy and precision depending of the investigated *in vitro* system. Therefore, Omnisphero allows to identify the most adequate software in regard to accuracy and precision for neuronal quantification for a given *in vitro* system.

As mentioned above most software requires the user to optimize a variety of parameters for automated image analysis on a sample set of images (Carpenter et al. 2006; Harrill et al. 2010, 2011b; Radio and Mundy 2008). To successfully do so, the user needs to have sophisticated knowledge of these parameters. Therefore we developed a supervised learning algorithm in Omnisphero, which utilizes user-defined objects to automatically adjust the evaluation parameters. This enables the user e.g. to optimize neuronal recognition for another *in vitro* system by simply creating a new training set via manual annotation. Therefore Omnisphero can be adjusted to analyze different neural *in vitro* systems.

In summary Omnisphero, BrdeLuxe and other existing software approaches are valuable sources for novel algorithms and new tools, but are standalone programs and cover only a limited set of endpoints. Therefore, it would be highly desirable to implement the new software approaches developed in this thesis into a platform like the Cell Profiler. This would on the one hand expand the available algorithms for endpoint evaluation in the CellProfiler towards 3D *in vitro* systems and on the other hand the new developed visualization and comparison tools would add the important possibility to judge accuracy and precision of different algorithms. Furthermore, the supervised learning algorithm would facilitate user-friendliness allowing even users without any expertise in image analysis to run analyses on their images. The implemented algorithms in the CellProfiler would on the other hand allow to enlarge the portfolio of endpoints of the Neurosphere Assay including e.g., protein distributions or cell cycle endpoints. Implementation of Omnisphero would also enlarge the

application domain of Omnisphero's algorithms to other neuronal *in vitro* systems by opening it to a larger community of researchers. Furthermore, some algorithms like the one for assessing migration distance could be translated to assess such endpoints in non-neural cultures like in tumor-spheroids, in which cell migration is quantified as an indicator for invasiveness of tumor cells (Vinic et al. 2013).

4. Abstract

Neurodevelopmental toxicants represent a serious threat for society, clearly demonstrating the need for developmental neurotoxicity (DNT) testing. However, testing according to the current guidelines based on animal experiments is extremely time- and cost-intensive. Therefore, alternative testing approaches based on *in vitro* studies in combination with novel tools and strategies as proposed in the Tox21 concept are highly desirable. A promising *in vitro* system for DNT testing are neural progenitor cells (NPCs) grown as 3D neurospheres, which mimic several basic processes of fetal brain development, like migration and differentiation, *in vitro*.

In the present dissertation a new DNT testing workflow of chemicals within the 3D neurosphere system employing high content image analyses (HCA) was developed. Therefore, suitable sample preparation and automated microscope scanning protocols as well as self-developed software were designed. We developed the software Omnisphero to assess classical neuronal endpoints like neuronal quantification and morphology as well as the neurosphere-specific endpoints dealing with spatial distribution of cells within the entire well like migration distance, migration pattern and neuronal density distributions. For regional quantification of $BrdU^+$ (Bromodeoxyuridine) cells in brain slices *in vivo* the software BrdeLuxe was developed.

This thesis demonstrates the capability of Omnisphero to assess relevant endpoints of the 'Neurosphere Assay' for medium throughput DNT substance screening: the effects of three model substances with known effects on relevant developmental endpoints (methylmercury, acrylamide, epidermal growth factor (EGF)) and one so far unknown DNT compound (epigallocatechin gallate, EGCG) were assessed. For neurospheres treated with the model substances, Omnisphero reached a detection power (DP) of 80-85% and a false positive rate (FPR) of 10-15% for neuronal quantification outperforming foreign automated evaluations (Thermo Scientific; DP: 50%, FPR: 40%). The high DP and low FPR was shown to be crucial for assessing neuronal morphology, since the high FPR of the foreign software caused an introduction of artificial branching points. Omnisphero also assessed the neurosphere-specific endpoint ‘radial cell migration’ by identifying the neurosphere core as a single object and determining migration distance as an average of the distances between the rim of the neurosphere core and all nuclei positions, obtained for the Array Scan technology, with the furthest migration distances with comparable precision than manual evaluations. Another self-written algorithm for the first time quantified positioning of individual cell types within the identified migration area leading to a distance-dependent density distribution. For the so far unknown DNT compound EGCG Omnisphero generated a substance-specific fingerprint with neurosphere endpoints that were established for HCA. This specific fingerprint was well distinguishable from other investigated compounds and could be attributed to the mode of action of disrupted cell adhesion. Altered adhesion was caused by EGCG interfering with laminin-integrin binding. This caused a chaotic glia phenotype and subsequent disturbance of neuronal migration. These *in vitro* results were compared to *in vivo* data from EGCG treated rats by assessing positioning of BrdU (bromodeoxyuridine)-labeled cells in cortical brain slices by a second algorithm developed within this work, BrdeLuxe, allowing an *in vitro in vivo* comparison.

In conclusion, HCA of neurospheres is a promising technique for DNT medium throughput screening which might be used in safety and efficacy testing in the future – with additional features also for *in vivo* evaluations.

5.Zusammenfassung

Entwicklungsneurotoxische Substanzen stellen eine ernste Bedrohung für die Gesellschaft dar und erfordern daher geeignete Methoden zur Erfassung von Entwicklungsneurotoxizität (ENT). Jedoch sind Tests nach den momentanen Richtlinien, welche auf Tierversuchen basieren, extrem kosten- und zeitaufwändig. Daher sind alternative Testmethoden basierend auf *in vitro* Studien in Kombination mit neuen Technologien und Strategien, wie sie innerhalb des Tox21 Konzeptes vorgeschlagen werden, in hohem Masse wünschenswert. Ein vielversprechendes *in vitro* System für ENT Prüfung stellen neurale Progenitorzellen (NPCs), kultiviert als 3D Neurosphäre dar, da sie einige wesentliche Prozesse der Gehirnentwicklung wie Migration und Differenzierung *in vitro* nachahmen.
In der vorliegenden Dissertation wurde ein Workflow zur Erfassung entwicklungsneurotoxischer Substanzeigenschaften im 3D Neurosphärenmodel mittels "High Content" Bildanalysen entwickelt. Dafür wurden geeignete Probenpräparations-, automatische Bildaufnahmeprotokolle und eine eigene Auswertungssoftware entwickelt. Die Auswertsoftware "Omnisphero" analysiert klassische Endpunkte wie neuronale Quantifizierung und Morphologie sowie Neurosphären-spezifische Endpunkte, die die räumliche Verteilung von Zellen im gesamten Well betreffen, wie Migrationsdistanz, Migrationsmuster und neuronale Dichteverteilungen. Für die räumliche Quantifizierung von BrdU (Bromdeoxyuridin)$^{+}$-Zellen in Gehirnschnitten *in vivo* wurde die Software "BrdeLuxe" entwickelt.
Diese Arbeit belegt die Leistungsfähigkeit von Omnisphero, relevante Endpunkte des "Neurosphären Assays" für Substanzprüfungen im mittleren Durchsatz zu analysieren. Hierzu wurden die Effekte von drei Modellsubstanzen mit bekannten Effekten auf entwicklungsrelevante Endpunkte (Methyl-quecksilber, Acrylamid, epidermaler Wachstumsfaktor) und die bislang unbekannte ENT Substanz Epigallocatechingallat (EGCG) untersucht. Für die mit Modellsubstanzen behandelten Neurosphären erreichte Omnisphero eine Detektionsfähigkeit (DP) von 80-85 % mit einer Falscherkennungsrate (FPR) von 10-15% für die neuronale Quantifizierung und übertraf damit andere automatische Auswertungssysteme (Thermo Scientific; DP: 50%, FPR: 40%). Die Relevanz einer hohen DP und niedrigen FPR für die Analyse der neuronalen Morphologie wird dadurch deutlich, dass die hohe FPR der bisher genutzten Software zu einer Identifizierung von artifiziellen Verzweigungspunkten in Neuriten führt. Omnisphero analysiert des Weiteren den Neurosphären-spezifischen Endpunkt "radiale Zellmigration" mit vergleichbarer Präzision wie manuelle Messungen, indem der Neurosphärenkern als einzelnes Objekt identifiziert und die Migrationsstrecke als Mittelwert der Distanz zwischen dem Rand des Neurosphärenkerns und den am weitesten migrierten Zellkernpositionen, welche durch die Array Scan Technologie bestimmt wurden, berechnet wird. Ein weiterer selbst entwickelter Algorithmus quantifiziert erstmalig die Position einzelner Zelltypen innerhalb der identifizieren Migrationsfläche und erfasst damit Abstands-abhängige Dichteverteilungen. Für die bis dahin unbekannte ENT Substanz EGCG konnte mit Omnisphero ein Substanz-spezifischer Fingerabdruck mittels der für HCA etablierten Neurosphärenendpunkte generiert werden. Dieser spezifische Fingerabdruck war eindeutig von denen anderer Substanzen abgrenzbar und konnte auf eine gestörte Zelladhäsion zurückgeführt werden. Die beeinträchtigte Adhäsion wurde durch die Störung der Laminin-Integrin Bindung durch EGCG hervorgerufen. Diese führte zu einem chaotischen Glia-Phänotyp und einer anschließenden beeinträchtigten neuronalen Migration. Diese *in vitro* Ergebnisse wurden mit *in vivo* Daten von EGCG behandelten Ratten verglichen, indem die Positionierung von BrdU markierten Zellen in Großhirnrindenschichten mittels eines zweiten Algorithmus, BrdeLuxe, analysiert wurde und dadurch einen *in vitro in vivo* Vergleich ermöglichte.
Zusammenfassend kann die Schlussfolgerung getroffen werden, dass die HCA von Neurosphären eine vielversprechende Technik für die ENT Prüfung im mittleren Durchsatz darstellt, welche in Sicherheits- und Wirksamkeitsstudien in der Zukunft Anwendung finden könnte - mit erweiterten Applikationen für *in vivo* Analysen.

List of abbreviations

2D	Two-dimensional
3D	Three-dimensional
BrdU	bromodeoxyuridine
CTB	Cell titer blue
DAPI	4',6-diamidino-2-phenylindole
DNT	developmental neurotoxicity
DP	detection power
EFSA	European Food Safety Authority
EGCG	epigallocatechin Gallate
EGF	epidermal growth factor
EPA	Environmental Protection Agency
ESC	embryonic stem cell
FGF	fibroblast growth factor
FP	false positive
FPR	false postive rate
GFAP	glial fibrillary acidic protein
HCA	High Content Analysis
iPSC	induced pluripotent stem cell
IQ	intelligence quotient
KE	key event
LOAECs	lowest observable adverse effect concentrations
LOAEL	lowest-observed-adverse-effect level
LOEC	lowest observed effect concentration
MeHgCl	methylmercury-chloride
MOA	mode of action
NOAEL	no-observed-adverse-effect level
NPC	neural progenitor cell
NRC	National Research Council
PCB	polychlorinated biphenyl
PDL	poyl-D-lysine
PI	propidium diode
QSAR	quantitative structure–activity relationship
RPF	relative potency factor
SAR	structure–activity relationship
TEF	toxicity equivalent factor

TN	true negative
TP	true positive
TP	true positive
USEPA	United States Environmental Protection Agency
WOA	weight of evidence

References

Abbott BD, Held GA, Wood CR, Buckalew AR, Brown JG, Schmid J. 1999. AhR, ARNT, and CYP1A1 mRNA quantitation in cultured human embryonic palates exposed to TCDD and comparison with mouse palate in vivo and in culture. Toxicol. Sci. 47:62–75; doi:10.1093/toxsci/47.1.62.

Abràmoff MD, Magalhães PJ, Ram SJ. 2004. Image processing with imageJ. Biophotonics Int. 11:36–41; doi:10.1117/1.3589100.

Alépée N, Bahinski A, Daneshian M, Wever B De, Fritsche E. 2014. State-of-the-Art of 3D Cultures (Organs-on-a-Chip) in Safety Testing and Pathophysiology. ALTEX 31:441–477; doi:http://dx.doi.org/10.14573/altex1406111.

Anderl JL, Redpath S, Ball AJ. 2009. A neuronal and astrocyte co-culture assay for high content analysis of neurotoxicity. J. Vis. Exp. 1–6; doi:10.3791/1173.

Andersen SL. 2003. Trajectories of brain development: Point of vulnerability or window of opportunity? Neurosci. Biobehav. Rev. 27:3–18; doi:10.1016/S0149-7634(03)00005-8.

Ankley GT, Bennett RS, Erickson RJ, Hoff DJ, Hornung MW, Johnson RD, et al. 2010. Adverse outcome pathways: A conceptual framework to support ecotoxicology research and risk assessment. Environ. Toxicol. Chem. 29:730–741; doi:10.1002/etc.34.

Ayuso-Sacido A, Moliterno JA, Kratovac S, Kapoor GS, O'Rourke DM, Holland EC, et al. 2010. Activated EGFR signaling increases proliferation, survival,and migration and blocks neuronal differentiation in post-natal neural stem cells. J. Neurooncol. 97:323–337; doi:10.1007/s11060-009-0035-x.

Bal-Price A, Crofton KM, Leist M, Allen S, Arand M, Buetler T, et al. 2015a. International STakeholder NETwork (ISTNET): creating a developmental neurotoxicity (DNT) testing road map for regulatory purposes. Arch. Toxicol. 89:269–287; doi:10.1007/s00204-015-1464-2.

Bal-Price A, Crofton KM, Sachana M, Shafer TJ, Behl M, Forsby A, et al. 2015b. Putative adverse outcome pathways relevant to neurotoxicity. Crit. Rev. Toxicol. 8444:83–91; doi:10.3109/10408444.2014.981331.

Bal-Price AK, Coecke S, Costa L, Crofton KM, Fritsche E, Goldberg A, et al. 2012. Advancing the Science of Developmental Neurotoxicity (DNT): Testing for Better Safety Evaluation. ALTEX 29: 202–15.

Barczyk M, Carracedo S, Gullberg D. 2010. Integrins. Cell Tissue Res. 339:269–280; doi:10.1007/s00441-009-0834-6.

Barker RA, de Beaufort I. 2013. Scientific and ethical issues related to stem cell research and interventions in neurodegenerative disorders of the brain. Prog. Neurobiol. 110:63–73; doi:10.1016/j.pneurobio.2013.04.003.

Baumann J, Barenys M, Gassmann K, Fritsche E. 2014. Comparative human and rat "neurosphere assay" for developmental neurotoxicity testing. Curr. Protoc. Toxicol. 59:12.21.1–12.21.24; doi:10.1002/0471140856.tx1221s59.

Baumann J, Gassmann K, Masjosthusmann S, DeBoer D, Bendt F, Giersiefer S, et al. 2015. Comparative human and rat neurospheres reveal species differences in chemical effects on neurodevelopmental key events. Arch. Toxicol.; doi:10.1007/s00204-015-1568-8.

Bellanger M, Pichery C, Aerts D, Berglund M, Castaño A, Čejchanová M, et al. 2013. Economic benefits of methylmercury exposure control in Europe: Monetary value of neurotoxicity prevention. Environ. Heal. 12:3; doi:10.1186/1476-069X-12-3.

Bernal J. 2005. Thyroid Hormones and Brain Development. Vitam. Horm. 71:95–122; doi:10.1016/S0083-6729(05)71004-9.

Bertrand N, Castro DS, Guillemot F. 2002. Proneural genes and the specification of neural cell types. Nat. Rev. Neurosci. 3:517–530; doi:10.1038/nrn874.

Bland JM, Altman DG. 1986. Statistical methods for assessing agreement between two methods of clinical measurement. Lancet 1:307–10; doi:10.1016/s0140-6736(86)90837-8.

Bondy SC, Campbell A. 2005. Developmental neurotoxicology. J. Neurosci. Res. 81:605–12; doi:10.1002/jnr.20589.

Brannen CL, Sugaya K. 2000. In vitro differentiation of multipotent human neural progenitors in serum-free medium. Neuroreport 11:1123–1128; doi:10.1097/00001756-200004070-00042.

Breier JM, Gassmann K, Kayser R, Stegeman H, De Groot D, Fritsche E, et al. 2010. Neural progenitor cells as models for high-throughput screens of developmental neurotoxicity: state of the science. Neurotoxicol. Teratol. 32:4–15; doi:10.1016/j.ntt.2009.06.005.

Breier JM, Radio NM, Mundy WR, Shafer TJ. 2008. Development of a high-throughput screening assay for chemical effects on proliferation and viability of immortalized human neural progenitor cells. Toxicol. Sci. 105:119–33; doi:10.1093/toxsci/kfn115.

Buc-Caron MH. 1995. Neuroepithelial progenitor cells explanted from human fetal brain proliferate and differentiate in vitro. Neurobiol. Dis. 2:37–47; doi:10.1006/nbdi.1995.0004.

Carpenter AE, Jones TR, Lamprecht MR, Clarke C, Kang IH, Friman O, et al. 2006. CellProfiler: image analysis software for identifying and quantifying cell phenotypes. Genome Biol. 7:R100; doi:10.1186/gb-2006-7-10-r100.

Chalmers-Redman RM, Priestley T, Kemp JA, Fine A. 1997. In vitro propagation and inducible differentiation of multipotential progenitor cells from human fetal brain. Neuroscience 76:1121–1128; doi:10.1016/S0306-4522(96)00386-7.

Claudio L, Kwa WC, Russell AL, Wallinga D. 2000. Testing methods for developmental

neurotoxicity of environmental chemicals. Toxicol. Appl. Pharmacol. 164:1–14; doi:10.1006/taap.2000.8890.

Coecke S, Goldberg AM, Allen S, Buzanska L, Calamandrei G, Crofton K, et al. 2007. Workgroup Report: Incorporating In Vitro Alternative Methods for Developmental Neurotoxicity into International Hazard and Risk Assessment Strategies. Environ. Health Perspect. 115:924–931; doi:10.1289/ehp.9427.

Collins FS, Gray GM, Bucher JR. 2008. Toxicology. Transforming environmental health protection. Science 319:906–907; doi:10.1126/science.1154619.

Crofton KM, Mundy WR, Lein PJ, Bal-Price A, Coecke S, Seiler AEM, et al. 2011. Developmental neurotoxicity testing: recommendations for developing alternative methods for the screening and prioritization of chemicals. ALTEX 28:9–15; doi:10.14573/altex.2011.1.009.

Crofton KM, Mundy WR, Shafer TJ. 2012. Developmental neurotoxicity testing: A path forward. Congenit. Anom. (Kyoto). 52:140–146; doi:10.1111/j.1741-4520.2012.00377.x.

Cukierman E, Pankov R, Stevens DR, Yamada KM. 2001. Taking cell-matrix adhesions to the third dimension. Science 294:1708–1712; doi:10.1126/science.1064829.

Culbreth ME, Harrill JA, Freudenrich TM, Mundy WR, Shafer TJ. 2012. Comparison of chemical-induced changes in proliferation and apoptosis in human and mouse neuroprogenitor cells. Neurotoxicology 33:1499–510; doi:10.1016/j.neuro.2012.05.012.

Das KP, Freudenrich TM, Mundy WR. 2004. Assessment of PC12 cell differentiation and neurite growth: a comparison of morphological and neurochemical measures. Neurotoxicol. Teratol. 26:397–406; doi:10.1016/j.ntt.2004.02.006.

Dragunow M. 2008. High-content analysis in neuroscience. Nat. Rev. Neurosci. 9:779–88; doi:10.1038/nrn2492.

Dulabon L, Olson EC, Taglienti MG, Eisenhuth S, McGrath B, Walsh CA, et al. 2000. Reelin binds alpha3beta1 integrin and inhibits neuronal migration. Neuron 27:33–44; doi:10.1016/S0896-6273(00)00007-6.

ECHA. 2012. Briefing from Day 1 – ECHA-MSCA interaction: Experts Workshop on Read-across Assessment. 1–11.

Echeverri CJ, Perrimon N. 2006. High-throughput RNAi screening in cultured cells: a user's guide. Nat. Rev. Genet. 7:373–84; doi:10.1038/nrg1836.

EFSA. 2013. Scientific Opinion on the developmental neurotoxicity potential of acetamiprid and imidacloprid. EFSA J. 11:3471, 44 pp; doi:10.2903/j.efsa.2013.3471.

Eto K. 1997. Pathology of Minamata Disease. Toxicol. Pathol. 25:614–623; doi:10.1177/019262339702500612.

Fawcett T. 2006. An introduction to ROC analysis. Pattern Recognit. Lett. 27:861–874; doi:10.1016/j.patrec.2005.10.010.

Fritsche E, Cline JE, Nguyen N-H, Scanlan TS, Abel J. 2005. Polychlorinated Biphenyls Disturb Differentiation of Normal Human Neural Progenitor Cells: Clue for Involvement of Thyroid Hormone Receptors. Environ. Health Perspect. 113:871–876; doi:10.1289/ehp.7793.

Fritsche E, Gassmann K, Schreiber T. 2011. Neurospheres as a Model for Developmental Neurotoxicity Testing. L.G. Costa, G. Giordano, and M. Guizzettieds. Vitr. Neurotoxicology Methods Protoc. 758:99–114; doi:10.1007/978-1-61779-170-3.

Gassmann K, Abel J, Bothe H, Haarmann-Stemmann T, Merk HF, Quasthoff KN, et al. 2010. Species-specific differential AhR expression protects human neural progenitor cells against developmental neurotoxicity of PAHs. Environ. Health Perspect. 118:1571–7; doi:10.1289/ehp.0901545.

Gassmann K, Baumann J, Giersiefer S, Schuwald J, Schreiber T, Merk HF, et al. 2012. Automated neurosphere sorting and plating by the COPAS large particle sorter is a suitable method for high-throughput 3D in vitro applications. Toxicol. Vitr. 26:993–1000; doi:10.1016/j.tiv.2012.04.025.

Gibb S. 2008. Toxicity testing in the 21st century: A vision and a strategy. Reprod. Toxicol. 25:136–138; doi:10.1016/j.reprotox.2007.10.013.

Goldman LR, Koduru S. 2000. Chemicals in the environment and developmental toxicity to children: a public health and policy perspective. Environ. Health Perspect. 108 Suppl:443–448; doi:10.2307/3454535.

Grandjean P, Landrigan PJ. 2006. Developmental neurotoxicity of industrial chemicals. Lancet 368:2167–2178; doi:10.1016/S0140-6736(06)69665-7.

Grandjean P, Landrigan PJ. 2014. Neurobehavioural effects of developmental toxicity. Lancet Neurol. 13:330–338; doi:10.1016/S1474-4422(13)70278-3.

Greene LA, Tischler AS. 1976. Establishment of a noradrenergic clonal line of rat adrenal pheochromocytoma cells which respond to nerve growth factor. Proc. Natl. Acad. Sci. U. S. A. 73:2424–2428; doi:10.1073/pnas.73.7.2424.

Harrill JA, Freudenrich TM, Machacek DW, Stice SL, Mundy WR. 2010. Quantitative assessment of neurite outgrowth in human embryonic stem cell-derived hN2 cells using automated high-content image analysis. Neurotoxicology 31:277–90; doi:10.1016/j.neuro.2010.02.003.

Harrill JA, Freudenrich TM, Robinette BL, Mundy WR. 2011a. Comparative sensitivity of human and rat neural cultures to chemical-induced inhibition of neurite outgrowth. Toxicol. Appl. Pharmacol. 256:268–80; doi:10.1016/j.taap.2011.02.013.

Harrill JA, Freudenrich TM, Robinette BL, Mundy WR. 2011b. Comparative sensitivity of human and rat neural cultures to chemical-induced inhibition of neurite outgrowth. Toxicol. Appl. Pharmacol. 256:268–80; doi:10.1016/j.taap.2011.02.013.

Harrill JA, Robinette BL, Freudenrich T, Mundy WR. 2013. Use of high content image

analyses to detect chemical-mediated effects on neurite sub-populations in primary rat cortical neurons. Neurotoxicology 34:61–73; doi:10.1016/j.neuro.2012.10.013.

Harrill JA, Robinette BL, Mundy WR. 2011c. Use of high content image analysis to detect chemical-induced changes in synaptogenesis in vitro. Toxicol. In Vitro 25:368–87; doi:10.1016/j.tiv.2010.10.011.

Hossini AM, Megges M, Prigione A, Lichtner B, Toliat MR, Wruck W, et al. 2015. Induced pluripotent stem cell-derived neuronal cells from a sporadic Alzheimer's disease donor as a model for investigating AD-associated gene regulatory networks. BMC Genomics 16:84; doi:10.1186/s12864-015-1262-5.

Humphries JD, Byron A, Humphries MJ. 2006. Integrin ligands at a glance. J. Cell Sci. 119:3901–3903; doi:10.1242/jcs.03098.

Hynes RO. 2002. Integrins: Bidirectional, allosteric signaling machines. Cell 110:673–687; doi:10.1016/S0092-8674(02)00971-6.

JCGM JCFGIM. 2008. JCGM 200 : 2008 International vocabulary of metrology — Basic and general concepts and associated terms (VIM) Vocabulaire international de métrologie — Concepts fondamentaux et généraux et termes associés (VIM). Int. Organ. Stand. Geneva ISBN 3:104; doi:10.1016/0263-2241(85)90006-5.

Jorissen R. 2003. Epidermal growth factor receptor: mechanisms of activation and signalling. Exp. Cell Res. 284:31–53; doi:10.1016/S0014-4827(02)00098-8.

Kadereit S. 2012. Compound selection for in vitro modeling of developmental neurotoxicity. Front. Biosci. 17:2442; doi:10.2741/4064.

Kageyama R, Ohtsuka T, Shimojo H, Imayoshi I. 2008. Dynamic Notch signaling in neural progenitor cells and a revised view of lateral inhibition. Nat. Neurosci. 11:1247–1251; doi:10.1038/nn.2208.

Kamentsky L, Jones TR, Fraser A, Bray MA, Logan DJ, Madden KL, et al. 2011. Improved structure, function and compatibility for cellprofiler: Modular high-throughput image analysis software. Bioinformatics 27:1179–1180; doi:10.1093/bioinformatics/btr095.

Kim D-S, Ross PJ, Zaslavsky K, Ellis J. 2014. Optimizing neuronal differentiation from induced pluripotent stem cells to model ASD. Front. Cell. Neurosci. 8:1–16; doi:10.3389/fncel.2014.00109.

Kleinstreuer NC, Yang J, Berg EL, Knudsen TB, Richard AM, Martin MT, et al. 2014. Phenotypic screening of the ToxCast chemical library to classify toxic and therapeutic mechanisms. Nat. Biotechnol. 32:583–91; doi:10.1038/nbt.2914.

Krewski D, Acosta Jr. D, Anderson M, Anderson H, Bailar III JC, Boekelheide K, et al. 2010. TOXICITY TESTING IN THE 21ST CENTURY: A VISION AND A STRATEGY. Toxicol Env. Heal. B Crit Rev. 13:51–138; doi:10.1080/10937404.2010.483176.TOXICITY.

Krug AK, Balmer N V, Matt F, Schönenberger F, Merhof D, Leist M. 2013. Evaluation of a human neurite growth assay as specific screen for developmental neurotoxicants. Arch.

Toxicol. 87:2215–31; doi:10.1007/s00204-013-1072-y.

Landrigan PJ, Schechter CB, Lipton JM, Fahs MC, Schwartz J. 2002. C HILDREN ' S H EALTH Environmental Pollutants and Disease in American Children : Estimates of. Environ. Health Perspect. 110: 721–728.

Leist M, Hartung T. 2013. Inflammatory findings on species extrapolations: humans are definitely no 70-kg mice. Arch. Toxicol. 87:563–567; doi:10.1007/s00204-013-1038-0.

Lie D-C, Colamarino SA, Song H-J, Désiré L, Mira H, Consiglio A, et al. 2005. Wnt signalling regulates adult hippocampal neurogenesis. Nature 437:1370–1375; doi:10.1038/nature04108.

Liebner S, Czupalla CJ, Wolburg H. 2011. Current concepts of blood-brain barrier development. Int. J. Dev. Biol. 55:467–476; doi:10.1387/ijdb.103224sl.

Lim JH, Gibbons HM, O'Carroll SJ, Narayan PJ, Faull RLM, Dragunow M. 2007. Extracellular signal-regulated kinase involvement in human astrocyte migration. Brain Res. 1164:1–13; doi:10.1016/j.brainres.2007.06.020.

Lobo MVT, Alonso FJM, Redondo C, López-Toledano MA, Caso E, Herranz AS, et al. 2003. Cellular characterization of epidermal growth factor-expanded free-floating neurospheres. J. Histochem. Cytochem. 51:89–103; doi:10.1177/002215540305100111.

Moors M, Cline JE, Abel J, Fritsche E. 2007. ERK-dependent and -independent pathways trigger human neural progenitor cell migration. Toxicol. Appl. Pharmacol. 221:57–67; doi:10.1016/j.taap.2007.02.018.

Moors M, Rockel TD, Abel J, Cline JE, Gassmann K, Schreiber T, et al. 2009. Human neurospheres as three-dimensional cellular systems for developmental neurotoxicity testing. Environ. Health Perspect. 117:1131–8; doi:10.1289/ehp.0800207.

Moors M, Vudattu NK, Abel J, Krämer U, Rane L, Ulfig N, et al. 2010. Interleukin-7 (IL-7) and IL-7 splice variants affect differentiation of human neural progenitor cells. Genes Immun. 11:11–20; doi:10.1038/gene.2009.77.

Mundy WR, Radio NM, Freudenrich TM. 2010. Neuronal models for evaluation of proliferation in vitro using high content screening. Toxicology 270:121–30; doi:10.1016/j.tox.2010.02.004.

Neubig RR, Spedding M, Kenakin T, Christopoulos A. 2003. International Union of Pharmacology Committee on Receptor Nomenclature and Drug Classification. XXXVIII. Update on terms and symbols in quantitative pharmacology. Pharmacol. Rev. 55:597–606; doi:10.1124/pr.55.4.4.and.

NRC. 2007. Toxicity Testing in the 21st Century: A Vision and a Strategy | The National Academies Press.; doi:10.17226/11970.

OECD. 2014. CHAPTER 3: Guidence on grouping of chemicals. ENV/JM/MONO 141.

OECD. 2013. THE WORKING PARTY ON CHEMICALS , PESTICIDES AND BIOTECHNOLOGY ENV / JM / MONO (2010) 46 Unclassified. Development 33:1–16; doi:ENV/JM/MONO(2007)10.

Påhlman S, Mamaeva S, Meyerson G, Mattsson ME, Bjelfman C, Ortoft E, et al. 1990. Human neuroblastoma cells in culture: a model for neuronal cell differentiation and function. Acta Physiol. Scand. Suppl. 592: 25–37.

Påhlman S, Ruusala AI, Abrahamsson L, Mattsson ME, Esscher T. 1984. Retinoic acid-induced differentiation of cultured human neuroblastoma cells: a comparison with phorbolester-induced differentiation. Cell Differ. 14:135–144; doi:10.1016/0045-6039(84)90038-1.

Pampaloni F, Reynaud EG, Stelzer EHK. 2007. The third dimension bridges the gap between cell culture and live tissue. Nat. Rev. Mol. Cell Biol. 8:839–845; doi:10.1038/nrm2236.

Pardridge WM. 2006. *Introduction to the Blood-Brain Barrier: Methodology, Biology and Pathology*.

Patlewicz G, Roberts DW, Aptula A, Blackburn K, Hubesch B. 2013. Workshop: Use of “read-across” for chemical safety assessment under REACH. Regul. Toxicol. Pharmacol. 65:226–228; doi:10.1016/j.yrtph.2012.12.004.

Piper DR, Mujtaba T, Keyoung H, Roy NS, Goldman SA, Rao MS, et al. 2001. Identification and Characterization of Neuronal Precursors and Their Progeny From Human Fetal Tissue. J Neurosci Res. 66:356–368; doi:10.1055/s-0029-1237430.Imprinting.

Powers DMW. 2011. EVALUATION: FROM PRECISION, RECALL AND F-MEASURE TO ROC, INFORMEDNESS, MARKEDNESS & CORRELATION. J. Mach. Learn. Technol. 2: 37–63.

Price JH, Goodacre A, Hahn K, Hodgson L, Hunter EA, Krajewski S, et al. 2002. Advances in molecular labeling, high throughput imaging and machine intelligence portend powerful functional cellular biochemistry tools. J. Cell. Biochem. 39:194–210; doi:10.1002/jcb.10448.

Radio NM, Freudenrich TM, Robinette BL, Crofton KM, Mundy WR. 2010. Comparison of PC12 and cerebellar granule cell cultures for evaluating neurite outgrowth using high content analysis. Neurotoxicol. Teratol. 32:25–35; doi:10.1016/j.ntt.2009.06.003.

Radio NM, Mundy WR. 2008. Developmental neurotoxicity testing in vitro: models for assessing chemical effects on neurite outgrowth. Neurotoxicology 29:361–76; doi:10.1016/j.neuro.2008.02.011.

Ramm P, Alexandrov Y, Cholewinski A, Cybuch Y, Nadon R, Soltys BJ. 2003. Automated screening of neurite outgrowth. J. Biomol. Screen. 8:7–18; doi:10.1177/1087057102239779.

Reif DM, Judson RS, Martin M, Breier JM, Houck KA, Mundy WR, et al. 2015. Use of Neural

Models of Proliferation and Neurite Outgrowth to Screen Environmental Chemicals in the ToxCast Phase I Library. Appl. Vitr. Toxicol. 1:1–9; doi:10.1089/aivt.2014.0009.

Reubinoff BE, Itsykson P, Turetsky T, Pera MF, Reinhartz E, Itzik A, et al. 2001. Neural progenitors from human embryonic stem cells. Nat. Biotechnol. 19:1134–1140; doi:10.1038/nbt1201-1134.

Reynolds BA, Tetzlaff W, Weiss S. 1992. A multipotent EGF-responsive striatal embryonic progenitor cell produces neurons and astrocytes. J. Neurosci. 12: 4565–4574.

Rice D, Barone SJ. 2000. Critical Periods of Vulnerabilityfor the Developing Nervous System : Evidence from Humans and Animal Models Development of the Brain in Utero. EHP 108: 511–533.

Ridler TW, Calvard S. 1978. Picture Thresholding Using. IEEE Trans. Syst. Man Cybern. smc-8: 630–632.

Rodier PM. 1995. Developing brain as a target of toxicity. Environ. Health Perspect. 103:73–76; doi:10.1289/ehp.95103s673.

Russell WMS, Burch RL. 1959. *The Principles of Humane Experimental Technique*.

Schettler T. 2001. Toxic threats to neurologic development of children. Environ. Health Perspect. 109:813–816; doi:sc271_5_1835 [pii].

Schreiber T, Gassmann K, Götz C, Hübenthal U, Moors M, Krause G, et al. 2010. Polybrominated diphenyl ethers induce developmental neurotoxicity in a human in vitro model: evidence for endocrine disruption. Environ. Health Perspect. 118:572–8; doi:10.1289/ehp.0901435.

Slikker W. 1994. Principles of developmental neurotoxicology. Neurotoxicology 15: 11–6.

Suzuki Y, Isemura M. 2001. Inhibitory effect of epigallocatechin gallate on adhesion of murine melanoma cells to laminin. Cancer Lett. 173:15–20; doi:10.1016/S0304-3835(01)00685-1.

Svendsen CN, Fawcett JW, Bentlage C, Dunnett SB. 1995. Increased survival of rat EGF-generated CNS precursor cells using B27 supplemented medium. Exp. Brain Res. 102:407–414; doi:10.1007/BF00230645.

Svendsen CN, Skepper J, Rosser AE, Ter Borg MG, Tyres P, Ryken T. 1997. Restricted growth potential of rat neural precursors as compared to mouse. Dev. Brain Res. 99:253–258; doi:10.1016/S0165-3806(97)00002-3.

Swedlow J, Goldberg I, Brauner E, Sorger P. 2003. Informatics and quantitative analysis in biological imaging. Science (80-.). 300:100–102; doi:10.1126/science.1082602.Informatics.

Thermo_Fisher_Scientific. 2010a. Thermo Scientific Cellomics ® Neuronal Profiling V4. 1–112.

Thermo_Fisher_Scientific. 2010b. Thermo Scientific Cellomics ® Target Activation V 4. 1–

58.

Tollefsen KE, Scholz S, Cronin MT, Edwards SW, de Knecht J, Crofton K, et al. 2014. Applying Adverse Outcome Pathways (AOPs) to support Integrated Approaches to Testing and Assessment (IATA). Regul. Toxicol. Pharmacol. 70:629–40; doi:10.1016/j.yrtph.2014.09.009.

Tong W, Welsh WJ, Shi L, Fang H, Perkins R. 2003. STRUCTURE – ACTIVITY RELATIONSHIP APPROACHES AND APPLICATIONS. Environ. Toxicol. Chem. 22:1680–1695; doi:10.1897/01-198.

Ullian EM, Sapperstein SK, Christopherson KS, Barres BA. 2001. Control of synapse number by glia. Science 291:657–61; doi:10.1126/science.291.5504.657.

UNEP. 1999. Guidelines for the Identification of PCBs and Materials Containing PCBs. United Nations Environ. Program. 40.

USEPA. 2000. Supplementary Guidance for Conducting Health Risk Assessment of Chemical Mixtures.

Vinic M, Box C, Zimmermann M, Eccles SA. 2013. Target Identification and Validation in Drug Discovery. Target Identif. Valid. Drug Discov. 986:187–214; doi:10.1007/978-1-62703-311-4.

Wang D, Lagerstrom R, Sun C, Bishof L, Valotton P, Gotte M. 2010. HCA-Vision: Automated Neurite Outgrowth Analysis. J. Biomol. Screen. 15:1165–1170; doi:10.1177/1087057110382894.

Wang NCY, Zhao QJ, Wesselkamper SC, Lambert JC, Petersen D, Hess-wilson JK. 2012. Application of computational toxicological approaches in human health risk assessment . I . A tiered surrogate approach. Regul. Toxicol. Pharmacol. 63:10–19; doi:10.1016/j.yrtph.2012.02.006.

Wilson MS, Graham JR, Ball AJ. 2014. Multiparametric High Content Analysis for assessment of neurotoxicity in differentiated neuronal cell lines and human embryonic stem cell-derived neurons. Neurotoxicology 42:33–48; doi:10.1016/j.neuro.2014.03.013.

Wu S, Blackburn K, Amburgey J, Jaworska J, Federle T. 2010. A framework for using structural, reactivity, metabolic and physicochemical similarity to evaluate the suitability of analogs for SAR-based toxicological assessments. Regul. Toxicol. Pharmacol. 56:67–81; doi:10.1016/j.yrtph.2009.09.006.

Yamada KM, Cukierman E. 2007. Modeling Tissue Morphogenesis and Cancer in 3D. Cell 130:601–610; doi:10.1016/j.cell.2007.08.006.

Acknowledgements

At this point I would like to acknowledge all people who enabled this dissertation.

I would like to thank my supervisor Prof. Dr. Ellen Fritsche for the opportunity to perform my thesis in her working group and for the great support during the entire dissertation.

I would like to thank Prof. Lutz Schmitt for his cross-faculty supervision enabling this dissertation and for being my mentor.

Special thanks go to my colleague Thomas Temme and his supervisor Prof. Dr. Axel Mosiq for doing the programming work of the new developed software presented in this study and for Thomas to be a wonderful master student.

I would like to thank all my colleagues for their support, the productive working atmosphere, the fruitful discussions and helpful tips. I would like to thank Janette Goniwiecha for introducing me to the cell culture and assays. Special thanks go to Dr. Marta Barenys who assisted me in writing the publications, statistical analysis and general questions. Many thanks also to Farina Bendt who greatly assisted me in carrying out many experiments used in the presented publications. Furthermore I would like to thank Maxi Hofrichter, Laura Nimtz und Stefan Masjosthusmann for having always time to discuss and to help out. I especially appreciate the friendships originated during the dissertation and all the together free time activities.

I would like to thank Katharina Dach for structuring and motivating me throughout the entire dissertation and for her great support and help in all situations.

Finally I would like to thank my family and my other friends for their support and assistance during the stressful phases of this dissertation.

Many thanks for everything!

Eidesstattiche Erklärung/Declaration

Hiermit versichere ich an Eides statt, dass ich die vorliegende Arbeit „Entwicklung und Anwendung von informatischen Methoden für die "High Content" Bildanalyse (HCA) von neuralen Zellen“ selbständig verfasst und ausschließlich die von mir angegebenen Hilfsmittel verwendet habe. Die Dissertation wurde in der vorgelegten oder einer ähnlichen Form noch bei keiner anderen Institution eingereicht. Ich habe bisher keine erfolglosen Promotionsversuche unternommen.

I declare that I have developed and written the enclosed Thesis “Development and application of computational tools for high content image analysis (HCA) of neural cells” completely by myself, and have not used sources or means without declaration in the text. Any thoughts from others or literal quotations are clearly marked. The Thesis was not used in the same or in a similar version to achieve an academic grading elsewhere.

Martin Schmuck

Düsseldorf, November 2015